PENETRANT TRANSPORT IN COAL NETWORK STRUCTURES BETWEEN 35°C AND 150°C

Jorge M. Olivares and Nikolaos A. Peppas*
School of Chemical Engineering
Purdue University
West Lafayette, Indiana 47907

Keyword: coal network, penetrant transport, Case-II transport

INTRODUCTION

The dynamics of penetrant swelling of macromolecular coal systems can provide important information about the structure of the coal itself and its interactions with vapors and liquids. For example, it is possible to identify the thermodynamic state of the coal network. Inflections or dips in the time-sorption curve may be attributed to specific relaxations of the macromolecular coal system. If the coal is in the glassy state, one can determine whether the sorption is due to Fickian diffusion and/or due to relaxations of the macromolecular coal chains and estimate values of the diffusion coefficient and of the relaxation constants.

Increased concentration of penetrant in a macromolecular coal system has the same effect as increase of the temperature. As sorption continues, the density of the coal decreases thus allowing increased bond rotations and mobility. In addition, the favorable energetics involved in sorption provide the energy required for motion. Thus the glass transition temperature is lowered by the presence of the penetrant.

In previous work from our laboratory (1-7) we have examined the mechanism of penetrant transport in coal networks at low temperatures using pyridine (1-6) and various other amines (7). We have concluded that at low temperature (below 50°C) the mechanism of pyridine transport is non-Fickian or Case-II and that the size of the samples tested may shift the overall coupling of the diffusional and relaxational mechanisms.

Analysis of the sorption data can be accomplished by various means. For example, a convenient method of analysis involves fitting of the sorption data (4) to the empirical equation,

$$\frac{M_t}{M_\infty} = kt^n \qquad (1)$$

Here, M_t is the mass of solvent imbibed at time t, M_∞ is the mass of solvent imbibed at long times, and k is a constant which depends on the structural characteristics of the material and on the solvent/material interactions. The exponent, n, is used to indicate the type of diffusion and to infer state changes in the macromolecular systems. For a thin slab, when n equals 0.5, the diffusion is Fickian. When n is 1.0, Case II transport occurs. Finally, values of n between 0.5 and 1.0 indicate anomalous transport. If n > 1.0, the swelling material is likely to craze and fracture due to the tremendous osmotic pressure differences at the accelerating and advancing front. This type of transport mechanism is known as Super Case II transport.

* Correspondence

Up to now only one research contribution from our laboratory (8) has examined the change in temperature as a method to decouple the diffusion and relaxation phenomena. In the present work we examine the transport of various penetrants in coal sections at moderate temperatures.

EXPERIMENTAL PART

Coal samples were supplied by the Pennsylvania State University Coal Bank (PSU). Table 1 includes pertinent information provided by PSU for the coals used in this investigation.

Table 1. Analysis of Coal Samples Used

PSOC Code No.	County, State	Rank	%C (dmmf)	%H (dmmf)	%MM (dry)
418	Titus, TX	LigA	69.9	6.1	27.5
791	Titus, TX	LigA	72.2	5.3	20.7
247	Burke, ND	LigA	75.5	4.8	12.7
312	Navajo, AR	HVC	78.3	5.7	7.5
853	Delta, CO	HVC	80.1	5.0	3.7
402	Craig, OK	HVA	82.4	5.6	18.4
341	Jefferson, PA	HVA	86.0	5.7	14.5
384	Sullivan, PA	SAn	94.1	3.5	24.1

The techniques presented here for preparing uncontaminated thin section specimens of coal are based on the method of preparation employed by Brenner (9). Uncontaminated coal samples were prepared using a paraffin-based adhesive which could be completely removed from the sample. A chunk of coal was ground flat in a direction parallel to the geographic bedding plane on a horizontal diamond grinding wheel using progressively finer diamond grits. The flat surface of the coal was then heat cemented to a pre-conditioned microscope slide. When the hexane-soluble, paraffin-based, thermoplastic adhesive (Paraplast, American Scientific Products) had hardened, the coal chunk was cut with a diamond saw leaving approximately a two millimeter thick slab of coal mounted on the glass slide. The slab was then ground using a vertical diamond grinding wheel to the desired final thickness. The thin section specimens of coal were removed from the glass slide by soaking in n-hexane for several hours. Hexane did not swell the coal sample. After a few days of immersion, the solvent was removed, the samples were oven-dried at 60°C and stored in a dry nitrogen atmosphere at room temperature until use. The uncontaminated samples obtained ranged in thickness from 100 μm to 1500 μm. Thin coal sections, 200 μm to 1200 μm thick, of 1 mg to 10 mg were dried and cut in squares. They were introduced to one of the chambers of a thermogravimetric analyzer (TGS-2, Perkin Elmer, Norwalk, Connecticut) and the whole system was calibrated. The electrobalance system of the TGS-2 was purged with a continuous stream of nitrogen passing through three traps filled with N,N-dimethyl formamide (DMF) or pyridine. By adjusting the flow rate of nitrogen it was possible to control the evaporation rate of DMF or pyridine and, therefore, the ratio in the gaseous phase. Therefore, it was possible to conduct dynamic DMF uptake experiments at different activities. In addition, because of the microfurnace available in the thermogravimetric system, it was possible to carry out experiments at various temperatures.

RESULTS AND DISCUSSION

Selected data of pyridine and DMF uptake as a function of time and temperature are presented in Figures 1 through 6. In all cases, the diffusion time has been normalized with respect to the square of the sample thickness, t/l^2. In addition, all graphs present the amount of penetrant adsorbed per gram of dry coal, M_t/M_c.

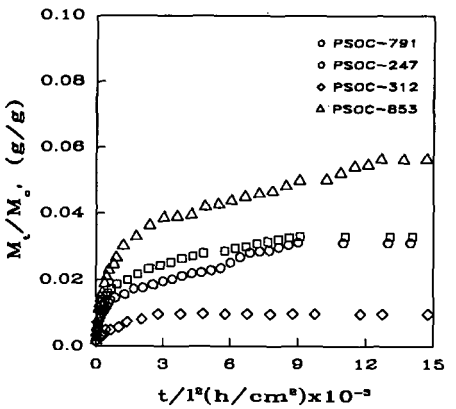

Fig. 1. Pyridine uptake in thin coal sections at 35°C.

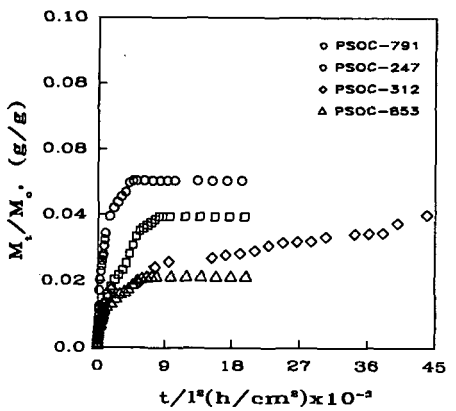

Fig. 2. Pyridine uptake in thin coal sections at 100°C.

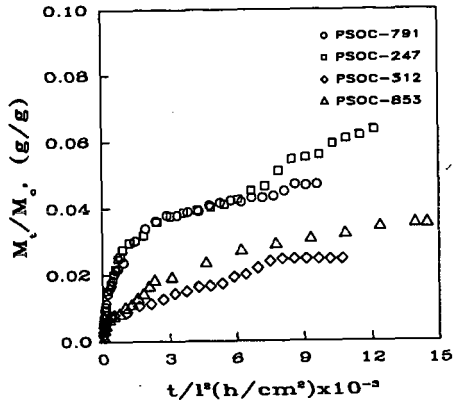

Fig. 3. Pyridine uptake in thin coal sections at 150°C.

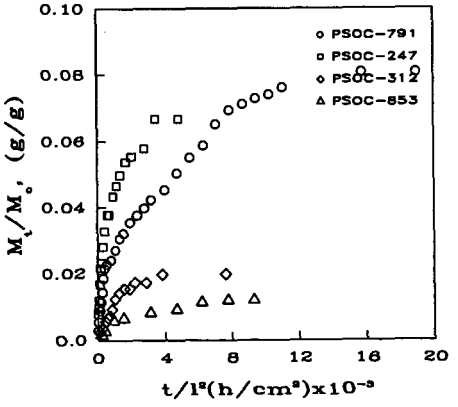

Fig. 4. DMF uptake in thin coal sections at 35°C.

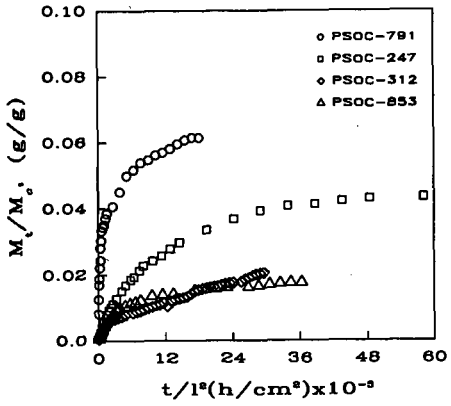

Fig. 5. DMF uptake in thin coal sections at 100°C.

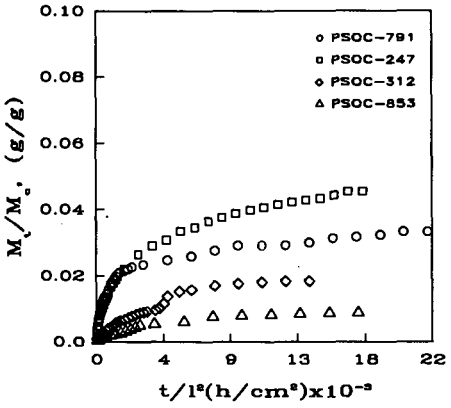

Fig. 6. DMF uptake in thin coal sections at 150°C.

These results were analyzed using equation (1) and the value of k and n are reported in Tables 2 and 3, respectively.

Table 2
Analysis of Pyridine Uptake by Coal Samples Using Equation (1)

PSOC	Temperature (°C)	n	95% CI for n	k	95% CI for k
791	35	0.42	0.06	8.6×10^{-4}	2.3×10^{-4}
247	35	0.56	0.05	4.3×10^{-4}	1.1×10^{-4}
312	35	0.34	0.12	5.1×10^{-4}	2.6×10^{-4}
853	35	0.61	0.09	4.6×10^{-4}	2.0×10^{-4}
-	-	-	-	-	-
791	100	0.47	0.04	1.2×10^{-3}	2.4×10^{-4}
247	100	0.61	0.03	1.8×10^{-4}	3.3×10^{-5}
312	100	0.32	0.04	1.4×10^{-3}	3.5×10^{-4}
853	100	0.68	0.09	1.2×10^{-4}	4.4×10^{-5}
-	-	-	-	-	-
791	150	0.41	0.02	1.4×10^{-3}	1.4×10^{-4}
247	150	0.58	0.08	6.9×10^{-3}	2.8×10^{-3}
312	150	0.32	0.04	4.2×10^{-2}	9.1×10^{-3}
853	150	0.61	0.09	4.2×10^{-3}	2.0×10^{-3}

Table 3
Analysis of DMF Uptake by Coal Samples Using Equation (1)

PSOC	Temperature (°C)	n	95% CI for n	k	95% CI for k
791	35	0.49	0.05	8.8×10^{-4}	2.4×10^{-4}
247	35	0.51	0.04	1.5×10^{-3}	2.9×10^{-4}
312	35	0.74	0.13	6.5×10^{-5}	3.6×10^{-5}
853	35	0.62	0.29	6.6×10^{-5}	5.6×10^{-5}
-	-	-	-	-	-
791	100	0.47	0.07	1.6×10^{-3}	5.5×10^{-4}
247	100	0.67	0.03	5.7×10^{-5}	1.0×10^{-5}
312	100	0.52	0.03	9.6×10^{-5}	1.7×10^{-5}
853	100	0.70	0.04	3.3×10^{-5}	8.3×10^{-6}
-	-	-	-	-	-
791	150	0.59	0.06	3.2×10^{-4}	9.5×10^{-5}
247	150	0.55	0.03	3.9×10^{-4}	7.1×10^{-5}
312	150	0.61	0.02	6.7×10^{-5}	9.9×10^{-6}
853	150	0.65	0.04	2.4×10^{-5}	5.2×10^{-6}

These results indicate that anomalous transport is observed in some samples of coal, especially at the higher degree of crosslinking, exemplified by the high carbon content of the coal samples. No Case-II transport was observed, and the results indicate a slight decoupling of diffusion and relaxation at higher temperatures.

This work was supported by a grant from the Department of Energy (PETC).

REFERENCES

1. N.A. Peppas and L.M. Lucht, *Chem. Eng. Commun., 37*, 333 (1985).
2. B.D. Barr-Howell, N.A. Peppas and D.N. Winslow, *Chem. Eng. Commun., 43*, 301 (1986).
3. B.D. Barr-Howell, N.A. Peppas and T.G. Squires, *J. Appl. Polym. Sci., 31*, 39 (1986).
4. P.L. Ritger and N.A. Peppas, *Fuel, 66*, 815 (1987).
5. L.M. Lucht and N.A. Peppas, *J. Appl. Polym. Sci., 33*, 1552 (1987).
6. B.D. Barr-Howell, J.M. Howell and N.A. Peppas, *Energy and Fuels, 1*, 181 (1987).
7. P.L. Ritger and N.A. Peppas, *Fuel, 66*, 1379 (1987).
8. B.D. Barr-Howell, J.M. Howell and N.A. Peppas, *Thermoch. Acta, 116*, 153 (1987).
9. D. Brenner, *Nature, 306*, 772 (1983).

The Relationships Between Coal Macromolecular Structure and Solvent Diffusion Mechanisms

Peter J. Hall, Harry Marsh and K. Mark Thomas
Northern Carbon Research Laboratories
University of Newcastle-upon-Tyne
Newcastle-upon-Tyne NE1 7RU
United Kingdom

Key Words: Macromolecular structure, diffusion, viscoelastic properties

Introduction

The diffusion of solvents through coal is the limiting step of many coal processes and measurement of the mechanism and kinetics of solvent diffusion has been the subject of numerous investigations[1,2]. It is generally accepted that solvent diffusion through coal is analogous to the diffusion of solvents through conventional glassy polymers and much of the formalism of the latter has been applied to coal[3]. The diffusion of solvents may vary between two extrema. If the diffusion is controlled by the concentration gradient between the center and the outside of the particle the diffusion mechanism is Fickian and, for diffusion into a sphere, the kinetics are expressed by the following expression[4]:

$$\frac{M(t)}{M_e} = 1 - \frac{6}{\pi^2}\sum_{n=1}^{\infty}\frac{1}{n}\exp(-Dn^2\pi^2 t/a) \qquad 1$$

where M(t) is the mass uptake at time t, Me is the equilibrium mass uptake, a is the particle radius and D is the diffusion coefficient. However, the mechanism of diffusion can deviate significantly from the Fickian mode when the diffusing solvent changes the viscoelastic properties of the glassy solvent. In the limit the diffusion of solvents is completely controlled by polymer relaxation and the solvent advances through the polymer with a well defined front such that ahead of the front the solvent concentration is zero and behind the front the solvent is at equilibrium concentration. Furthermore, ahead of the front the polymer is glassy and behind the front the solvent is rubbery. This kind of diffusion is referred to as "relaxation" or "Case II" diffusion and is characterized either by a polymer relaxation constant or the front velocity. Simple integration of the mass uptake at time t gives the following kinetic expression[5]:

$$\frac{M(t)}{M_e} = 1 - (1 - k_0 t / C_0 a)^3 \qquad 2$$

where k_0 is the relaxation constant and C_0 is the equilibrium solvent concentration. The

front velocity is k_o / C_o.

Diffusion mechanisms for solvents through coals has been shown to vary between there limits[2]. However, the structural features of the coal macromolecular structure or the details of the macromolecular/solvent interactions which determine diffusion mechanisms remain undefined and are the subject of this paper.

The method used to monitor the amount of solvent that has diffused into the solvent is Dynamic Volumetric Swelling (DVS). Essentially, the amount of volumetric swelling is monitored as a function of time. Only solvent that has diffused into the "bulk" structure can cause coal to swell so that this technique is insensitive to occluded solvent. At any time T, the amount of solvent that has diffused into the bulk is proportional to the amount of volumetric swelling, so that:

$$\frac{M(t)}{Me} = \frac{Q(t)}{Qe} \qquad 3$$

where Q(t) is the amount of volumetric swelling at time t and Qe is the equilibrium swelling. Graphically, to distinguish between the extremal modes of diffusion it is conventional to plot the normalized mass (or swelling) uptake as a function of root normalized time, $(t/t_e)^{1/2}$. Figure 1 shows the normalized plots for the theoretical Fickian and Relaxation diffusion modes. It can be seen that under this regime the normalized Fickian curve increases monotonically whereas the Relaxation controlled mode has an inflexion at low $(t/t_e)^{1/2}$.

Experimental

The apparatus was adapted from a design by Aida and Squires[6]. Essentially it consists of a glass cylinder 2 cm in diameter in which coal, supported by a quartz frit, interacts with the solvent. A light PTFE piston is placed on top of the coal and the increase in the height of the coal sample is monitored by a linear transducer connected to a microcomputer. The piston was of such a size as to allow a gap of about 1/4mm between the itself and the outer cylinder. The reaction chamber was surrounded by a constant temperature water bath, kept at 313K for these experiments. The coals were ground to between 60 and 30 Tyler mesh. With this particle size the diffusion of solvents through the coal bed was at least two orders of magnitude faster than diffusion into the particles. Coal was placed into the cylinder and the upper surface levelled. The initial height of the coal sample was measured and the piston and transducer placed on the coal. Solvent was introduced into the chamber to just below the frit and allowed to come to thermal equilibrium. Further solvent was added until the coal and piston were covered. The increase in sample height was monitored as a function of time. Since the approach to equilibrium swelling was asymptotic, the equilibrium time was chosen as the time to reach 99.5% of the equilibrium swelling value.

The coals were obtained from the coal bank of the Northern Carbon Research Laboratories and are described in Table 1. Two solvent sets were chosen, a set of

substituted pyridine molecules and a set of straight chain amines. The former were chosen because the steric properties of the molecules are similar but the basicity depends upon the substitution. In the latter, the molar volume increases with amine chain length whereas the basicity is relatively constant with amine chain length. The pK_b values and molar volumes of these solvent sets are given in Table 2.

Results and Discussion

Figure 2 shows the swelling curves for Gedling coal as a function of time. As would be expected, the time to equilibrium swelling (as defined above) increases as a function of amine chain length or molar volume. The amount of swelling also increases with amine molar volume, as observed by Green and West[7]. However, Figure 3 shows that when the swelling is normalized and plotted against root normalized time the curves have the same trajectory. Therefore all of the amines have the same swelling mechanism, regardless of molar volume.

Figure 4 shows the normalized DVS data for the substituted pyridine set. The diffusion changes from an anomalous mode for the pyridine and 2-methylpyridine to Fickian for the 2-fluoropyridine.

The principal mechanism of swelling for bases such as the amine and substituted pyridine sets appears to involve the disruption of inter chain hydrogen bonds[8,9]. Coal hydrogen bonds have a range of bond energy[9]. One result of this is that weaker bases, such as the 2-fluoropyridine, are able to disrupt only the weakest hydrogen bonds, stronger hydrogen bonds act as *de facto* crosslinks. As solvent basicity increases in the substituted pyridine set the solvents are able to disrupt increasing numbers of hydrogen bonds. Eventually a point is reached at which all of the hydrogen bonds are disrupted. This is manifested as a plateau in swelling/basicity curves[9].

One explanation of the progressive change from anomalous diffusion to Fickian diffusion could be that as the bases disrupt hydrogen bonds so the viscoelastic properties of the coals change from glassy to increasingly rubbery in the presence of the solvents. However, Figure 4 shows that pyridine and 2-methylpyridine have the same diffusion mechanism, even though their basicities are significantly different. This can be rationalized by noting that pyridine and 2-methylpyridine swell Gedling coal to the same extent[9] and, by hypothesis, disrupt the same number of hydrogen bonds.

Further corroborative evidence for the above theory comes from the diffusion mechanisms of the straight chain amine set. The amine chain length has little effect on molecular basicity and the observed increase in swelling with chain length has been attributed to the presence of increasingly larger molecules within the coal structure[7]. Green and West[7] have presented evidence to suggest that the molar amount of amine is absorbed per unit weight of coal is independent of amine size. This is consistent with the idea of

solvent basicity determining the number of hydrogen bonds disrupted.

From the above a consistent picture can be made of the factors which determine diffusion mechanisms for basic solvents. In its usual state Gedling coal is glassy at room temperature. When hydrogen bonds are disrupted by basic solvents the effective crosslink density decreases. There is an associated change of the coal viscoelastic properties as the coal becomes more rubbery. The degree to which coal becomes rubbery is a function of the density of hydrogen bonds disrupted. No assumptions are made about the mechanism by which basic solvents disrupt hydrogen bonds. However, the disruption of hydrogen bonds in itself may not be sufficient to change coal viscoelastic properties. Lucht *et al.*[10] have shown that Tg is reduced only to a limiting value of about 410K following sorption of pyridine vapor. There is a certain amount of evidence from work by Brenner[11] to suggest that solvent which makes coal rubbery is weakly associated in the coal structure. This may imply some sort of a solvent plasticization effect. These observations are not inconsistent with the picture presented above because during the uptake of liquids, for the Anomalous and Relaxation controlled diffusion, the concentration of solvent behind the solvent front must be sufficiently large to cause the rubbery behavior. In summary, the above picture only seeks to stresses that an essential part of the glass to rubber conversion is the disruption of hydrogen bonds. Recent, unpublished, work suggests that solvents which would be expected to have a plasticization effect similar to pyridine (such as chlorobenzene) in themselves do not change coal viscoelastic properties.

With the preceding in mind, an attempt can now be made to interpret the diffusion properties of a rank range of coals. The diffusion mechanisms are presented in Figure 5 with pyridine as the diffusing solvent. The lignite displays a Fickian diffusion and the diffusional mode becomes increasingly Relaxation controlled as rank increases. The diffusional mode for Cortonwood is well outside of the theoretical Relaxation controlled limit. Now, if the change in viscoelastic properties were simply a function of the density of hydrogen bonds disrupted then relaxation controlled behavior would be expected for coals with high oxygen contents. In fact the opposite is true. This can be rationalized by assuming that the change in viscoelastic property is, *ceteris paribus*, a function of the ratio of crosslink density before and after solvent diffusion *i.e.* (M_c/M_c+M_h). Where M_c is the covalent crosslink density and M_h is the hydrogen bond crosslink density. If this is indeed the case then the ratio of hydrogen bond to covalent (and other non-scissile) crosslinks increases as a function of coal rank in the range 50-87% carbon content. supportive evidence for this hypothesis comes from a body of data, derived from a variety of coal chemical and physical properties, which suggests that the crosslink density of coal reaches a minimum at about 87% carbon content[3,8].

There is no easy explanation in this framework for the behavior of Cortonwood coal. The swelling appeared to be a two-stage process with a quasi-equilibrium followed by a very slow approach to swelling equilibrium. A detailed picture of the factors influencing

coal diffusion mechanism requires more work. The role of solvent plasticization is unexplored.

Conclusions

The mechanism of diffusion of a solvent through a coal is, in part, determined by the degree to which the diffusing solvent changes the coal viscoelastic properties. One factor which influences this is the density of hydrogen bonds disrupted by the solvent in ratio to the non-scissile coal crosslinks. Solvent steric properties influence the kinetics, but not the mechanism of diffusion.

References

1. Hseih, S.T. and Duda, J.L., *Fuel*, **66**, 170, 1987.
2. Peppas, N.A. and Lucht, *Chem. Eng. Comm.*, **37**, 334, 1984.
3. Thomas, K.M. in *Carbon and Coal Gasification*, Eds Figureido, J.L. and Moulijn, J.A., NATO ASI Series E, 105, Martinus Nijhoff, Netherlands, 1986.
4. Crank, J., *The Mathematics of Diffusion*, Clarendon Press, UK, 1975.
5. Enscore, D.J., Hopfenberg, H.B. and Stannett, V.T., *Polymer*, **18**, 793, 1977.
6. Aida, T. and Squires, T.G., *ACS Fuel Division Preprints*, **30**, 95, 1985.
7. Green, T.K. and West, T.A., *Fuel*, **61**, 65, 1986.
8. Green, T.K., Kovac, J., Brenner, D. and Larsen, J.W., in *Coal Structure*, Ed Meyer, R.A., Academic Press, NY, 1982.
9. Hall, P.J., Thomas, K.M. and Marsh, H., *Fuel*, **67**, 863, 1988.
10. Lucht, L.M., Larson, J.M. and Peppas, N.A., *Energy and Fuels*, **1**, 56, 1987.
11. Brenner, D., *Fuel*, **63**, 1324, 1984.

Table 1

Coal	%C	%H	%O*	%N	%Mineral
ND Lignite	50.0	4.3	45.7	-	-
Gedling	81.6	5.2	9.4	1.7	2.8
Cresswell	84.5	5.5	5.9	1.9	3.0
Cortonwood	87.2	5.6	3.9	1.7	2.7

* by difference

Table 2

Solvent	pKb	Molar Volume (cm ^{3}/mol)
Propylamine	3.3	82.2
Butylamine	3.2	98.8
Propylamine	3.4	115.9
Hexylamine	3.4	132.1
2-methylpyridine	8.0	98.8
Pyridine	8.6	80.9
2-chloropyridine	13.5	94.6
2-fluoropyridine	14.4	86.1

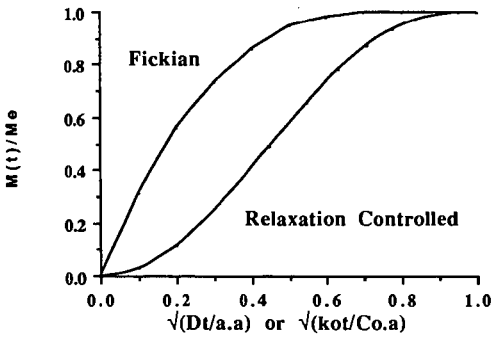

Figure 1. The normalized, theoretical, modes for Fickian and Relaxation-controlled diffusion into a sphere.

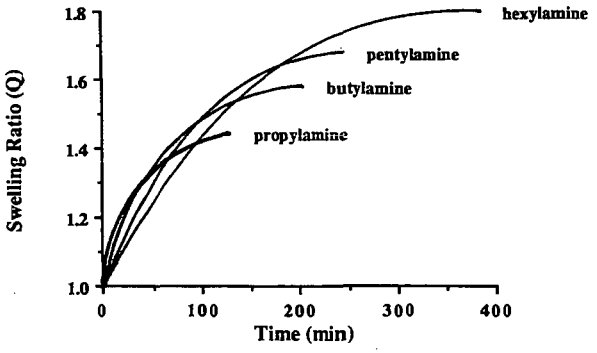

Figure 2. The dynamic volumetric swelling for straight chain amines in Gedling

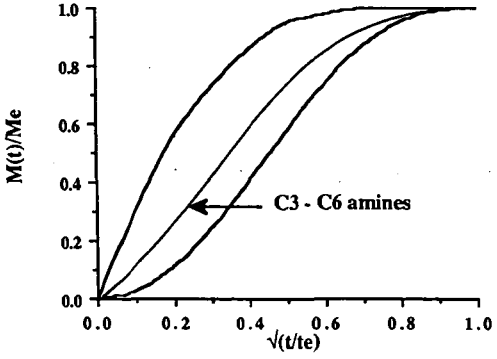

Figure 3. The diffusion mechanism for straight chain amines into Gedling coal at 313K as deduced from dynamic volumetric swelling.

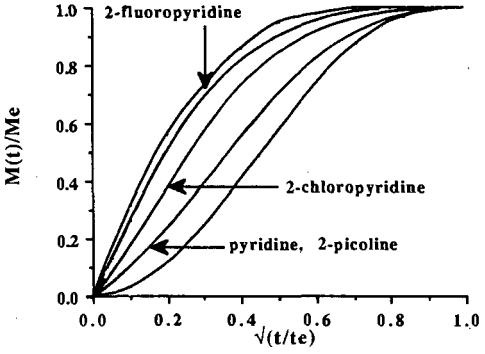

Figure 4. The diffusion mechanisms for substituted pydidines into Gedling coal at 313K, as deduced from dynamic volumetric swelling.

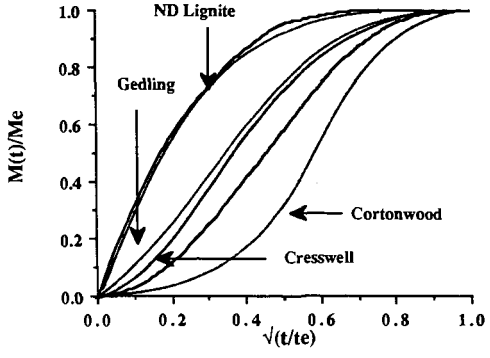

Figure 5. The diffusion mechanisms for pydidine into a range of coals at 313K, as deduced from dynamic volumetric swelling.

COAL SOLUBILITY AND SWELLING

Paul Painter, Yung Park, John Graf,
Maria Sobkowiak and Mike Coleman
Polymer Science Program
The Pennsylvania State University
University Park, PA 16802

Key Words: Coal solubility, coal swelling, hydrogen bonding

INTRODUCTION

The characterization of coal as a macromolecular network has resulted in a significant advance in our understanding of this complex material. By applying the theories of Paul Flory (1,2), the solubility (or, more accurately, extractability) and swelling of a coal can be used as a probe of structure (3-11). It is widely recognized however, that the original theories are flawed, particularly the Flory-Rehner treatment of the swelling of polymer networks (although it apparently benefits from the cancellation of errors (12)), and their application to coals is further limited by the presumed non-Gaussian behaviour of the "chains" and the realization that coal segments interact with each other and solvent through the formation of hydrogen bonds. Strong, specific interactions such as these are not accounted for in Flory's original equations describing the free energy of mixing and the contribution of the chemical potentials to the balance of forces involved in the swelling of a cross-linked network. We have recently developed an association model that can account for hydrogen bonding in polymer mixtures (13-16). The result is a Flory-Huggins equation accounting for the entropy of mixing and the dispersive (and other) non-hydrogen bonding forces described by a χ parameter, with an addition free energy term ΔG_H that accounts for the change in the number and type of hydrogen bonds that occur as a function of composition;

$$\frac{\Delta G_M}{RT} = \frac{\phi_A}{x_A} \ln \phi_A + \frac{\phi_B}{x_B} \ln \phi_B + \phi_A \phi_B \chi + \frac{\Delta G_H}{RT} \qquad (1)$$

where ϕ_A,ϕ_B are volume fractions and x_A,x_B are "degrees of polymerization", or, more accurately, the ratio's of the molar volumes of the components relative to a reference molar volume. The crucial points concerning this equation are:

1) The ΔG_H term is negative and favourable to mixing
2) The quantities used to calculate ΔG_H are determined experimentally and there are no adjustable parameters in this term
3) Phase behaviour is determined by the balance between the positive and unfavourable to mixing χ term and the favourable to mixing entropic and ΔG_H terms and the contribution of these terms to the derivatives of the free energy with respect to composition.

The equations for ΔG_H and its derivatives and the details of their specific application to coal have been presented elsewhere (17,18). Here we will concern ourselves with a brief outline of some of our most important recent results. Space does not permit a detailed description of the calculations, which will be presented in a set of three papers that are about to be submitted for publication (19-21). Our discussion will touch upon;

a) The determination of χ from solubility parameters.
b) The calculation of "hypothetical" phase diagrams for coal solutions
c) The calculation of the molecular weight between cross-link points from swelling measurements
d) The formulation of a new model for the description of coal swelling and its relationship to structure.

COAL SOLUBILITY PARAMETERS

If we are limiting its application to non-specific and (relatively) weak interactions, then the value of the Flory χ parameter can be estimated from solubility parameters using

$$\chi = \frac{V_B}{RT}\left(\delta_c - \delta_s\right)^2 + 0.34 \qquad (2)$$

where V_B is a reference volume and δ_c and δ_s are the solubility parameters of the coal and solvent, respectively. For an insoluble network the solubility parameter (δ_c) has been determined in one of two ways; from group contributions using, for example, the methods of van Krevelen (4,22) Hoy (23) or Small (24), of from swelling measurements. Unfortunately, both these methods involve difficulties and for coals lead to the prediction of very different solubility parameters, even when the effect of hydrogen bonding is minimized or excluded. For example, Larsen et al. (7) carefully examined the swelling of acetylated coals in non-hydrogen bonding solvents. An Illinois No. 6 and a Bruceton coal both gave a maximum degree of swelling for solvents with solubility parameters in the range 9-10 $(cal.cm^3)^{1/2}$. This value would then normally be taken as the proper value for coal, as it would give the minimum value for χ. However, a calculation of the corresponding solubility parameters using the atomic contribution method proposed by van Krevelen (4) gives values in the range 11-12 $(cal/cm^3)^{1/2}$, depending upon the precise value of the fraction aromaticity assumed for these samples. We found it difficult to understand precisely how van Krevelen obtained his parameters, as his methodology is not described, but on the basis of our calculations we believe it to be prone to large errors and fully of broad and perhaps unjustifiable assumptions, as we will discuss in detail elsewhere in a separate publication (19). The obvious choice would therefore seem to be the experimentally determined values. Paradoxically, we believe that van Krevelen's result is at least in the right range and the value obtained from maximum swelling is <u>not</u> the value for coal. This is not because of any problem with the experiments, but one that has its origins in free volume or compressibility effects that are ignored in simple theories of mixing.

In resolving the differences in the values of δ_c given by group contributions and swelling measurements we first observe that this problem is not unique to coal. Bristow and Watson (26) found that certain rubbers with solubility parameter values of the order of 9-10, gave maximum swelling in a series of n-alkanes with heptane, δ=7.4. This difference was demonstrated to be due to so-called free volume effects by Biros et al. (27), who applied Flory's equation-of-state theory (2). it is a relatively straightforward matter to show that such effects also account for the observed maximum in the swelling of coal. We have applied the.lattice fluid model of Sanchez and Lacombe (28-30) rather than Flory's theory, however.

The association formalism we use to describe hydrogen bond interactions and the Sanchez-Lacombe theory are both simple lattice models, so for future application it is more appropriate to combine these approaches, as we will report elsewhere (31), than to somehow graft an association model onto Flory's equation-of-state. Accordingly, using the equations of Sanchez and Lacombe (28-29) the Flory χ parameter can be written as:

$$\chi = \frac{\tilde{\rho}\Delta\varepsilon^*}{RT} + \frac{1}{\phi_2^2}\left[\tilde{T}_1\left(\tilde{\rho}_1 - \tilde{\rho}\right) + \frac{(1-\tilde{\rho})}{\tilde{\rho}}\ln(1-\tilde{\rho}) - \frac{(1-\tilde{\rho}_1)}{\tilde{\rho}_1}\ln(1-\tilde{\rho}_1) + \frac{1}{r}\ln(\tilde{\rho}/\tilde{\rho}_1)\right] \qquad (3)$$

or, more simply

$$\chi = \frac{\tilde{\rho}\Delta\varepsilon^*}{kT} + \beta^1 \qquad (4)$$

where $\tilde{\rho}$, $\tilde{T}$ are the reduced density and temperature (see references 27-29) and the subscripts 1 and 2 refer to components 1 and 2 of the mixture. The term $\Delta\varepsilon^*$ is given by

$$\Delta\varepsilon^* = \varepsilon_{11}^* + \varepsilon_{22}^* - 2\varepsilon_{12}^* \qquad (5)$$

and is the usual difference in the energy of 1-2 contacts relative to 1-1,2-2 contacts. If we make the geometric mean assumption

$$\varepsilon_{12}^* = \left(\varepsilon_{11}^* \ \varepsilon_{22}^*\right)^{1/2} \qquad (6)$$

then

$$\chi = \frac{\tilde{\rho}}{kT}\left[\left(\varepsilon_{11}^*\right)^{1/2} - \left(\varepsilon_{22}^*\right)^{1/2}\right]^2 + \beta^1 \qquad (7)$$

The correspondence of this equation to the solubility parameter approach can then be seen immediately by rewriting equation 1 on the basis of numbers of molecules rather than moles and transforming the subscripts:

$$\chi = \frac{V_1}{kT}\left(\delta_1 - \delta_2\right)^2 + \beta \qquad (8)$$

The solubility parameters are related to the cohesive energy densities (CED) and hence the lattice fluid parameters (28,29) through

$$\delta = (CED)^{1/2} = \left(\frac{\Delta E_v}{V}\right)^{1/2} = \left(\frac{\varepsilon^*}{v^*}\right)^{1/2} \tilde{\rho} \qquad (9)$$

where v^* is the average close packed volume of a segment and generally varies with composition (i.e., $v_1^* \neq v_2^*$). If we assume there is no dependence of the energies of interaction (ε_{11}^* etc.) on composition and use the identity $V_1 = v_1^*/\tilde{\rho}_1$, then equation (8) can be obtained directly from equation 7. Accordingly, in the solubility parameter approach we can identify the parameter β with so-called free volume or compressibility effects, while the $(\delta_1-\delta_2)^2$ term reflects exchange interaction energies that are assumed independent of composition. We must now face the following question: for coal is the value of β of the order of 0.34, as in many polymer systems, or are free volume differences such that there is a larger deviation? It is a relatively straightforward matter to use equation 3 to calculate χ for various coal/solvent mixtures. The necessary parameters for the solvents used by Larsen et al. (7) were obtained from Sanchez and Lacombe (28), while the parameters for coal were calculated from its coefficient of thermal expansion ($\alpha = 1 \times 10^{-5}$, from van Krevelen (34) and an assumed value of the solubility parameter of $\delta_c = 11.8$, a value estimated from van Krevelen's method (4). Coal-solvent interactions were also assumed to be given by the usual geometric mean assumption. The equations necessary for these calculations are given elsewhere (19) and here we simply present the result in Figure 1, a plot of χ vs δ_s. A coal with a solubility parameter of 11.8 $(cal/cm^3)^{1/2}$ has a minimum value of χ and hence a predicted maximum swelling with a solvent that has a solubility parameter of

about 10 $(cal/cm^3)^{1/2}$. A value of δ for an Illinois #6 coal of 11.4, as we estimate from a revised methodology (19) gives a predicted maximum swelling with non-hydrogen bonding solvents that have a solubility parameter in the range 9-10, corresponding to the value determined experimentally by Larsen et al. (7).

THE PHASE BEHAVIOUR OF SOLUTIONS OF COAL MOLECULES

An understanding of the solubility of a coal in various solvents can be obtained by a calculation of hypothetical phase diagrams. They are hypothetical in the sense that we assume that the coal is not cross-linked, but is simply a macromolecule. This macromolecule could be highly branched and with an extremely high molecular weight, but within the limitations of the simple lattice model applied here its equilibrium properties can be determined. This, in turn, allows an understanding of why a particular solvent is capable of extracting more (or less) soluble material than another and, as we will see, provides some fundamental insight into the variation of swelling behavior with temperature.

In a preliminary communication of this work (18) we calculated theoretical phase diagrams as a function of coal rank. the value of χ was estimated using van Krevelens method (4). As we will discuss in detail in a separate paper (19), we have little confidence in the precise value so calculated for any particular coal, but the trend with rank makes sense in terms of what we know about the structure of coal and the value appears to be in the right range. The calculation of the ΔG_H term and the derivatives of the free energy are described in previous publications (13-18). here we will discuss the calculated spinodals for three coals, an Illinois #6, PSOC 207 and PSOC 402, shown in Figures 2-4, as these results bear on the interpretation of swelling measurements.

For Illinois #6 coal we illustrate the spinodals obtained for mixing with three different solvents, pyridine, THF and benzene. For pyridine, we predict a typical inverted "U" shaped stability curve with an upper critical solution temperature near 25°C. Mixtures with THF and benzene are predicted to be far less miscible, with the stability limits calculated to be near the two composition extremes. An examination of Table 1, which lists the solvent parameters utilized here, together with some values for other solvents, immediately demonstrates why. Pyridine forms much stronger hydrogen bonds that the other solvents listed (as measured by the equilibrium constant K_A) and, in addition, its solubility parameter is closer to the range we estimate represents the most likely value for this coal (11-12 $(cal/cm^3)^{1/2}$). Thus, favorable interactions (coal solvent hydrogen bonds) are maximized and χ is minimized. This is a crucial point, correlation of coal swelling to a single parameter, chosen so as to represent χ or some measure of the strength of favorable interactions, can be misleading. It is the balance of favorable and unfavorable forces that is crucial.

The calculated spinodals for PSOC 207 and PSOC 402 in pyridine show progressively increasing values of the upper critical solution temperature (maximum value of the inverted "U") relative to Illinois #6 coal, a trend that largely reflects the increasing value of χ calculated for this coal-pyridine series. To reiterate, although the precise positions of these curves are obviously affected by the errors in calculating δ_c, we believe that this predicted trend in behavior should be reasonably accurate.

The calculated phase behaviours indicates that if these coals were not cross-linked they would be completely soluble in pyridine at elevated temperatures. This remains true even if we assume very high molecular weights for the coal molecules (the contribution of the combinatorial entropy from the coal is very small for the degree of polymerization x_B assumed in these calculations (x_B=100); changing this value to 1000 or 10,000 has only a minor effect on the calculated spinodals, as illustrated in our preceding publications (17,18)). Accordingly, we believe that these results strongly support the present generally held view that at least up to a certain carbon content, coals are cross-linked networks

THE SWELLING OF COAL

Hydrogen bonding affects the swelling of coal through its contribution to the chemical potential of the solvent $(\Delta G_H)_A$. The Flory Rehner equation, as modified by Kovac (32) and applied to coal by Larsen et al. (7),can then be written

$$\bar{M}_c = \frac{\rho_B V_A \phi_B^{1/3} + \rho_B V_A / N \phi_B^{1/3}}{-\left[\ln(1-\phi_B) + \phi_B + \chi \phi_B^2 + \left(\Delta \bar{G}_H\right)_A / RT \right]} \qquad (10)$$

where $\bar{M}_c$ is the number average molecular weight between cross link points and N represents the number of "clusters" between cross link points. Larsen et al. (7) studied the swelling of an extracted but otherwise unreacted Illinois #6 coal in pyridine. Using the reported swelling ration of about Q=2.4, we obtained the plots of $\bar{M}_c$, the number average molecular weight between cross link points against M_o, the assumed molecular weight of a coal cluster, shown in Figure 5. In this initial plot we put $(\Delta G_H)_A = 0$, i.e., we ignored hydrogen bonding. Results were obtained for four different assumed values of δ_{coal}, ranging from 9 to 12 and display the large sensitivity to χ noted by Lucht and Peppas (8). These results are dramatically altered if we now include the effect of hydrogen bonding, using equation 10. The effect of variations in χ is now greatly reduced, as can be seen from Figure 6, and the calculated values of M_c are now much smaller. this is a consequence of the large contribution of hydrogen bonding to the chemical potential of the solvent, i.e., the $(\Delta G_H)_A$ term dominates the χ term. A calculated molecular weight of about 500, or "degree of polymerization" of about 2 clusters, between cross-link points is determined. This appears to be too small to be reasonable, but we will defer a discussion of this point until after we consider some additional data.

Lucht and Peppas (9) have also studied the swelling of various coals in pyridine, including PSOC 207 and PSOC 402. These swelling measurements were conducted at three different temperatures, 35, 60 and 80°C, and the results of applying equation 10 to their data is shown in Figures 7 and 8. It can be seen that there are distinct differences in the calculated values of the molecular weight between cross-link points with much larger values being determined at high temperatures. Unlike Lucht and Peppas (8), we allowed χ to have its usual $1/T$ dependence, while the variation of the values of the equilibrium constants, and hence $(\Delta G_H)_A$, with temperature was determined through the usual vant Hoff relationship (14). Accordingly, it is not the temperature dependence of the solvent chemical potential that is responsible for such large differences. Only small variations might be expected due to the errors inherent in the various assumptions that are made concerning the form of the temperature dependence of the parameters over this fairly limited range. An explanation is immediately apparent if we examine the calculated solution phase diagrams shown in Figures 3 and 4, however. PSOC 207 and 402 are predicted to have upper critical solution temperatures near 75 and 125°C, respectively, these values being subject to the significant errors involved in estimating χ(19). Clearly, if the swollen network is at a temperature above this transition, in the single phase region, the coal should swell to the limit imposed by the nature of the network. Below this transition, however, there is a two phase region that is predicted for the coal primary chains in pyridine. The precise position of this transition for the network would be affected by the elastic forces between cross-link points, but clearly at some critical temperature solvent would be expelled leading to the phenomenon of gel collapse. The plots shown in Figures 7 and 8 suggest that this is precisely what we are observing in coal. PSOC 207 shows a large change in swelling and hence calculated molecular weight on going from 35°C to 60°C, but a small difference on going from 60°C to 80°C. In contrast, the major change for PSOC 402 appears to occur between 60°C and 80°C. We believe that these discontinuities in behaviour are due to expulsion of solvent from the swollen coal network. Our association model predicts this trend remarkably well; an examination of the calculated solution phase behaviours, shown in Figures 4 and 5, indicates that PSOC 402 has a higher UCST than PSOC 207. The absolute values of the transition are off by approximately 40°C, but this is not bad considering the errors in calculating χ and the probability that we should include a chain extension term in accounting for the phase behaviour of the gel.

If we now consider the values of the molecular weight obtained at the highest swelling temperature to be the most accurate, the predicted molecular weight between cross links is now more reasonable, but still small in terms of the inherent limitations of the model. If we further assume that the molecular weight of an average "cluster" is of the order of 200, this model predicts that the number of such

clusters between cross links is of the order of three for these coals. We must therefore, question whether it is at all appropriate to apply Flory's theory to coal, even in the modified form expressed by equation 10. We will suggest an alternative in the following section.

SWELLING BY DISINTERSPERSION

Even if we discount the flaws perceived by various authors in the original Flory-Rehner theory, its application to coal, even using the modified Gaussian statistics proposed by Kovac (32) and accounting for the contribution of hydrogen bonding, must be considered highly suspect. The results suggest that the number of aromatic "clusters" between crosslinks is small and such chains are certainly stiff. Nevertheless, we believe that it is possible to construct a simple model that provides at least a rough estimate of the molecular weight between cross-link points, although we do not formulate it in those terms.

This model is based on the very important observations of Bastide et al. (33) that the radius of gyration of the chains of a swollen polystyrene gel were equal, within the limits of experimental error, to that of the free chains in the same solvent, and did not vary when the degree of swelling was altered. On this basis it was proposed (34) that swelling was associated with a topological reorganization of the network, where the cross link points essentially rearrange their positions with only minor perturbations to the chain dimensions, a process that these authors labeled disinterspersion. We assume that the stiff molecules in coal essentially unfold in this manner and that the degree of swelling is then limited by the geometry of the system. A more complete account of our arguments is given in reference 1, but a schematic view of this process is illustrated in Figure 9. Strangely enough, we will argue that the coal "chains" are not straight rods, as shown in this figure, but follow random walk or perhaps self avoiding walk statistics. This is a second crucial point in the development of our simple model. It is important to realize that we are not making this claim on the basis of any argument concerning chain flexibility. Instead, we propose that this is a consequence of the heterogeneity of linkages that must occur in coal. A two dimensional view of simple aromatic units (benzene and naphthalene rings), linked by $-CH_2-$ and -O- groups, is shown in Figure 10. Even if we require on steric grounds that bonds in the ortho position are unlikely, the variety of other possibilities result in a chain that can be modeled by a set of virtual bonds, in this example shown linking the centers of the aromatic clusters, such that they trace out a (more-or-less) random walk or random flight. If the network then simply swells to the limit permitted by the "unfolding" of these chains, which behave as stiff, bent wires, then the relationship between the degree of swelling and the contour length of these chains follows from simple geometry. If we let the functionality of the network be equal to f and the average end-to-end distance between cross link points be equal to R_o ($=\langle r^2\rangle^{1/2}$), then we can pick a cross-link point in the swollen network at random and determine the volume of the chains in the volume (4/3) πR_0^3 following Bastide et al. (34). This is equal to fV_sN, where V_s is the volume occupied by each "repeat" unit and N is the number of repeat units in each primary chain. It then follows that the volume fraction of polymer in the swollen gel is given by

$$\phi = \frac{3fV_sN}{4N\pi R_o^3} \qquad (11)$$

The quantity R_o is related to N by the general relationship

$$R_o = aN^{\nu} \qquad (12)$$

where a is the length of an average unit and ν has a value in the range 0.5 to 1 (for a random walk ν = 0.5, a self avoiding walk ν = 0.6 and for a rigid rod ν = 1).

The parameter a, V_s and N are not easily defined for any particular coal, but, as we show in more detail in a separate publication (21), by defining these quantities on a per carbon atom basis we obtain

$$N_c^{(3\nu-1)} = \frac{3fV_c}{4\pi\phi a_c^3} n_c^{3(\nu-1)} \quad (13)$$

where N_c is the number of carbon atoms between cross-link points, V_c is the molar volume per carbon atom (which can be determined from the elemental composition and density), and a_c is the length of such a cluster (or virtual bond in Figure 10) divided by the number of carbon atoms (n_c, in that cluster. If we assume that as a result of the heterogeneities of the cross-link points and the limited degree of chain flexibility that can occur in a good solvent, $\nu = 0.6$, then plots of N_c vs n_c for various values of a_c can be constructed, as shown in Figure 11 (a value of $f = 3$ was assumed). The data used to obtain these plots was that of the Illinois #6 coal studied by Larsen et al. (7). If we assume an average of 8-9 carbon atoms per repeat or cluster, corresponding to a mixture of substituted benzene and naphthalene rings, with the former predominating, then it follows from known bond length and bond angle geometries that a_c is in the range 0.5 to 0.6, so that N_c would have a value somewhere between 25 and 45 carbon atoms, corresponding to approximately 3-5 clusters between each cross-link point. For a network with $f = 4$, this increases to a value between 4 and 7 (19).

CONCLUSIONS

We believe a number of important conclusions follow from this analysis, amongst the most significant of which are:

1) Solubility parameters for coal are not accurately determined from swelling measurements because of free volume effects.

2) The phase behaviour of the coal network/solvent has to be taken into account when conducting swelling measurements.

3) We predict that the phenomenon of gel collapse could occur in coal.

4) A simple model for coal swelling based on disinterspersion has been proposed, following the work of Bastide et al. (33,34).

ACKNOWLEDGEMENTS

We gratefully acknowledge the support of the Office of Basic Energy Sciences, Division of Chemical Sciences, Department of Energy, under Grant No. DE-FG02-86ER13537.

REFERENCES

1. Flory, P. J. Principles of Polymer Chemistry; Comell University Press: Ithaca: NY, 1953.
2. Flory, P. J. Selected Works of Paul J. Flory; Mandelkern, L., Mark, J. E., Suter, U. W., Yoon, Do. Y., Eds.; Stanford University Pres: Stanford, CA, 1985; Vol. I-III.
3. van Krevelen, D. W. Coal; Elsevier: New York, 1981.
4. van Krevelen, D. W. Fuel 1966, 45, 229.
5. Green, T.; Kovac, J.; Brenner, D.; Larsen, J. W. In Coal Structure; Meyers, R. A., Ed.; Academic: New York, 1982.
6. Larsen, J. W. In Chemistry and Physics of Coal Utilization; AIP Conference Proceedings, 70; Cooper, B. R., Petrakis, L., Eds.; AIP: New York, 1981.
7. Larsen, J. W.; Green, T. K.; Kovac, J. J. Org. Chem. 1985, 50, 4729.
8. Lucht, L. M.; Peppas, N. A. In chemistry and Physics of Coal Utilization, AIP Conference Proceedings 18; Cooper, B. R., Petrakis, L., Eds.; AIP: New York, 1981.
9. Lucht, L. M.; Peppas, N. A. Fuel 1987, 66, 803.
10. Lucht, L. M.; Peppas, N. A. J. Appl. Polym. Sci. 1987, 33, 2777.
11. Brenner, D. Fuel 1985, 64, 167.

12. DeGennes, P. G., Scaling concepts in Polymer Physics, Cornell University Press, Ithaca, NY, (1979).
13. Painter, P. C.; Park, Y.; Coleman, M. M., Macromolecules, 1988, 21, 66.
14. Painter, P. C.; Park, Y.; Coleman, M. M., Macromolecules, 1989, 22, 570.
15. Painter, P. C.; Park, Y.; Coleman, M. M., Macromolecules, 1989, 22, 580.
16. Painter, P. C., Graf, J. and Coleman, M. M. J. Chem. Phys. (submitted for publication).
17. Painter, P. C., Park, Y. and Coleman, M. M., Energy and Fuels, 1988, 2, 693.
18. Painter, P. C., Park, Y., Sobkowiak, M. and Coleman, M. M., ACS Fuel Chem. Div. Preprints, 1989, 34(2), 559.
19. Painter, P. C., Graf, J. and Coleman M. M., (to be submitted to Energy and Fuels).
20. Painter, P. C., Park, Y., Sobkowiak, M. and Coleman, M. M. (to be submitted to Energy and Fuels).
21. Painter, P. C., Graf, J., and Coleman, M. M. (to be submitted to Energy and Fuels).
22. van Krevelen, D. W. Fuel 1966, 45, 229.
23. van Krevelen, P. W., Properties of Polymers; Elsevier: Amsterdam, 1972.
24. Hoy, K. L., J. Paint Technol., 1970, 42, 76.
25. Small, P. A., J. Appl. Chem., 1953, 3, 71.
26. Bristow, G. M. and Watson W. F., Trans. Faraday, Soc., 1958, 54, 1731.
27. Biros, J. Zeman, L. and Patterson, D. Macromolecules, 1971, 4, 30.
28. Sanchez, I. C. and Lacombe, R. H. J. Phys. Chem. 1976, 80, 2352, 2568.
29. Sanchez, I. C. and Lacombe, R. H. Macromolecules, 1978, 11, 1145.
30. Sanchez, I. C. and Lacombe, R. H. J. Pol. Sci. Poly Letters Ed, 1977, 15, 71.
31. Painter, P. C., Graf, J. and Coleman, M. M., to be published.
32. Kovac, J. Macromolecules, 1978, 11, 362.
33. Bastide, J., et al., as reported by Candau, S., Bastide, J. and Delsanti, M., Advances in Polymer Science, 1982, 44, 27.
34. Bastide, J., Picot, C., Candau, S., J. Macromol. Sci., Phys. 1981, B19, 13.

Table 2. Parameters for Solvents at 25°C

SOLVENTS	V_s ($cm^3\ mol^{-1}$)	K_A ($kcal\ mol^{-1}$)	h_s ($kcal\ mol^{-1}$)	δ_s $(cal\ cm^{-3})^{1/2}$
PYRIDINE	81	284.87	8.9	10.6
THF	74.3	89.54	5.76	9.9
ACETON	74.3	58.9	4.03	9.9
DIETHYL ETHER	101.7	45.24	5.76	7.5
ACETONITRILE	55.4	23.56	2.03	11.8
BENZENE	82.2	1.41*	1.25	9.1

* Weak H-bonds between OH groups and π electrons have been proposed.

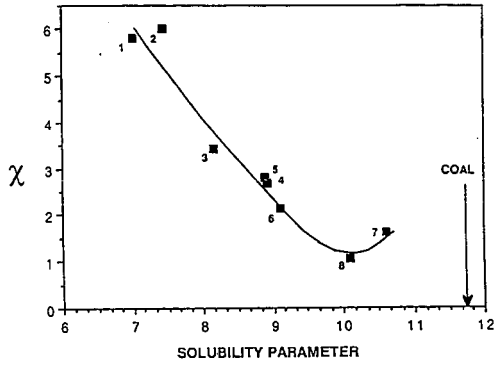

Figure 1. Plot of χ vs solubility parameters for the Illinois #6 coal and solvents studied by Larsen et al. (7).

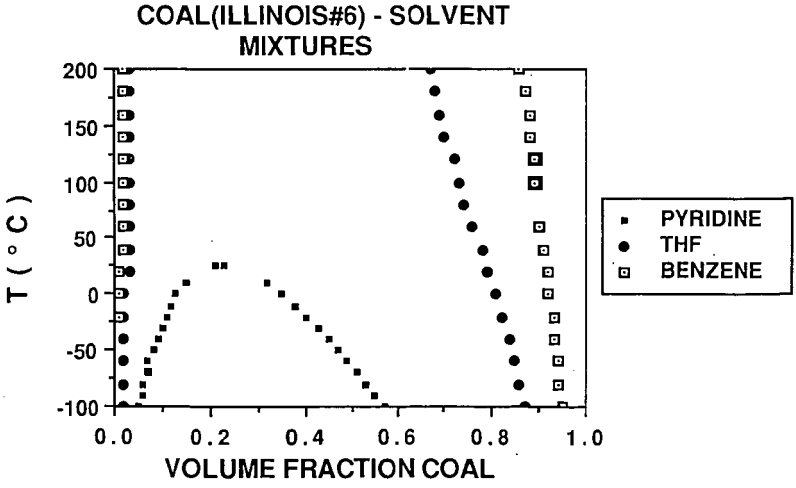

Figure 2. Phase diagram (spinodals) for an Illinois #6 coal mixed with various solvents.

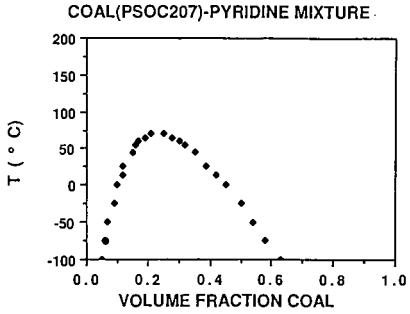

Figure 3. Phase diagram (spinodal) for PSOC 207-pyridine mixtures.

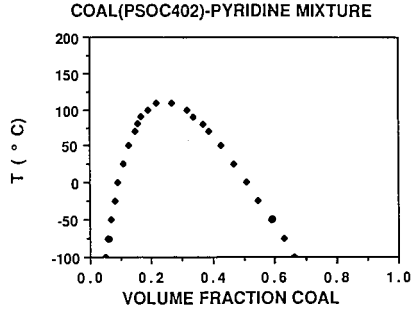

Figure 4. Spinodal for PSOC 402/pyridine mixtures.

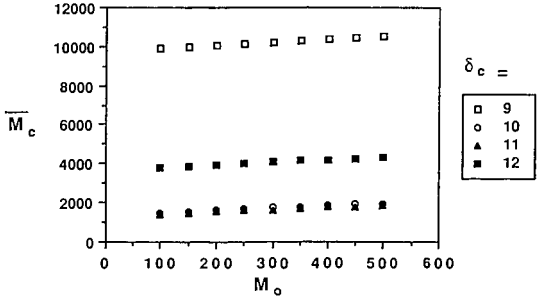

Figure 5. Plot of $\overline{M}_c$ vs M_o (see text) for Illinois #6 coal, ignoring hydrogen bonds.

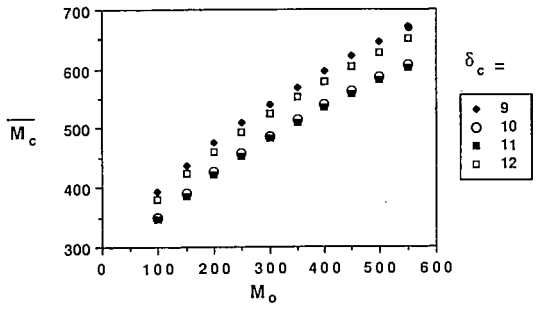

Figure 6. Plot of $\overline{M}_c$ vs M_o for Illinois #6 coal when hydrogen bonding is included.

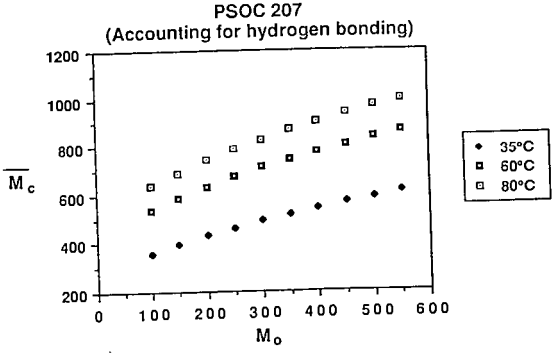

Figure 7. $\overline{M}_c$ vs M_o for PSOC 207.

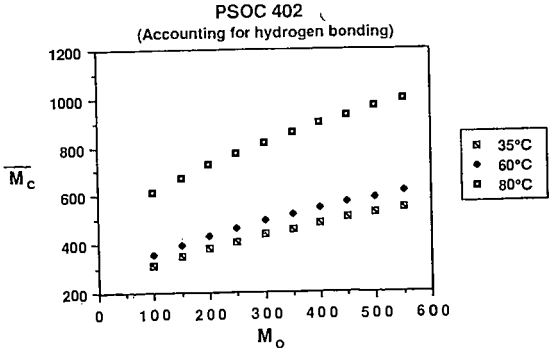

Figure 8. $\overline{M}_c$ vs M_o for PSOC 402

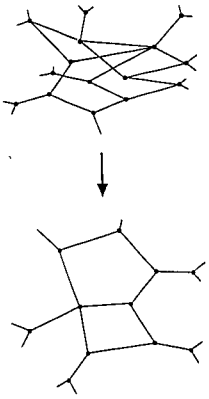

Fiture 9. Disinterspersion for a network of rigid rods.

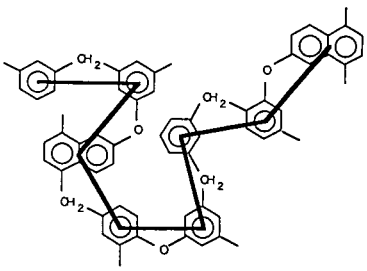

Figure 10. A random walk imposed by a pattern of substitution in a rigid chain.

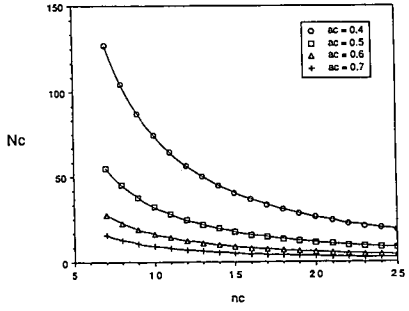

Figure 11. Plot of N_c (number of carbon atoms between cross link points) vs n_c (the number of carbon atoms per cluster).

SOLVENT-INDUCED ASSOCIATIONS OF HIGH-VOLATILE BITUMINOUS COALS

Masaharu Nishioka* and John W. Larsen

Corporate Research Science Laboratories
Exxon Research and Engineering Company
Clinton Township, Annandale, NJ 08801
(*Present address: BCR National Laboratory,
500 William Pitt Way, Pittsburgh, PA 15238)

Keywords: association; soaking; hydrogen bonds

INTRODUCTION

It is known that solvent-induced crystallization of amorphous polymers can occur below their glass transition temperatures.[1] This conformational change of the polymer chains into a lower free energy state is facilitated by the presence of the solvent. We recently reported a similar solvent-induced association between coal macromolecules.[2] This is analogous to the solvent-induced crystallization of amorphous polymers in that the amorphous coal macromolecules are altered to increase relatively strong intermolecular interactions leading to a lower free energy state.

It was previously observed that the pyridine extractability and optical anistrophy of Pittsburgh No. 8 coal decreased after heating at 115°C in chlorobenzene under nitrogen for seven days. Immersion in pyridine at room temperature for one day, followed by eliminating pyridine, had the same effect on pyridine extractability as exposure to hot chlorobenzene for a week. Treatment of the pyridine extract from the same coal with chlorobenzene (115°C, 1 week) resulted in about half of the formerly soluble extract becoming pyridine-insoluble. The physical interactions responsible for the solvent-induced conformational changes of coal macromolecules are relatively strong, because some of these interactions cannot be overcome by solvation with pyridine.

In this paper, the solvent-induced associations of several high-volatile bituminous coals were investigated in several solvents for various times. The scope and magnitude of the phenomenon in bituminous coals was investigated in several solvents for various times. The scope and magnitude of the phenomenon in bituminous coals was explored, though not exhaustively. Additional structural information on the changes occurring in these samples was obtained using FT-IR and X-ray diffraction.

EXPERIMENTAL SECTION

ACS reagents and HPLC grade solvents were used. Tetrahydrofuran (THF) was distilled before use, and the other solvents were used without further purification. The coal samples were obtained from Exxon Research and Engineering Co. and the Pennsylvania State University Coal Bank. Their elemental

analyses were given in the previous paper.[2] Coal samples were ground and sifted under a nitrogen atmosphere. Minus 60-mesh size coal particles were used in the experiments.

Samples (two-gram) were extracted with 200 mL of pyridine for 24 hours in a Soxhlet apparatus under nitrogen atmosphere. The coal extracts were dried to constant weight in a vacuum oven at 50°C after evaporation of the pyridine.

Approximately 5 grams of each coal sample was placed in 100 mL of solvent in a 250 mL flask or a 300 mL autoclave and magnetically stirred under nitrogen. The mixture was either stirred at room temperature, heated, or mildly refluxed in an oil bath or in an autoclave heater. The cooled mixture was dried using a rotary evaporator, mixed with methanol, and filtered, while being rinsed with methanol several times. The coal was dried to constant weight in the vacuum oven at 50°C.

O-methylation was carried out following the method of Liotta.[3] Two different O-methylated Pittsburgh No. 8 coals were prepared. One was obtained using normal conditions (exhaustive alkylation), and the other was partially alkylated by using a limited amount of alkylation reagents. For the latter reaction, 5 grams of coal samples was placed in 100 mL of THF, and 1.5 cm^3 of 1M tetrabutylammonium hydroxide in methanol and 0.2 cm^3 of iodomethane were used in the reactions.

Infrared spectra were obtained on an IBM 97/IR Series Fourier Transform Photoacoustic Infrared Spectrometer. Spectra were recorded from 256 scans at 8 cm^{-1} resolution against a reference of carbon black. Samples for infrared spectra were further evacuated for 12 hours at 100°C.

X-ray diffraction studies were carried out at ambient temperatures on a Phillips APD 3600 Automated Powder Diffractometer (Phillips Electronics Instruments, Inc., Mahwah, NJ) using CuK radiation (1.5418 A) at 45 kV, 40 ma. The diffractometer was equipped with a graphite monochrometer, theta-compensating slit, scintillation counter, and pulse-height selector. The X-ray data were collected, stored, and displayed using the APD 3600 data system.

RESULTS

Pittsburgh No. 8 coal was immersed or mildly refluxed in the following hot solvents for times as long as 28 days: chlorobenzene, toluene, toluene/ethanol (95/5 vol %), and H_2O. O-methylated Pittsburgh No. 8 coals were similarly treated in toluene for one week. These solvent-treated coals were dried and Soxhlet extracted with pyridine. The pyridine extraction yields are plotted in Figure 1. Figure 2 shows the changes in pyridine extractability (Soxhlet) with time for various high-volatile bituminous coals heated at 115°C in chlorobenzene. The solvent treatment resulted in decreasing amounts of pyridine extracts for all coals studied. Table I shows the change in pyridine Soxhlet extractability for Illinois No. 6 coal treated in chlorobenzene at different temperatures for 24 hours.

Structural differences between the original and the solvent-treated coals were investigated using photoacoustic Fourier transform infrared spectroscopy.

Absorptions due to hydrogen bonds in these samples were slightly different. Figure 3 shows overlay spectra (2810-3740 cm^{-1}) of the original, two-day, and four-week chlorobenzene-treated Pittsburgh No. 8 coals. No absorbance change between 3200-3516 cm^{-1} was observed for the untreated coal after soaking in methanol and drying. The four-day, one-week and two-week chlorobenzene-treated coals gave spectra almost identical to that of the two-day treated coal.

Changes in aromatic parallel stacking due to solvent treatment were surveyed using the X-ray diffraction [002] band.[4] The X-ray [002] deffraction peak of the Pittsburgh No. 8 coal is very weak, and no change resulted from chlorobenzene treatment. A pyridine extract from Pittsburgh No. 8 coal was treated with chlorobenzene at 115°C for a week, and the portion rendered insoluble by this treatment was isolated and subjected to X-ray analysis. No [002] band was observed.

DISCUSSION

One of the major secondary interactions in coals is hydrogen bonds.[5,6] Toluene and chlorobenzene cannot break hydrogen bonds in coals at room temperature.[5,7] However, it is possible that weak hydrogen bonds are broken thermally at higher temperatures, because such solvents swell coals more at higher temperatures.[8] The ability of chlorobenzene to disrupt the weak secondary interactions in coals is expected to be slightly greater than that of toluene, because of its greater interaction with coals as revealed by its higher solvent-swelling values. The ability of toluene containing ethanol to disrupt the weak secondary interactions should be greater than pure toluene since ethanol can participate in and break coal-coal hydrogen bonds while toluene cannot. Pyridine can break most, if not all, hydrogen bonds in coals at room temperature and so thoroughly disrupts these interactions.[5,7]

The relative rates of decrease in pyridine Soxhlet extraction yield of Pittsburgh No. 8 coal after solvent treatment (Figure 1) are consistent with the ability of the solvents to disrupt hydrogen bonds. The decrease was most rapid when the treating solvent was pyridine, slowest with toluene, and slightly faster with the toluene/ethanol mixed solvent than with pure toluene. The effect of chlorobenzene treatment was faster and larger than that of toluene over the 30-day period of the experiments. Hydroxyl groups can be capped by O-methylation, eliminating hydrogen bonds.[3] This treatment enhanced the rate of decrease of the pyridine Soxhlet extractability of toluene-treated coals.

The effect of solvent treatment on the hydrogen bonds present in this coal were studied by FT-IR using the band assignments recently reported by Painter *et al.*[6] There are four general types of hydrogen-bonded structures involving hydroxyl groups in coal. These are found between 3200 and 3516 cm^{-1}. In this study, the absorbance between 3200 and 3516 cm^{-1} was examined. The intensity of the aliphatic C-H stretching band at 2930 cm^{-1} was used as the reference in comparing the spectra. Weak hydrogen bonds were reduced after the solvent-induced conformational changes (Figure 3) as revealed by a decrease in the intensity of the IR peaks. Similar absorbance changes in hydrogen bonds have been observed for other coals used in this study. This loss is ascribed to a reduction in hydrogen bonding as a result of conformational changes.

It is proposed that solvent-induced conformational changes occur and that they require breaking secondary interactions. Direct structural evidence for hydrogen bond disruption has been obtained. Evidence for participation of other non-covalent interactions is indirect.

Pittsburgh No. 8 coal heated in boiling pyridine gave almost the same pyridine extraction yield as that of the starting coal if the pyridine was not removed from the treated coal.[2] Strong secondary interactions seem not to be produced in the pyridine-swollen state, but are formed during the pyridine-removal step. Probably, pyridine solvates the sites which can generate the strong secondary bonds so they form as pyridine is removed.[1]

Anisotropic solvent swelling of coals has been studied using thin sections.[7,8] Coals swell more perpendicular to the bedding plane than parallel to it. After swelling with pyridine and removing it with a nitrogen flow, the coal shrank parallel to the bedding plane and expanded perpendicular to it. Similarly, the coal initially shrinks parallel to the bedding plane and expands perpendicular to it when thin sections are treated with hot chlorobenzene or toluene and then dried with nitrogen.[10]

Optical anisotrophy in coals is well known.[11] Birefringence in coal thin sections and swollen thin sections was observed by Brenner.[9] The loss of optical anisotrophy in solvents at room temperature coincided with the solvent's ability to break secondary interactions.[9,12] The Birefringence of high-volatile bituminous coals apparently stems from a low degree of molecular orientation.[12] When macromolecules are in the glassy state, all large molecular chain motions are restricted, but segmental motion is not necessarily restricted.[13] The presence of a solvent in the coal macromolecules lowers the glass transition temperature.[14] Coal macromolecules may not be completely in the glassy state in cold pyridine, hot chlorobenzene or toluene, and some movement of coal can occur. The optical anisotropy of Pittsburgh No. 8 coal diminished after soaking in hot chlorobenzene.[2] The observed loss of optical anisotropy of Pittsburgh No. 8 coal after exposure to hot chlorobenzene provides additional evidence for conformational rearrangements in the swollen coal.

Pyridine breaks most or all of the hydrogen bonds in coals. Therefore, coal-coal hydrogen bonding will give no or a small effect on pyridine extractability. Since the pyridine extractability of the solvent-trested coal is smaller than that of the starting coal, it is likely that strong secondary interactions which are not hydrogen bonds are produced during the solvent-induced conformational change. An X-ray study of the effects of solvent treatment on the [002] band reveal no changes. The enhanced association does not include increased amounts of parallel face-to-face aromatic stacking. These imply that unknown complexes are involved in the new interactions.

A number of lines of evidence point to the solvent-induced association of coal molecules to a lower free energy state. Mined coals are in a metastable, strained state.[7] The existence of coals in a non-equilibrium state was shwon by swelling[7] and vapor uptake hysteresis.[15,16] These observations are presumably concerned with the initial movement of coal macromolecules during relaxation of the strained state as the coal is swollen by solvents. In high-volatile bituminous coals, physical interactions which cannot be broken by boiling pyridine are formed during pyridine removal, but are hardly formed in

the coal while it is fully pyridine swollen. The pyridine extract can aggregate during hot chlorobenzene treatment. These results demonstrate that the solvent-induced conformational change of coal macromolecules occurs with the coal achieving a lower free-energy state after relaxation. Secondary interactions originally present in the coal are broken and other secondary interactions are generated by the solvent-treatment. One view of this is schematically shown in Figure 4. The rates of disruption and formation of these secondary interactions will be dependent upon original coal properties, the interaction between the coal and the solvents used, and system conditions.

ACKNOWLEDGMENTS

We thank G. D. Cody, Jr. and M. Siskin for helpful discussions. The effort of J. C. Scanlon for making X-ray measurements is gratefully acknowledged.

REFERENCES

1. Jameel, H., Waldman, J., and Regenfeld, L., J. Appl. Polym. Sci., 1981, 26, 1975-1811, and references cited in the paper.

2. Nishioka, M. and Larsen, J. W., Energy & Fuels, submitted.

3. Liotta, R., Fuel, 1979, 58, 724-728.

4. Hirsh, P. B., Proc. Royal Soc. (London), 1954, A226, 143-169.

5. Larsen, J. W. and Baskar, A. J., Energy & Fuels, 1987, 1, 230-232.

6. Painter, P. C., Sobkowiak, M., and Youtcheff, J., Fuel, 1987, 66, 973-978.

7. Cody, G. D., Jr., Larsen, J. W., and Siskin, M., Energy & Fuels, 1988, 2, 340-344.

8. Sanada, Y. and Honda, H., Fuel, 1966, 45, 451-456.

9. Brenner, D., Fuel, 1985, 64, 167-456.

10. Jeffreys, H. E. and Cody, G. D., Jr., unpublished data.

11. van Krevelen, D. W., Coal; Elsevier: New York, 1961, Chapter 17.

12. Cody, G. D., Jr., Larsen, J. W., and Siskin, M., unpublished data.

13. Barr-Howell, B. D., Howell, J. M., and Peppas, N. A., Energy & Fuels, 1987, 1, 181-1186.

14. Lucht, L. M., Larson, J. M., and Peppas, N. A., Energy & Fuels, 1987, 1, 56-58.

15. Ritger, P. L. and Peppas, N. A., Fuel, 1987, 66, 1379-1388, and the preceding series of papers.

16. Hsieh, S. T. and Duda, J. L., Fuel, 1987, 66, 170-178.

TABLE I. PYRIDINE SOXHLET EXTRACTION YIELDS (WT %) OF ILLINOIS NO. 6 COAL AFTER SOAKING IN CHLOROBENZENE AT DIFFERENT TEMPERATURES FOR 24 HOURS

Temperature (°C)	Extraction Yield (wt %)
23	27
115	19
200	16
300	24 + tar (20)*

*Tar was recovered during methanol rinsing. The yield is wt % of the coal.

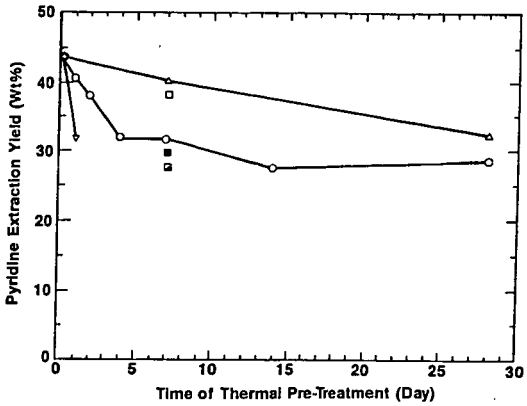

Figure 1. Change of pyridine extractability (Soxhlet) of Pittsburgh No. 8 coal immersed in solvents and dried, (▽) room temperature pyridine, (○) 115°C chlorobenzene, (△) 100°C toluene, (□) 107°C toluene/ethanol (95/5 vol %) and 100°C toluene for completely (◪) and partly (■) O-methylated coal.

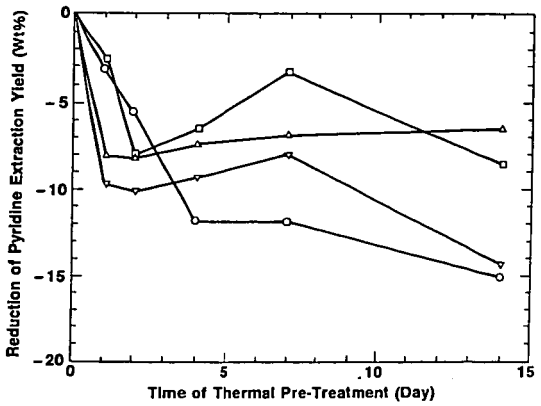

Figure 2. Difference of pyridine extraction (Soxhlet) yields between chlorobenzene-treated coals and starting coals for various ranks of high volatile bituminous coals. Key: (△) Wandoan, (▽) Illinois No. 6, (○) Pittsburgh No. 8, and (□) PSOC-1336.

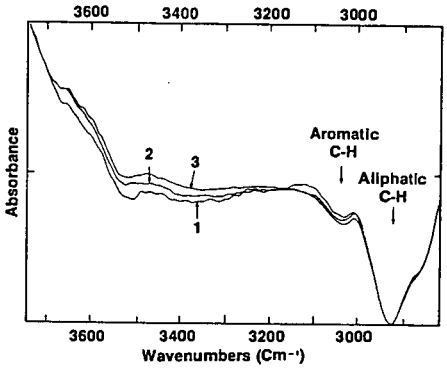

Figure 3. Overlay photoacoustic infrared Fourier transform spectra of (1) starting, (2) 2-day chlorobenzene-treated, and (3) 4-week chlorobenzene-treated Pittsburgh No. 8 coals.

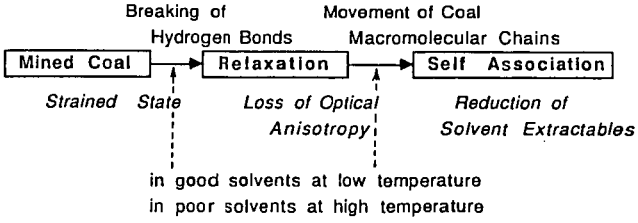

Figure 4. Schematic diagram for solvent-induced conformational changes of macromolecules in high-volatile bituminous coals.

RANK DEPENDENCE OF ASSOCIATIVE EQUILIBRIA OF COAL MOLECULES IN SOLVENTS

M. Nishioka*

Exxon Research and Engineering Company, Clinton Township, Annandale, NJ 08801
*Present address: BCR National Laboratory
500 William Pitt Way
Pittsburgh, PA 15238

Keywords: associative equilibrium; extraction rate; intermolecular interaction

Introduction

Solvent-induced association (a conformational change) of several high-volatile bituminous coals was observed in hot toluene, hot chlorobenzene, and cold pyridine.[1,2] It was proposed that the solvent-induced conformational change is due to two concerted processes: breaking secondary interactions originally present and forming new secondary interactions in a lower free energy state. This implies that associative equilibria between coal moleculea will exist in solvents. In this paper, the rank dependence of the associative equilibria and intermolecular interactions is investigated.

Experimental Section

All ACS and HPLC grade chemicals were uaed without further purification. The coal samples were obtained from Exxon Research and Engineering Co., and the Pennsylvania State University Coal Bank. Their elemental analyses were reported in the previous paper.[1] Coal samples were ground and sifted under a nitrogen atmosphere. Minus 60 mesh particles were used in the experiments.

Approximately 2 to 5 g of each coal sample were placed in a 250 mL flask in 100 mL of pyridine and either stirred at room temperature or refluxed (115°C) under dry N_2 in an oil bath. One series of cooled samples was dried using a rotary evaporator, mixed with methanol, filtered, and rinsed with methanol several times. The coal was then dried to constant weight in the vacuum oven at 50°C. Another series of samples was filtered and the wet residues promptly Soxhlet-extracted.

The Diels-Alder reaction has been reported.[1] Maleic anhydride adducts formed using phenol solvent were precipitated in methanol, filtered, and then Soxhlet-extracted with methanol for 24 hrs. in order to eliminate by-products formed by reactions of maleic anhydride and phenol before removal of non-reacted maleic anhydride by Soxhlet extraction with H_2O. The by-products were easily extracted with methanol, which was verified by using a blank experiment without coal. The major molecular masses of by-products from coal, and those obtained using the blank experiment, were the same: 270, 322, and 362. Infrared spectra and X-ray diffraction studies were carried out as previously described.[2]

Results and Discussion

Pyridine extractability rectilinearly increases up to ca. 87 wt% C coal (named here as A-region), then decreases sharply with rank (87-90 wt% C: B-region).[3] At still higher rank (>90 wt% C: C-region), only a few percent is extracted.

Pyridine extraction rate was compared for each region coal, and selected results are shown in Figure 1. A-region coal was promptly extracted within one or two days, while more than seven days were required for the extraction of B-region coal to be completed under the same conditions. C-region coal yields extract slowly, and the ultimate extractability is very small.

Pyridine extractability of the A-region coal was greater at the boiling point (115°C) than at room temperature,[1] but extraction yields of the A-region coal at 115°C and at 180°C were similar.[3,4] However, pyridine extractability of the B-region coal at 180°C is much greater than that at 115°C.[4]

Since it was first reported by Harger and Illingworth[5,6] that coals preheated at 200 to 400°C in an inert atmosphere give much higher yields of extract than unheated coals, the preheating effect has been investigated by several groups, and recently reviewed.[7] Solvent extractability increases with preheating temperature, reaches a maximum, and then declines.[3,8] However, the pyridine and chloroform extraction yields of the A-region coal were only slightly increased by preheating to 300°C, while the B-region coal was much more extractable after preheating at temperatures below 300°C.[3] The dependence of the preheating effect on coal rank was recently studied by preheating at 250°C for 24 hrs.[7] The effect was highly rank-dependent. Tetrahydrofuran extraction yields of higher-rank coals increased after preheating, while those of lower-rank coals decreased. These data show that A and B-region coals differ in their response to heating.

Heating the A-region coal at 115°C in chlorobenzene for seven days caused a decrease in pyridine extractability.[1] The same solvent treatment was given to a B-region coal, PSOC-1300 (89.9% C), in this study, but the pyridine extraction yield (24 hrs) of this treated coal increased to 18 wt% from 7 wt%. Figure 2 shows the change in pyridine extraction yields caused by soaking coal in pyridine at the boiling point for seven days for various A- and B-region coals. The pyridine extractabilities of coals dried after soaking in pyridine at room temperature for one day are also included in this figure. Pyridine extractabilities of the B-region coals significantly increased after soaking in pyridine at the boiling point for seven days contrary to those of the A-region coals. Pyridine extractabilities of the coals dried after soaking in pyridine at room temperature decreased for the A-region coals, but slightly increased for the B-region coals. These data show that the pyridine extractabilities of the A- snd B-region coals after trestment with pyridine and chlorobenzene result in opposites.

Aggregations are seen in phsse separation phenomena such as precipitation, gelation, and crystallization. Dormans and van Krevelen[3] studied precipitation from a pyridine soluble Soxhlet-extract at room temperature. Pyridine extracts from the A-region coal did not form precipitates after 240 hrs, while those from the B- and C-region coals yielded precipitates amounting to between 10 and 30 wt% of the extract. In the present study, the pyridine extract of an A-region coal, PSOC-1336 (84.1% C), was concentrated, filtered, and held at room temperature under nitrogen. The extract with concentration of 13.4 mg/cm^3 showed no precipitate after 14 days, while the extract with concentration of 55.3 mg/cm^3 precipitated 0.5 wt% of the extract after 5 days. The precipitate could be easily seen at the bottom of a flask. Concentrated pyridine extracts of other A-region coals, Illinois No. 6 (79.9% C) and Pittsburgh No. 8 (83.8% C), also formed precipitates if their concentration were more than 100 mg/cm^3. van Krevelen's work suggests that high temperature (Soxhlet extraction) extracts of the B- and

C-region coals easily associate at low (room) temperature. The present work shows that high temperature extracts of the A-region coal do not associate at low temperature when diluted, but concentrated extracts do tend to associate.

All of the above data are summarized in Table I. These data can be understood as the result of change of the equilibrium state of coal molecules in solvents. The associative equilibria seem to be highly rank-dependent.

From the above results, it is suggested that extractability may be controlled by the equilibrium state between a solvent and coal. This is amendable to a quantitative treatment.

Assume that a complex A·B equilibrates with each component A and B in a solvent.

$$A \cdot B \underset{\upsilon_{-1}}{\overset{\upsilon_1}{\rightleftharpoons}} A + B \qquad (1)$$

If the complex A·B is not extractable, components A and B are extractable with a solvent, and the rate υ_1 is much greater than the rate υ_{-1}, the extraction rate of each component is given as

$$\frac{dE}{dt} = k_1 (E_\infty - E) \quad (\upsilon_1 \gg \upsilon_{-1}) \qquad (2)$$

where E and E_∞ are concentrations (or extraction yields) given as follows

$$A \cdot B \underset{\upsilon_{-1}}{\overset{\upsilon_1}{\rightleftharpoons}} A + B$$

E_∞	0	0	at initial time
$E_\infty - E$	E	E	at time t

(3)

Therefore, an extraction yield at given time is

$$E = E_\infty (1 - e^{-k_1 t}) \qquad (4)$$

where E_∞ and k_1 are regarded as an ultimate extraction yield and an extraction rate constant, respectively. A similar equation was derived by Oele et al.[9] for the extractive disintegration of bituminous coals at high temperatures (150 to 350°C) in an anthracene oil and β-naphthol. They assumed a zero order process for a forward disintegration at the initial step and additionally a first order process for a backward integration when extraction proceeds. Equation (4) is a first order rate. The rate constant k_1 is determined by extraction yields E_1 and E_2 at two different times t_1 and t_2,

$$k_1 = \frac{\ln \dfrac{E_\infty - E_1}{E_\infty - E_2}}{t_2 - t_1} \qquad (5)$$

or by measurement of increment of extraction by half (τ)

$$k_1 = \frac{\ln 2}{\tau} \qquad (6)$$

Calculated values using Equstion (4) are shown in Figure 1 as well as experimental results for extractability versus extraction time. Extraction rate can be approximated by using Equation (4). Therefore, the dissociation of the coal-coal interactions can be thought of the major rate determining step in an extraction process. The slow rate of Soxhlet extraction is attributed to the slow dissociation (small k_1) of aggregated clusters. The stronger the physical interactions are, the smaller will be the rate constants k_1. The poorer solvents are for the extract, the smaller rate constants k_1 will be. In the case of very small rate constants, high temperature could be required to overcome the activation energy to allow dissociation of components.

Since high temperatures and good solvents are apparently needed to dissociate the aggregated clusters in the B- and C-region coals (Table I), chemical reactivity for these coals should be promoted at the higher temperatures and good solvents which lead to dissociation, while that for the A-region coal should not be enhanced even at the same condition. The Diels-Alder reaction has been utilized to weaken the interaction between polynuclear aromatics in coals.[1,10] In this work, maleic anhydride was reacted with each region coal in phenol at 115 and 180°C, and the product was pyridine-extracted.[1,10] Increased extractability at 180°C was observed for all coals, but the increases for B- and C-region coals were much greater than that of the A-region coal. A-region extractability increased by 1/3, while the B- and C-region extractabilities increased by factors of 7 and 15, reapectively. The enhancements of pyridine extractabilities for the B- and C-regions coals were particularly remarkable aa compared with the results obtained by using a chlorobenzene solvent (115°C).

The IR absorptions between 1700 and 1750 cm^{-1} assigned to carbonyl vibrations in maleic anhydride adducts are shown in Figure 3 for a starting C-region coal, PSOC-688 (92.0%C), and its maleic anhydride adducts reacted under various conditions. These results demonstrate more maleic anhydride incorporation at higher temperature, although the Diels-Alder reaction is reversible and low temperatures are preferred for adduct formation. Pyridine is a good solvent but cannot be used for this reaction, because this solvent catalyzes the polymerization of maleic anhydride.[10] These reaults suggest that the intermolecular interaction dissociable at high temperature play an important structural role in the B- and C-region coals and is responsible for the differencea in behaviors shown in Table I for each region coal.

Figure 4 shows the change in the X-ray diffraction [002] band caused by reaction with maleic anhydride. This band is due to the parallel stacking of aromatic systems.[11] The magnitude and half-width of the maleic anhydride adduct of the PSOC-668 reacted in chlorobenzene at 115°C was identical with that of starting coal. The parallel stacking was obviously reduced after the maleic anhydride reaction in phenol at 180°C. This result implies that the incorporation of maleic anhydride decreases the number of face-to-face aromatic stacks, and that the face-to-face interaction may be responsible, in part, for the association in high-rank coal.

References

1. Nishioka, M.; Larsen, J. W. Energy & Fuels in press.
2. Nishioka, M.; Larsen, J. W. Prepr. Am. Chem. Soc. Div. Fuel Chem. 1990.
3. Dormans, H. N. M.; van Krevelen, D. W. Fuel 1960, 39, 273-292.
4. Illingworth, S. R. Fuel 1922, 24, 213-219.
5. Harger, J. J. Soc. Chem. Ind. 1914, 33, 389-392.
6. Illingworth, S. R. J. Soc. Chem. Ind. 1920, 39, 111-118.
7. Nishioka, M.; Larsen, J. W. Energy & Fuels 1988, 2, 351-355.
8. Wynne-Jones, W. F. K.; Blayden, H. E.; Shaw, F. Brennstaff-Chem. 1952, 33, 201-206.
9. Oele, A. P.; Waterman, H. I.; Goedkoop, M. L.; van Krevelen, D. W. Fuel 1951, 30, 169-178.
10. Quinga, E. M. Y.; Larsen, J. W. Energy & Fuels 1987, 1, 300-304.
11. Hirsh, P. B. Proc. Royal Soc. (London) 1954, A226, 143-169.

Table I. Differences in Behaviors in Extraction, Soaking, and Sitting Extract for Each Region Coal.

%C (daf)	A <87	B 87-90	C[a] >90
1.Pyridine extraction rate	fast	slow	
2.Temperature (115°C & 180°C) effect on pyridine extraction	small	large	
3.Preheating (200-400°C) effect on pyridine extraction	small	large	
4.Immersion in pyridine and removal of the solvent before pyridine extraction	decrease in extractability	increase in extractability	
5.Soaking in hot toluene or chlorobenzene before pyridine extraction	decrease in extractability	increase in extractability	
6.Precipitation of Soxhlet pyridine extracts at room temperature	precipitation[b]	no precipitation	

[a]Differences are very samll because of very small ultimate extractability.
[b]Precipitation occurs only at high concentration.

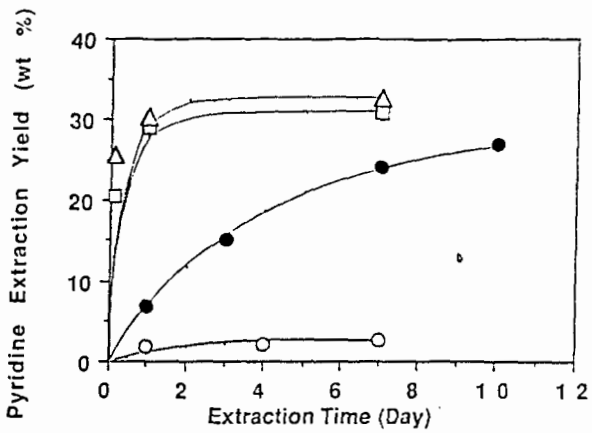

Figure 1. Pyridine extractability versus extraction time. Key: (□) Illinois No. 6 (79.9%C) (E_∞ = 31.2, k_1 = 2.3), (Δ) PSOC-1336 (84.1%C) (E_∞ = 32.8, k_1 = 2.3), (●) PSOC-1300 (89.9%C) (E_∞ = 29.0, k_1 = 0.26), and (○) PSOC-688 (92.0%C) (E_∞ = 2.7, k_1 = 0.43).

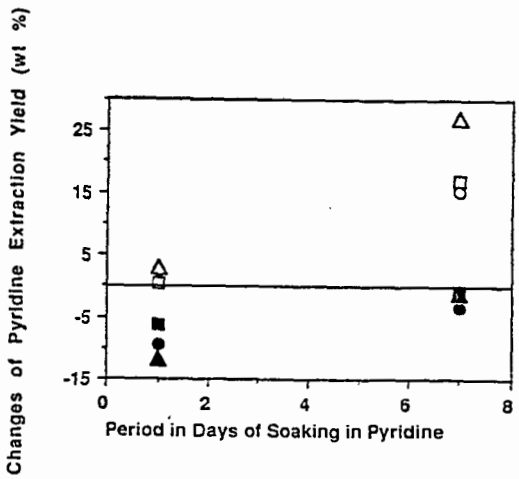

Figure 2. Changes of pyridine extractabilities of the A and B-region coals immersed in pyridine at the boiling point for seven days and their dried coals after immersing in pyridine at room temperature for one day. Key: (Δ) PSOC-991 (89.4%C), (□) PSOC-1300 (89.9%C), (○) PSOC-721 (88.5%C), (■) Illinois No. 6 (79.9%C), (◒) PSOC-1336 (84.1%C), and (▲) Pittsburgh No. 8 (83.8%C).

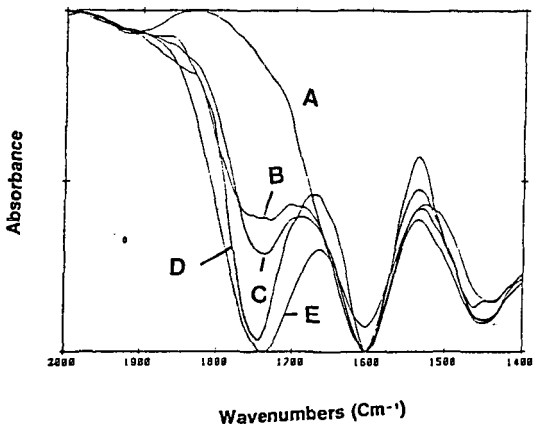

Figure 3. Overlay photoacoustic infrared Fourier transform spectra assigned to the carbonyl groups of (A) starting coal and maleic anhydride adducts of PSOC-688 reacted under selected solvents and temperature. Conditions of Diels-Alder reaction: (B) in chlorobenzene at 115°C, (C) in phenol at 115°C, (D) in phenol at 180°C, and (E) in 1,2-dichlorobenzene at 180°C.

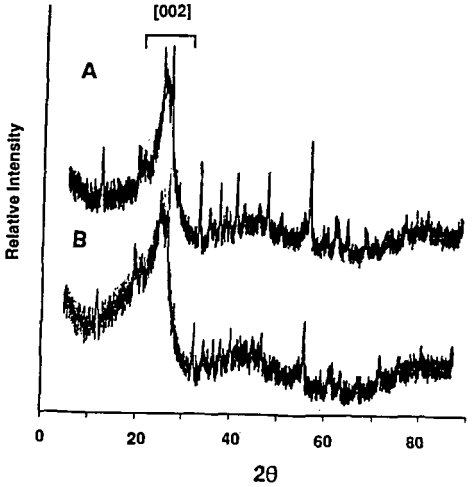

Figure 4. X-ray diffraction patterns of [002] band of maleic anhydride adducts of PSOC-688 reacted (A) in chlorobenzene at 115°C and (B) in phenol at 180°C.

COAL ANALYSIS BY TG-FTIR

P.R. Solomon, M.A. Serio, R.M. Carangelo, and R. Bassilakis
Advanced Fuel Research, Inc.
87 Church Street, East Hartford, CT 06108 USA

KEYWORDS: Coal, Analysis, Pyrolysis, Combustion, TGA, FTIR

INTRODUCTION

Thermogravimetric analysis has been employed in coal science to perform a number of characterizations including: proximate analysis (1), kinetics of weight loss (2,3) char reactivity (4-9) and gas adsorption measurements (10). A complimentary technique, evolved product analysis, has been employed to study pyrolysis product distributions and kinetics (11-18) functional group compositions (14,19-21), and temperature programmed desorption (22-24).

We have developed a TG-FTIR instrument which combines thermogravimetric analysis (TGA) with evolved product analysis by Fourier Transform Infrared (FT-IR) spectroscopy. FT-IR analysis of evolved products has advantages over mass spectroscopy in allowing analysis of very heavy products, and over gas chromatography in speed. To analyze coal, a sequence of drying, pyrolysis and combustion is employed to obtain: proximate analysis, volatiles composition, volatiles kinetics, and relative char reactivity. The application of TG-FTIR to coal and petroleum source rock has recently been described (25,26). The purpose of this paper is to describe the most recent improvements in the apparatus.

EXPERIMENTAL

Apparatus - A schematic of the instrument is presented in Fig. 1. Its components are as follows: a DuPont™ 951 TGA; a hardware interface (including a furnace power supply); an Infrared Analysis 16 pass gas cell with transfer optics; a MICHELSON 110 FT-IR; (Resolution: 4 cm^{-1}, Detector: MCT). A helium sweep gas is employed to bring evolved products from the TGA directly into the gas cell. This instrument package is now available commercially as the TG/plus from Bomem, Inc.

The most difficult volatiles to analyze are the heavy decomposition products which condense at room temperature, such as tars from coal. In the TG/plus, the high conductivity helium sweep gas and the rapid cooling causes these products to form an aerosol which is fine enough to follow the gas through the analysis cell. The cell is connected without restrictions to the sample area. The aerosol is also fine enough that there is little scattering of the infrared beam and it is thus attenuated as though the tar was in the gas phase.

Procedure - As an example of the analysis procedure, the pyrolysis and oxidation of a lignite is described. More detail can be found in Refs. 25 and 26. Figure 2a illustrates the weight loss from this sample and the temperature history. A 35 mg sample of Indian Head Zap lignite, loaded in the sample basket of the DuPont™ 951, is taken on a 30°C/min temperature excursion in the helium sweep gas, first to 150°C where it is held for 4 minutes to dry, then to 900°C for pyrolysis. The temperature is held at 900°C for 3 minutes. After cooling to 250°C, a small flow of O_2 is added to the furnace at the 57 minute mark and the temperature is ramped at 30°C/min to 700°C (or higher) for oxidation.

During this excursion, infrared spectra are obtained once every thirty seconds. As discussed previously (25,26), the spectra show absorption bands for CO, CO_2, CH_4, H_2O, SO_2, COS, C_2H_4, olefins, HCl, and NH_3. The spectra above 400°C also show aliphatic, aromatic, hydroxyl, carbonyl and ether bands from tar. The evolution of gases derived from the IR absorbance spectra are obtained by a quantitative analysis program which employs a database of integration regions and calibration spectra for different compounds. The routine decides which regions of each calibration spectrum to use for best quantitation with the least interferences. The routine is fast so the product analysis is displayed during the actual experiment.

Figure 2b illustrates the integral of the evolution curves to obtain cumulative evolved product amounts. Because the data are quantitative, the sum of these curves match the weight loss as

determined by the TGA balance. Discrepancies occur in this match because of missing components such as H_2 which cannot be seen by IR and H_2S which is very difficult to see. Secondly, when O_2 is introduced, the balance shows a net gain in weight due to O_2 chemisorption.

Calibration - To calibrate the instrument, known flows for calibration gases were mixed with a fixed flow of sweep gas and passed through the gas cell. Reference spectra were collected and the flow rate was varied to provide spectra over the range of expected concentrations. The quantitative analysis program employs the spectrum which most closely matches the experimental amplitudes since Beer's law (absorption is proportional to concentration) is not valid for many light gases.

Calibration spectra cannot be employed in the same way for tar since the absorptivity of any band varies with the tar compositions. Instead, the evolution of tar is derived by using the spectrum of a Pittsburgh Seam coal tar as a calibration standard. This coal tar has all the functional group features (but at different intensities) characteristic of coal tars. Its use as a reference spectrum determines the important tar functional group regions whose amplitudes provide a qualitative tar evolution profile for other coals. The tar's evolution determined in this manner typically exhibits a sharply peaked function with increasing temperature as shown in Fig. 3a.

To quantitatively determine the tar loss, it is assumed that the qualitative tar evolution profile is proportional to the rate of loss of tar. This will be true when the functional group compositions of the tar does not change with temperature, a condition which holds over most of the tar evolution profile as indicated by examining the infrared spectra at various times during its evolution. To determine the constant of proportionality for each sample, the tar loss profile is compared to the rate of weight loss from the balance minus the rate of weight loss for all the gases. This quantity is presented in Fig. 3b. The proportionality constant is picked by performing a least squares fit between the two curves over the region of tar evolution, except for parts where other gases are evolving quickly and might introduce error. The proportionality constant varies systematically from 0.86 times the absorptivity for Pittsburgh Seam coal for Zap lignite to 1.56 times Pittsburgh Seam coal for Pocahontas in agreement with the lower absorptivity of the aromatic components in the higher rank coals.

Routine calibration of the instrument is performed on a monthly basis using calcium oxalate. A typical evolution profile is presented in Fig. 4. The calcium oxalate has three weight loss regions yielding H_2O, CO_2, and CO. The agreement between the sum of gases and weight loss shows that the calibration and the sweep gas flow rate are accurate. The positions of peaks compared to a known reference validates the accuracy of the thermocouple temperature measurement. To check for possible leaks in the system and the absence of oxygen in the helium sweep gas, graphite is run periodically. If there are no leaks and the helium is of high purity, no appreciable weight loss or CO_2 evolution is experienced during the pyrolysis cycle.

Samples - The coals analyzed were Argonne premium coal samples. The characterization of these samples has appeared elsewhere (27). In addition, demineralized coals were produced using the technique of Bishop and Ward (28). This technique removes both discrete minerals as well as organically bound alkali or alkaline earth metals. Oxidized samples were prepared in an oven at 100°C or at room temperature in air.

RESULTS AND DISCUSSION

Analysis of Argonne Coals - Analyses were performed for eight Argonne coals at both 3°C/min and 30°C/min. Results for three coals for the pyrolysis cycle (30°C/min) are presented in Figs. 5 to 7. Figures 5a to 7a presents the weight losses and temperature profiles. Also presented (dashed line) is the sum of species (tar, CH_4, H_2O, CO_2, CO, SO_2, and NH_3). In general, the sum of species is within a few percent of the weight loss.

The evolution of tar and aliphatic gases is presented in Figs. 5c to 7c. These tar evolution profiles typically consist of a low temperature peak or shoulder followed by a narrow larger peak. The low temperature peak is believed to be due to the evaporation of unattached "guest" molecules (the molecular phase). The higher temperature peak is due to the release of coal fragments by bond breaking, evaporation and transport (29). In Fig. 5c, these peaks are labeled 1 (molecular phase) and 2 (pyrolysis).

Methane evolution is presented in Figs. 5e to 7e. Methane evolution occurs in two closely spaced peaks. The low temperature peak is initiated coincident with the initiation of tar evolution, but reaches a maximum at a slightly higher temperature than the maximum tar peak. The temperature for the maximum evolution varies little with rank but the temperature of initiation of methane evolution decreases with decreasing rank. The second peak appears as a shoulder on the high temperature side of the first peak. In Fig. 5e, these peaks are labeled **1** (methane loose) and **2** (methane tight).

Water evolution is presented in Figs. 5b to 7b. Water appears first at low temperature when the coal's moisture is evolved. For all coals, a prominent water peak also occurs simultaneously with the tar peak. This suggests that the chemistry responsible for this peak is either related to the free radicals produced, or the increase in fluidity (and hence mobility for bi-molecular interactions), both of which occur during tar formation. Burnham et al. (17) report the coincidence of the tar peak with the low temperature peaks for CO_2 and H_2S, which supports the idea that tar evolution is associated with the decomposition of heteroatom functionalities. There is also a higher temperature H_2O peak and a lower temperature peak or shoulder accompanying CO_2 evolution in low rank coals. In Fig. 7b, these peaks are labeled **1** (moisture), **2** (water extra loose, associated with early CO_2 evolution), **3** (water loose, associated with tar evolution), and **4** (water tight).

Figures 5d to 7d present the results for CO_2. Wyodak (Fig. 7d) which is typical of low rank coals, shows three peaks between 200 and 900°C labeled **2** (extra loose associated with H_2O), **3** (loose associated with tar evolution and H_2O evolution) and **4** (CO_2 tight). There is also a very low temperature peak labeled **1** (occurring only for the lowest rank coals) whose origin is presently unknown. Higher rank coals usually have peaks **3** and **4** but not peak **2** unless they are oxidized. Peak **2** is one of the regions affected most by oxidation. In addition, the evolution of CO_2 is often complicated in high rank coals by the evolution of CO_2 from carbonates such as calcite (Fig. 6d) and siderite.

The evolution of CO is presented in Figs. 5f to 7f. Low rank coals exhibit three peaks labeled **3**, **4**, and **5** as shown in Fig. 7f. Peaks **3** and **4** coincides with the CO_2 peaks **3** and **4**, while peak **5** has no accompanying peaks for H_2O or CO_2. CO peaks also can be seen accompanying the CO_2 calcite peak (see Fig. 6). High rank coals appear to have only the high temperature peak **5**.

Results for other gases are presented in parts g to i of Figs. 5 to 7. The C_2H_2 yield shown in Figs. 5g to 7g occurs in a narrow evolution peak which lags the tar peak but precedes the methane. The ammonia evolution in Fig. 5h to 7h appear to coincide with the start of CO evolution (Figs. 5f to 7f). The SO_2 peak near 28 minutes (Figs. 5i to 7i) appears to coincide with one of the COS peaks (Figs. 5j to 7j).

Sample results for the combustion cycle are presented in Fig. 8. Since oxygen is added, the reported weight loss is for the elements C, H, S, not the oxide. This will make the sum of the elements (C, H, and S) lost less than the total measured weight loss, the difference being the oxygen in the char. The combustion cycle is dominated by the evolution of CO_2, CO, and SO_2. The sum of the C, H, and S in these species is in reasonable agreement with the weight loss.

Analysis of Minerals - The identification of evolution peaks due to minerals was made by performing TG/plus analysis of reference minerals and demineralized coals. An important contributor is calcite. The major reaction is the evolution of CO_2 near 800°C. There are also small amounts of CO and H_2O evolved. The CO_2 peak is almost identical in shape and position to that exhibited by the Illinois No. 6 coal in Fig. 6e. When the Illinois coal was demineralized (dashed line) the 800°C CO_2 peak disappears. The demineralized coal also shows a small increase in the tar yield and little moisture, but no other major changes.

Several high rank coals (Pocahontas, Upper Freeport, and Pittsburgh) showed CO_2 peaks at about 525°C which disappeared with demineralization. The 520°C peak appears to be due to siderite based on the discussion by Raask (30).

Volatile Kinetics - The TG-FTIR analysis can be used to study product evolution kinetics. We have compared in Fig. 19, the temperature for the maximum hydrocarbon evolution rate for the Argonne coals as a function of rank at 0.05 and 0.5°C/sec. Duplicate runs were all within ±4°C. The peak temperatures as well as the shape of the tar peaks are in good agreement with the results of

Burnham et al. obtained using a Rock-Eval analyzer (17) and a Triple-Quadrupole Mass Spectrometer (TQMS). The 50 to 65°C shift in temperatures with heating rate corresponds to activation energies approximately between 45 and 60 Kcal/mole. The variation in the rate of thermal decomposition is in part responsible for the variation of ignition behavior with rank (31).

Functional Group Composition - The TG-FTIR analysis provides information on the coal's functional group composition since it is the functional group composition which gives rise to the variation in gas yields. Figure 9b shows the variation in oxygen containing products with rank. Low rank coals have a high content of oxygen functional groups.

Figure 9c presents the data for tar and CH_4 yields. Methane increases systematically with increasing rank. High volatile bituminous coals have the most tar. Tar yields are related to soot formation in combustion (31) to fluidity (32), and to yields in liquefaction (33) or mild gasification (34). The tar functional group composition can also be obtained from the infrared spectra during tar evolution.

Char Properties - The TG-FTIR analysis provides two measurements related to char reactivity. The first is the weight gain of the char which occurs when oxygen is added early in the combustion cycle (see Fig. 2b). This weight gain is proportional to the concentration of active sites which are accessible to O_2. The second measurement is of the temperature required to produce a specified rate of weight loss during the oxidation cycle. As discussed previously, this critical temperature T_{cr} is related to the reactivity (4-7). The higher the reactivity, the lower T_{cr}.

Figure 9d compares both the oxygen chemisorbed and T_{cr} as functions of the oxygen in the coal. There is a systematic decrease in T_{cr} and an increase in oxygen chemisorbed with increasing oxygen. The interplay of decomposition kinetics and reactivity control the ignition behavior and burnout in combustion or gasification (31).

CONCLUSIONS

A single TG-FTIR analysis provides an extensive coal characterization with regard to the decomposition kinetics, char reactivity, functional group compositions and conversion behavior.

ACKNOWLEDGEMENT

Work was supported by the U.S. Department of Energy, Morgantown Energy Technology Center under Contract No. DE-AC21-86MC23075 and under NSF SBIR Grant No. ISI-8703520.

REFERENCES

1. Ottaway, M., *Fuel*, **61**, 713-716, (1982).
2. Ciuryla, V.T., Weimer, R.F., Bivans, A., and Motika, S.A., *Fuel*, **58**, 748, (1979).
3. van Krevelen, D.W., van Heerden, C., and Huntjens, F.J., *Fuel*, **30**, 253, (1951).
4. Solomon, P.R., Serio, M.A., and Heninger, S.G., *ACS Div. of Fuel Chem. Preprints*, **31**, (3), 200-209, (1986).
5. Best, P.E., Solomon, P.R., Serio, M.A., Suuberg, E.M., Mott, W.R, Jr., and Bassilakis, R., *ACS Div. of Fuel Chem. Preprints*, **32**, (4), 138-146, (1987).
6. Serio, M.A., Solomon, P.R., Bassilakis, R., and Suuberg, E.M., *ACS Div. of Fuel Chem. Preprints*, **34**, (1), 9-21, (1989).
7. Serio, M.A., Solomon, P.R., Bassilakis, R., and Suuberg, E.M., The Effects of Minerals on Coal Reactivity, Int. Conf. on Coal Science, Japan, (10/89).
8. Jenkins, R.G., Nandi, S.P., and Walker, P.L., Jr., *Fuel*, **52**, 288, (1973).
9. Sahu, R., Levendis, Y.A., Flagan, R.C., and Gavalas, G.R., *Fuel*, **67**, 275-283, (1988).
10. Suuberg, E.M., Calo, J.M., and Wojtowicz, W., *ACS Div. of Fuel Chem. Preprints*, **31**, (3), 186-193, (1986).
11. Juntgen, H. and van Heek, K.H., *Fuel Proc. Tech*, **2**, 261, (1979).
12. Winans, R.E., McBeth, R.L., and Neill, P.H., *ACS Div. of Fuel Chem. Preprints*, **33**, (3), 85-90, (1988).
13. Chakravarty, T., Windig, W., Hill, G.R., and Meuzelaar, H.L.C., *Energy & Fuels*, **2**, (4), 400-405, (1988).
14. Solomon, P.R. and Hamblen, D.G., Finding Order in Coal Pyrolysis Kinetics, Topical Report

submitted to U.S. Department of Energy under Contract No. DE-AC21-FE05122, 1983, also *Progress in Energy and Combustion Science*, **9**, 323-361, (1983).
15. Fitzgerald, D. and van Krevelen, D.W., *Fuel*, **38**, 17, (1959).
16. Campbell, J.H., *Fuel*, **57**, 217, (1978).
17. Burnham, A.K., Oh, M.S., Crawford, R.W., and Samoun, A.M., *Energy & Fuels*, **3**, (1), 42-55, (1989).
18. Weimer, R.F. and Ngan, D.Y., *ACS Div. of Fuel Chem. Preprints*, **24**, (3), 129-140, (1979).
19. Attar, A. and Dupuis, F., *ACS Div. of Fuel Chem. Preprints*, **23**, (2), 44-53, (1978).
20. Attar, A. and Hendrickson, G.G., *Coal Structure*, (R.A. Meyers, Ed.), Academic Press, NY, Chapter 5, p. 131, (1982).
21. LaCount, R.B., Anderson, R.R., Friedman, S., and Blaustein, B.D., *Fuel*, **66**, 909-913, (1987).
22. Hall, P.J. and Calo, J.M., *Energy & Fuels*, **3**, (3), 370-376, (1989).
23. Zhang, Z.G., Kyotani, T., and Tomita, A., *Energy & Fuels*, **3**, 566-571, (1989).
24. Kyotani, T., Zhang, Z.G., Hayashi, S. and Tomita, A., *Energy & Fuels*, **2**, 1136, (1988).
25. Carangelo, R.M., Solomon, P.R., and Gerson, D.G., *Fuel*, **66**, 960-967, (1987).
26. Whelan, J.K., Solomon, P.R., Deshpande, G.V., and Carangelo, R.M., *Energy and Fuels*, **2**, 65, (1988).
27. Vorres, K.S., "Users Handbook for the Argonne Premium Coal Sample Program", Supported by US DOE, Contract No. W-31-109-ENG-238; (1989).
28. Bishop, M. and Ward, D.L., *Fuel*, **37**, 191, (1958).
29. Solomon, P.R., Hamblen, D.G., Carangelo, R.M., Serio, M.A., and Deshpande, G.V., *Energy & Fuels*, **2**, 405, (1988).
30. Raask, E., *Mineral Impurities in Coal Combustion; Behavior, Problems, and Remedial Measures*, Hemisphere Publishing Corp., NY, (1985).
31. Solomon, P.R., Chien, P.L., Carangelo, R.M., Best, P.E., and Markham, J.R., *22nd Symposium (Int) on Combustion*, The Combustion Institute, Pittsburgh, PA, 211, (1988).
32. Solomon, P.R., Best, P.E., Yu, Z.Z., and Deshpande, G.V., *ACS Div. of Fuel Chem. Preprints*, 34, (3), 895-906, (1989).
33. Serio, M.A., Solomon, P.R., Kroo, E., Bassilakis, R., Malhotra, R., and McMillen, D., "Fundamental Studies of Retrograde Reactions in Direct Liquefaction", Proceedings of the Direct Liquefaction Contractor's Meeting, (Oct. 2-4, 1989).
34. Khan, M.R., Serio, M.A. Malhotra, R., and Solomon, P.R., *ACS Div. of Fuel Chem. Preprints*, **34**, (4), 1054-1061, (1989).

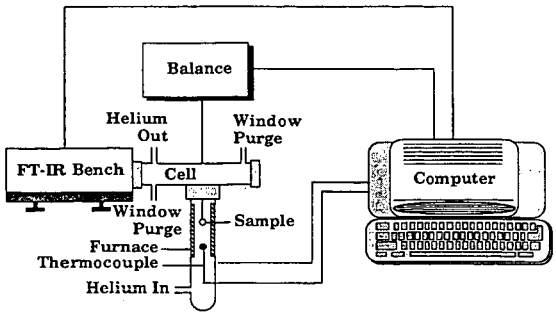

Figure 1. Schematic of TG/plus.

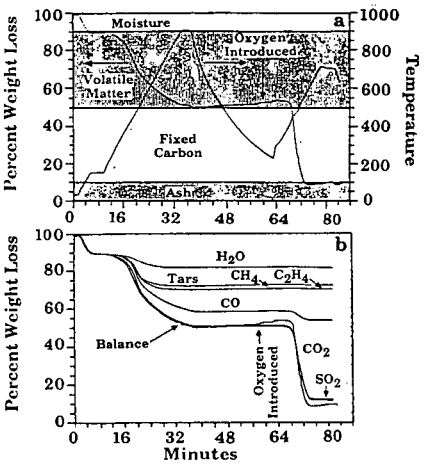

Figure 2. TG-FTIR Analysis of a Lignite.
a) Temperature History and Weight Loss.
b) Species Contributions to Weight Loss.

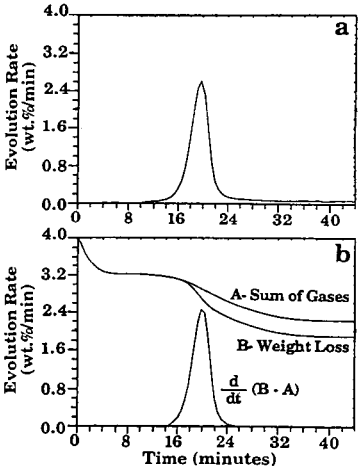

Figure 3. Calibration of Tar Absorptivity.
a) Tar Absorption Profile. b) Weight Loss Minus the Sum of Gases.

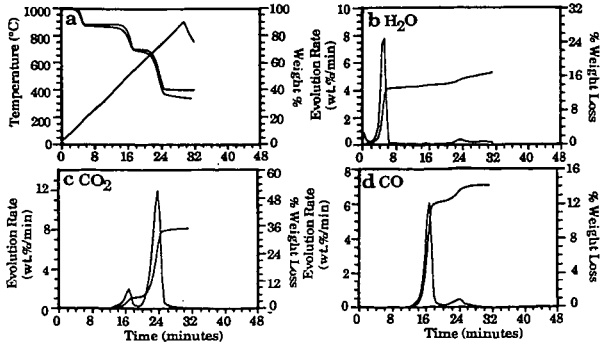

Figure 4. Pyrolysis of Calcium Oxylate. a) Weight Loss (solid), Sum of Evolved Products (dashed), and Temperature Profile. b) H_2O Evolution, c) CO_2 Evolution, and d) CO Evolution.

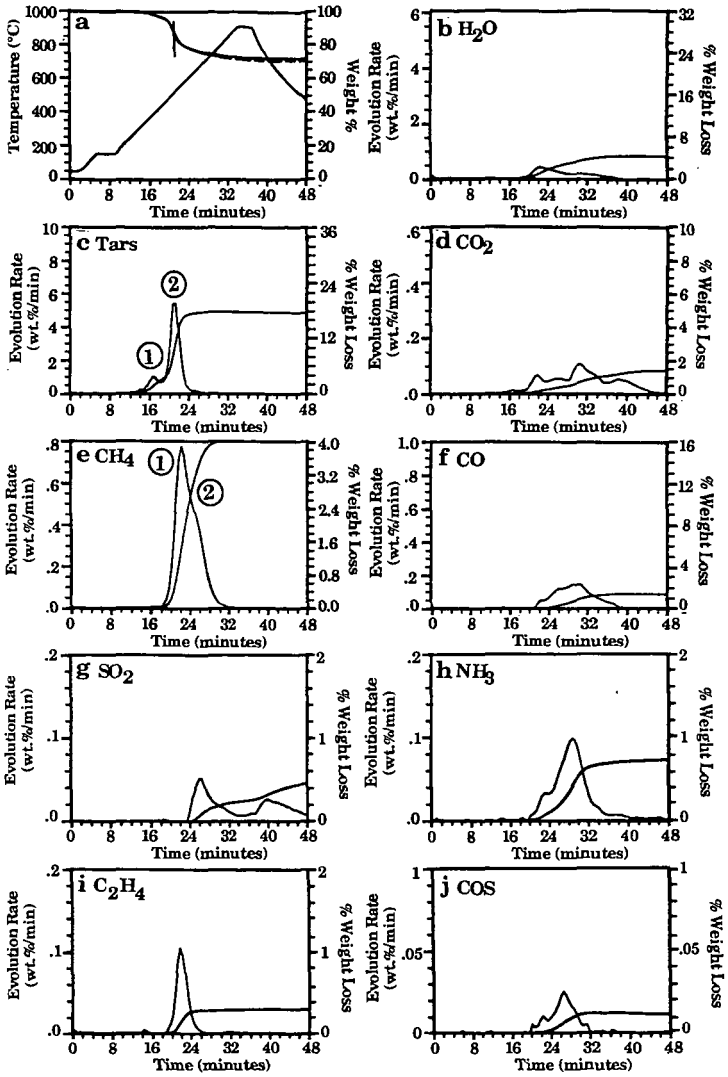

Figure 5. TG-FTIR Analysis of Upper Freeport Bituminous Coal during the Pyrolysis Cycle. a) Weight Loss (solid), Sum of Evolved Products (dashed), and Temperature Profile. b) H_2O Evolution Rate and Integrated Amounts Evolved, c) Tar Evolution Rate and Integrated Amounts Evolved, d) CO_2 Evolution Rate and Integrated Amounts Evolved, e) Methane Evolution Rate and Integrated Amounts Evolved, f) CO Evolution Rate and Integrated Amounts Evolved, g) SO_2 Evolution Rate and Integrated Amounts Evolved, h) NH_3 Evolution Rate and Integrated Amounts Evolved, i) C_2H_4 Evolution Rate and Integrated Amounts Evolved, and j) COS Evolution Rate and Integrated Amounts Evolved.

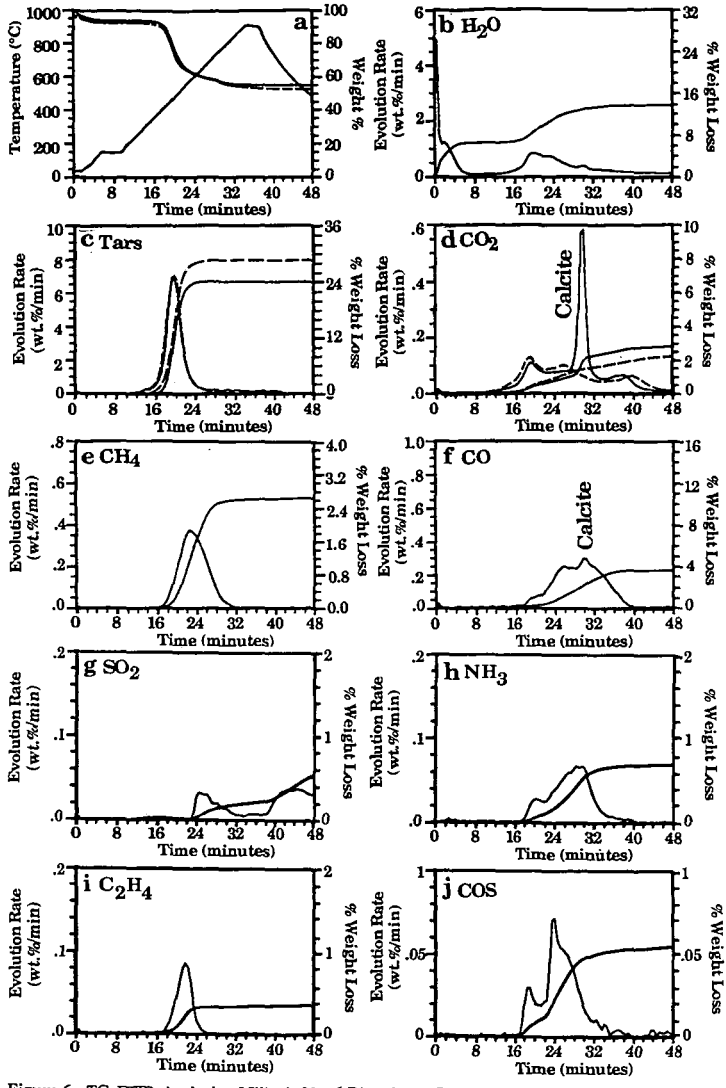

Figure 6. TG-FTIR Analysis of Illinois No. 6 Bituminous Coal during the Pyrolysis Cycle. a) Weight Loss (solid), Sum of Evolved Products (dashed), and Temperature Profile. b) H_2O Evolution Rate and Integrated Amounts Evolved, c) Tar Evolution Rate and Integrated Amounts Evolved (raw coal (solid line) demineralized coal (dashed line)), d) CO_2 Evolution Rate and Integrated Amounts Evolved (raw coal (solid line) demineralized coal (dashed line)), e) Methane Evolution Rate and Integrated Amounts Evolved, f) CO Evolution Rate and Integrated Amounts Evolved, g) SO_2 Evolution Rate and Integrated Amounts Evolved, h) NH_3 Evolution Rate and Integrated Amounts Evolved, i) C_2H_4 Evolution Rate and Integrated Amounts Evolved, and j) COS Evolution Rate and Integrated Amounts Evolved.

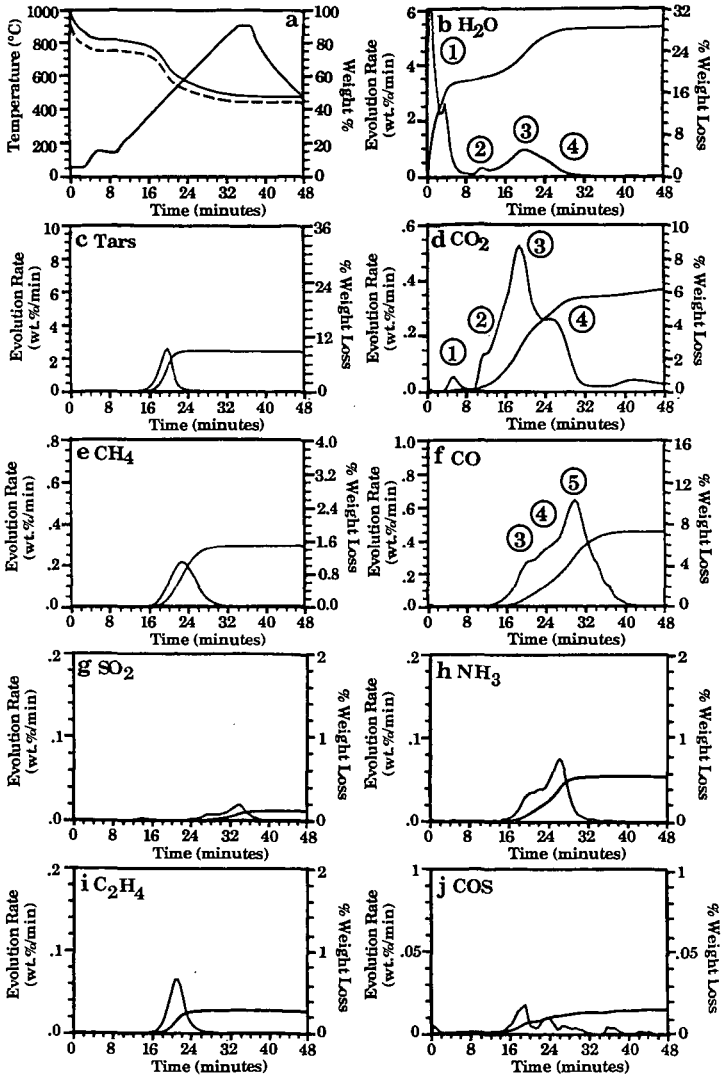

Figure 7. TG-FTIR Analysis of Wyodak Subbituminous Coal during the Pyrolysis Cycle. a) Weight Loss (solid), Sum of Evolved Products (dashed), and Temperature Profile. b) H_2O Evolution Rate and Integrated Amounts Evolved, c) Tar Evolution Rate and Integrated Amounts Evolved, d) CO_2 Evolution Rate and Integrated Amounts Evolved, e) Methane Evolution Rate and Integrated Amounts Evolved, f) CO Evolution Rate and Integrated Amounts Evolved, g) SO_2 Evolution Rate and Integrated Amounts Evolved, h) NH_3 Evolution Rate and Integrated Amounts Evolved, i) C_2H_4 Evolution Rate and Integrated Amounts Evolved, and j) COS Evolution Rate and Integrated Amounts Evolved.

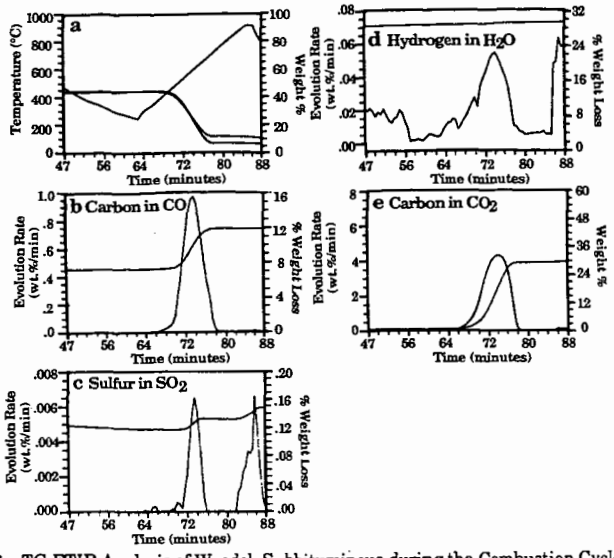

Figure 8. TG-FTIR Analysis of Wyodak Subbituminous during the Combustion Cycle. a) Weight Loss (solid), Sum of Evolved Products (dashed), and Temperature Profile. b) Carbon in CO Evolution Rate and Integrated Amount Evolved. c) Sulfur in SO_2 Evolution Rate and Integrated Amount Evolved. d) Hydrogen in H_2O Evolution Rate and Integrated Amount Evolved. e) Carbon in CO_2 Evolution Rate and Integrated Amount Evolved.

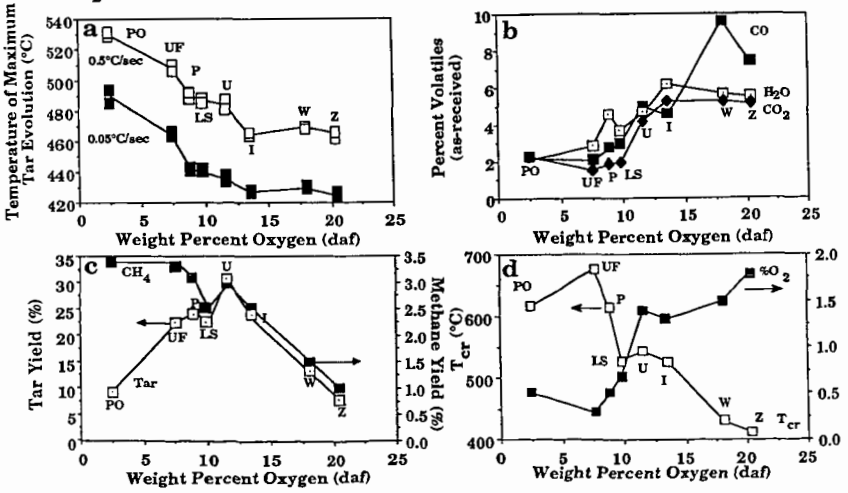

Figure 9. Variation of Coal Pyrolysis Properties with Rank. a) Rank Variation of Tar Evolution Temperature, b) Rank Variation of Oxygenated Gases c) Rank Variation of CH_4 and Hydrocarbons and d) Rank Variation of T_{cr} and Oxygen Chemisorption.

AGING STUDIES OF BITUMINOUS COAL BY ESCA AND FTIR

Cara L. Weitzsacker, James J. Schmidt
Joseph J. Gardella, Jr.*
Department of Chemistry and Surface Science Center
University of Buffalo, SUNY, Buffalo, NY 14214

Keywords: ESCA of coal, FTIR of coal, coal aging

ABSTRACT

Electron Spectroscopy for Chemical Analysis (ESCA or XPS) and transmission Fourier Transform Infrared Spectroscopy (FTIR) were used to examine aged bituminous coals. The coals were obtained from the Illinois #6, Kentucky #9, Pittsburgh and Upper Freeport seams. THe coals were stored under either ambient air, mine site tap water or nitrogen as they were exposed first to cold weather (10 C), warm weather (25 C) and the following cold season. Samples over the time periods were analyzed as raw, milled and processed coals. Emphasis was placed on changes in C, O, N and S functionalities on the surface by ESCA analysis, and in the bulk by transmission FTIR.

INTRODUCTION

The aging of coal is of interest both to the fuel and coking industry due to the physical and chemical changes aging causes. The changes can affect the behavior and properties of coal, and therefore affect the coal as it is processed and utilized. In the majority of cases, the effects are negative. Oxidation, a major mechanism in the aging process, can decrease the fuel value of coal. Processing can become more problematic as aging occurs. (1-3)

Storage of coal is where significant oxidation can occur as coal ages. (1,2) Coal is commonly stored in large stockpiles open to weather conditions. In this study, storage conditions were modified to investigate what effects they may have on controlling or inhibiting aging. (4) Samples were stored under nitrogen gas, tap water or ambient air.

EXPERIMENTAL

Coal samples, obtained by Otisca Industries, Ltd., were collected as they were brought up out of the mine. Coal was collected from the Illinois #6, Kentucky #9, Pittsburgh and Upper Freeport seams. The coal was placed under one of three atmospheres upon collection: nitrogen, ambient air or local mine site tap water.

Upon arrival at Otisca, the samples were riffled and crushed to 30m x 0 following ASTM methods, and returned to their respective environments. The coal was stored in 5 gallon pails holding approximately 17 lbs. each, and exposed to local weather during cold weather (10 C), the following

warm season (25 C) and another cold season. Individual samples were taken after each weather exteme. Samples were analyzed as raw samples, milled samples, and milled and processed samples. Raw coal was reduced to 60m x 0. Milled samples were ball milled to 15 m x 0. Processed samples were first milled and then agglomerated using pentane. At this point mineral matter was removed.

Initially a set of samples from each seam was analyzed before exposure to weather to establish a baseline for the aging study. The handling, analysis, and results of these analyses were presented in a previous preprint.(5)

The samples received from Otisca were handled as previously described (5). Analysis was done using a Perkin - Elmer Physical Electronics 5100 ESCA spectrometer using a non - monochromatized Mg K_{α} X - ray source under the conditions 300W, 20mA and 15kV. Transmission FTIR spectra were collected on a Nicolet 7199A FTIR spectrometer with an MCT detector, taking 1000 scans, and a Mattson Alpha Centauri FTIR spectrometer with DTGS detector, taking 32 scans.

RESULTS AND DISCUSSION

In the previous study (5), the baseline samples were analyzed to establish what information can be obtained from the ESCA and FTIR analyses. In that study it was shown that as the samples went from raw to milled to processed there was a decrease in mineral matter. In the milled samples, mineral surfaces were generally covered by a thin film of organic matter. In the processed samples, most mineral matter was separated from the coal during agglomeration. It was also shown there was no significant difference in the baseline samples due to differing storage conditions.

In this study, the trends from raw to milled to processed coal were observed throughout the storage period, as would be expected. No major differences due to storage conditions were observed, but some difference was seen in the nitrogen stored samples.

As the coal aged (see Table 1), changes in the surface percent atomic concentration (%AC), oxygen to carbon ratios (O/C), and peak shape changes were examined. Changes in %AC carbon and oxygen would be an indication of oxidation, as would peak shape changes. Peak shape changes were examined in the FTIR spectra.

As the coal aged, trends were investigated in percent atomic concentrations. The inorganic elements such as Al and Si showed no notable changes over the storage period. Sulfur also remained consistent throughout aging, and nitrogen exhibited only minor fluctuations over the aging period. The largest change was seen in %AC carbon of the raw samples. There was an increase of up to 10 %AC between the baseline and first aged samples in all 4 seams. See Figure 1. There were slight variations through to the 7th batch, with only Illinois showing a significant decrease in %AC C. See Figure 2.

The milled samples showed a slight decrease in %AC from

the baseline to 1st aged sample. Slight decreases were seen in batch 4 or 5 in all seams, with the largest seen in the Pittsburgh samples.

In the processed samples, The %AC C was consistent through batch 1 - 7 except for the Kentucky seam, where a decrease was seen over batch 4 - 6, with an increase in the 7th batch.

Looking at what effect the storage conditions had, very little change was observed. In all four seams, no significant change in %AC C was seen in the air or water stored. Differences due to nitrogen storage was only significant in the Upper Freeport seam.

The trend in %AC total oxygen decreased through the processed samples due to the removal of minerals. Surface organic oxygen was calculated using the method of Perry and Grint (3), by subtracting oxygen as SiO_2 and Al_2O_3 . There were fluctuations in %AC surface organic oxygen as the samples aged. The least fluctuation was seen in the Pittsburgh seam, the most in the Upper Freeport seam.

The calculated %AC surface organic oxygen was used to calculate O/C ratios. An increase in this ratio would indicate oxidation of the coal was occurring. The largest difference in O/C ratio between treatments was seen in the Illinois and Upper Freeport seams, the least in Kentucky and Pittsburgh. No trend of increasing O/C ratio was seen except in Illinois raw samples. See Figure 3.

Peak shape changes were only notable for C, O, N and S. The C 1s envelope exhibited no gross changes as the samples aged. Slight increases in the shoulder and tailing towards the high binding energy side were observed over all treatments through batch 7. This would indicate a slight increase in the oxidized carbon functionalities and possibly a slight increase in aromatic carbon. See Figure 4.

The O 1s envelope has contributions from both organic and inorganic species. It is a broad slightly assymmetric peak. As the coal aged, a more distinct shoulder was seen towards low binding energy. The most severe case was seen in the processed samples. The inorganic matter was largely removed at this point. The shoulder was due to organic (carbon - bound) oxygen. See Figure 5.

The S 2p peak shape didn't vary much over the storage period. The presence of one or two peaks and the relative intensities of these two peaks varied. No solid trends were seen between the seams. In the Kentucky seam raw samples, there was one peak in the water stored sample and baseline nitrogen stored, but two peaks in the air stored and last nitrogen stored. The relative intensity of these two peaks varied as well. In the water stored milled baseline samples, the inorganic/oxidized organic species peak (5) was more intense than the organic species peak. In the 3rd batch sample, the relative intensities were reversed. See Figure 6. In the Upper Freeport samples, the trend was reversed for the respective samples. No definite trend was seen in or

between the seams.

The infrared results reflected the removal of the mineral matter with decreases in intensity of inorganic peaks. There was little difference between raw and milled samples, but there was significant difference between raw and processed samples. There were some differences in general between the seams, particularly in the 1400 - 700 cm-1, region where bands corresponding to clay mineral matter appears. Kentucky and Pittsburgh had less of this matter than Illinois and Upper Freeport. This was most evident in the raw and milled samples.

No major changes were obvious from the infrared spectra. Over the four seams there was one trend in the 1800 - 1650 cm-1 region. In the early samples there was a small peak at approximately 1730 cm-1 or a shoulder between 1800 - 1650 cm-1. As the coal aged this small peak became less intense or the shoulder less prominent. This indicates there may be a decrease in carbonyl as the coal aged. See Figure 7.

CONCLUSIONS

This study shows that no major oxidation, either in the bulk or at the surface, was evidenced in these studies over the time period and temperature range they were stored at based on these analyses.

ACKNOWLEDGEMENTS

Support for this work has been provided by the Department of Energy under Contract # DE - AC22 - 87PC79880 DOE Pittsburgh Energy Technology Center with a subcontract to Otisca Industries, Ltd.

REFERENCES

1. Gethner, Jon S., FUEL 1987, **66**, 1091

2. Huffman, Gerald P.; Huggins, Frank E.; Dunmyre, George R.; Pignocco, Arthur J.; Lin, Mon - Ching, FUEL 1985, **64**, 849

3. Perry, David L.; Grint, Alan, FUEL 1983, **62**, 1024

4. Fred Simmons, private communications

5. Weitzsacker, Cara L.; Schmidt, James J.; Gardella, Jr., Joseph A., ACS Fuel Div. Preprint, 1989, **34**, 545

TABLE 1

Batch #	Storage History
1	baseline
2,3	1st cold season
4,5	warm season
6,7	2nd cold season

FIGURE 1

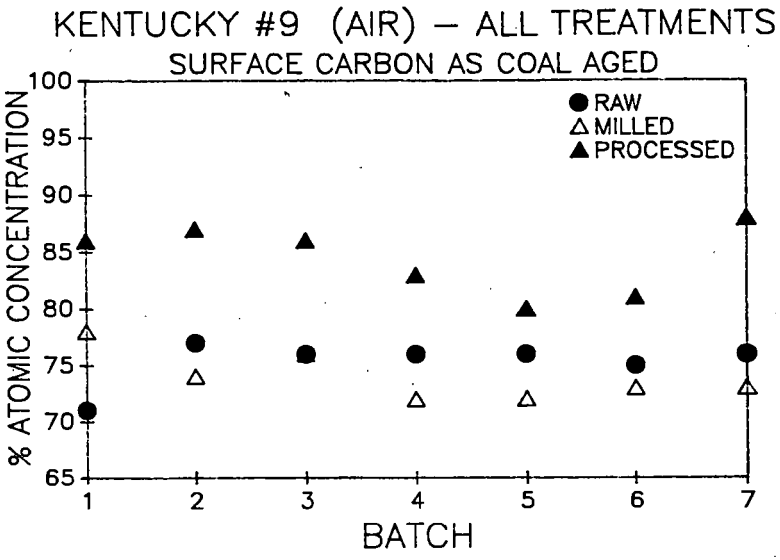

FIGURE 2

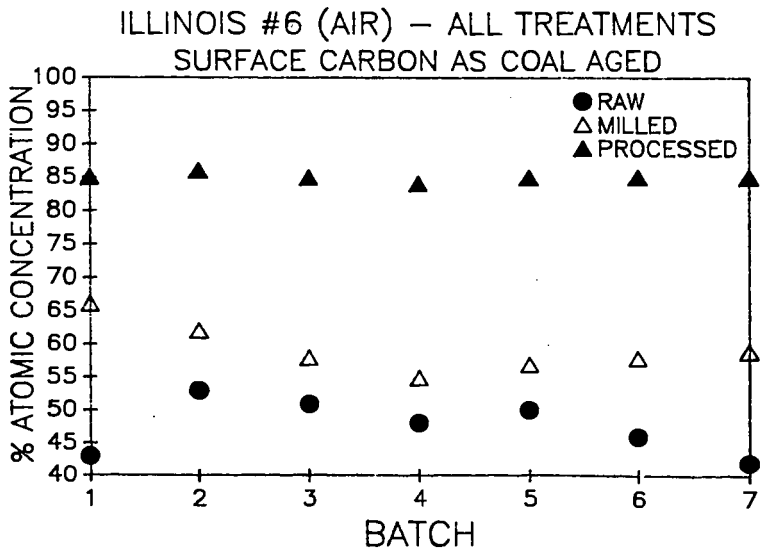

FIGURE 3

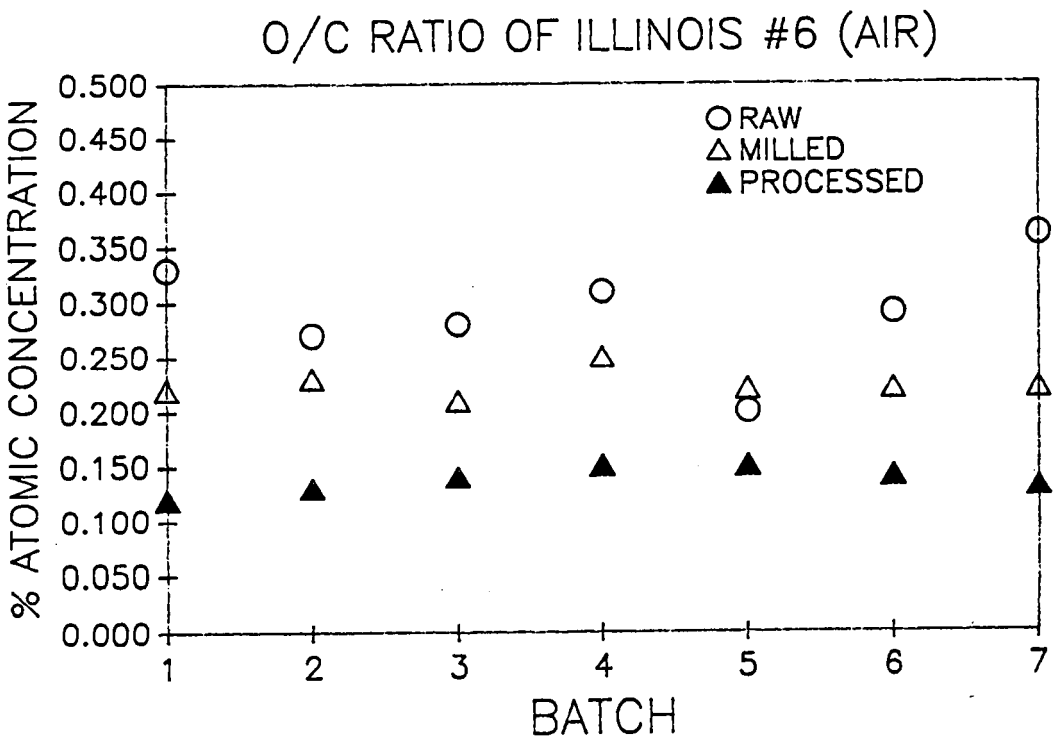
O/C RATIO OF ILLINOIS #6 (AIR)
% ATOMIC CONCENTRATION
0.500
0.450
0.400
0.350
0.300
0.250
0.200
0.150
0.100
0.050
0.000
RAW
MILLED
PROCESSED
1
2
3
4
5
6
7
BATCH

FIGURE 4

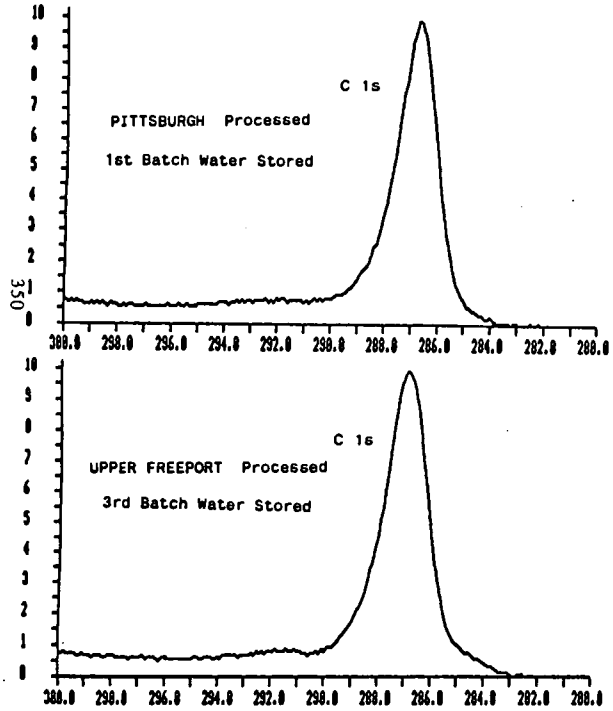

FIGURE 5

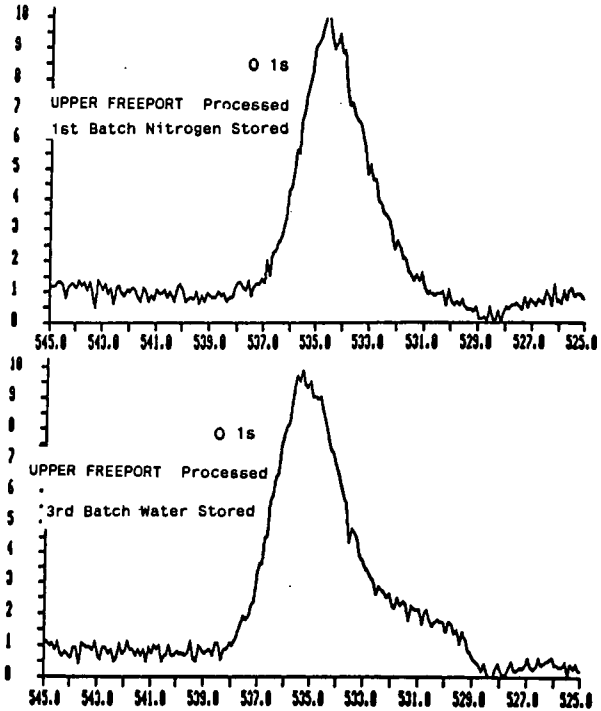

FIGURE 6

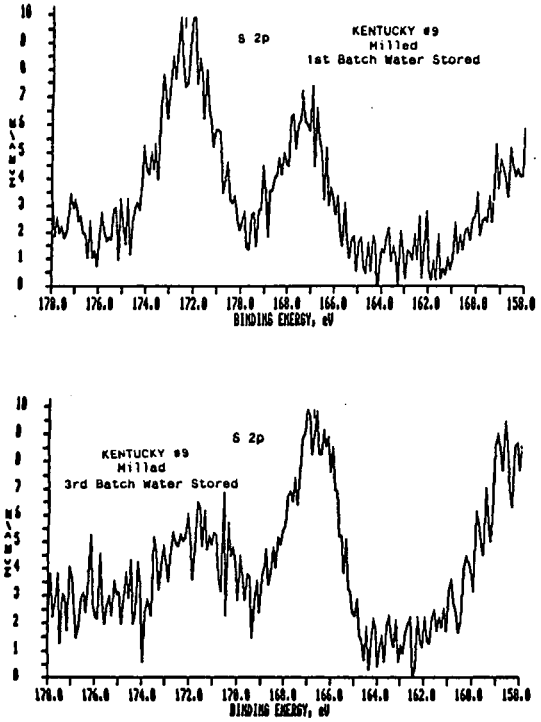

FIGURE 7

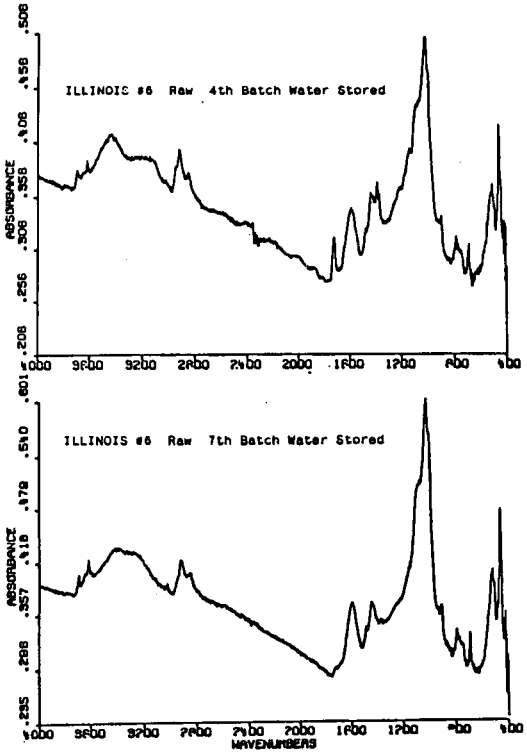

THE EFFECTS OF HYDROTHERMAL TREATMENT ON WYODAK COAL

David S. Ross, Albert S. Hirschon, Doris S. Tse, and Bock H. Loo
SRI International
Menlo Park, CA 94025

Keywords: hydrous pyrolysis, hydrothermal treatment, Wyodak

INTRODUCTION

There are a number of accounts of the treatment of coal with steam, including the recent work of Beinkowski et al.,[1] Brandes and Graff, [2,3] and Kahn, et al.[4] These efforts sought benefits to liquefaction and pyrolytic tar yields, and described changes in both the composition and the behavior of the coals. In other work Rozgonyi et al. described ash and sulfur reductions in steam-treated coal,[5] and some of our recent work with Illinois No. 6 coal in hot liquid water is described in a paper elsewhere in these preprints.[6]

The hydrothermal conditions used in these efforts are reminiscent of the hydrous pyrolysis studies conducted in research dealing with the accelerated maturation of oil shale.[7,8] Source rocks are heated in liquid water at temperatures in the 300-350°C range, resulting in the net production of alkanes and other hydrocarbons, in contrast to the case for dry pyrolysis where olefins are produced. The claim that hydrous pyrolysis actually mimics the natural process has been questioned recently,[9,10] but the phenomenology is unquestioned.

The work described here is an attempt to bridge the two areas. We are seeking to understand the changes brought about in Wyodak coal by liquid water in the range 150-350°C in terms of its structure. We expect the results of this work to provide some insight into any benefits such treatment provides liquefaction and volatiles production.

EXPERIMENTAL

Our work was conducted with Wyodak samples from the Argonne Premium Coal Bank. In most cases the starting coal was dried in an oven at 60°C/1 torr/20 hr, a pretreatment that resulted in a loss of water representing about 30% of the coal mass. In some runs the as received coal was used, and we found no difference in behavior following hydrothermal treatment. The as received coal was used as well in a control run where the treatment was conducted with no added water. In that case the water in the coal may have contributed to the subsequent pyrolytic behavior, as described below.

The hydrothermal treatment was conducted in a 45 ml stainless steel reactor with a tightly fitting Pyrex insert. Sufficient water was used to assure in each case that a liquid phase was present at temperature, and the reactor was charged with 33-50 atm (500-750 psi) nitrogen (cold). The run temperatures (°C) and respective vapor pressures of water (atm) were 150/4.6, 250/38, and 350/160. After treatment the coal/water mixture was centrifuged directly in the insert, most of the water removed by pipette and saved for later analysis, and the coal removed in an N_2-purged glove bag. The remaining superficial water was then removed in a stream of dry nitrogen.

The bulk of the analysis was conducted by pyrolysis field ionization mass spectrometry (py-FIMS). The heating rate used throughout was 2.5°C/min, and spectra were recorded at nominally 30° intervals from ambient to 500°C. In some cases quantities of volatiles from the treated coal were transferred at 120°C via vacuum transfer to bulbs for analysis by conventional mass spectrometry. In addition to the parent-peak spectra, py-FIMS output included volatility data, and values for the weight average molecular weights ($\bar{M}_w$) of the fractions.

Analysis of the water fractions were conducted by first saturating the aqueous phase with NaCl, and then extracting with methylene chloride. The extracts were then analyzed by gas chromatography, and identification confirmed by comparison with authentic samples.

BACKGROUND

Bienkowski et al. reported on the abundance of alkylated phenols and dihydroxybenzenes both in the pyrolysis tars of Wyodak coal, and in the water collected following steam treatment.[1] Kahn et al. similarly identified a large collection of phenols in the treatment water.[2] These results are expected based on the lignin residues present in this rank of coal.[11]

There is also a wide range of biomarkers reported for the extracts of Wyodak coal in work by Baset, et al. who studied benzene/ethanol extracts and pyrolysates evolved directly from the heated coal.[12] The extracts included ferruginol and retene, and they sought but found no pristane. The presence of the

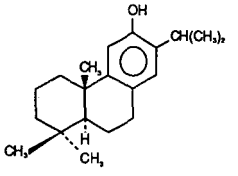

ferruginol

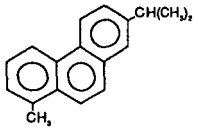

retene

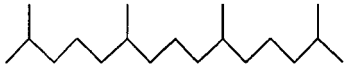

pristane

corresponding olefin pristene in the pyrolysate, however, suggested that the alkane or a precursor was bound to the coal, and then released as the olefin when the coal was heated.

The geochemical studies on oil shale could be related to these findings, with the account by Hoering of specific interest.[8] In that work the treatment of preextracted Messel shale in liquid water at 330°C/3 days generated petroleum hydrocarbons including long chain normal alkanes, aromatics, and biomarkers. When D_2O was used, deuterium was heavily incorporated into the hydrocarbons. Hoering's control results and the distributions of isotopic isomers essentially ruled out preexisting, trapped hydrocarbons, and the results suggested that the hydrocarbons were not merely freed, but rather generated in some manner by the water.

RESULTS

We conducted a number of experiments with hydrothermal treatments at 150° and 250°C, with the majority of the work at 350°C. Analyses of the recovered coals included py-FIMS and simple analyses of recovered water and volatiles samples.

Recovered Water, Direct Volatiles Analyses, and Elemental Analysis

As expected, analysis of the recovered water from 350°C treatment runs showed the presence of phenols and dihydroxybenzenes. The most prominent products were catechol (o-$(OH)_2$Ph) and phenol in a ratio of about 2/1. Other products found in smaller quantities were resorcinol (m-$(OH)_2$Ph) and hydroquinone (p-$(OH)_2$Ph), with the ratio catechol/(resorcinol + hydroquinone) ≈ 6/1.

The same materials were pulled from the coal heated to 120°C in a vacuum line transfer, and identified by conventional mass spectrometry. In this case phenol was the most prominent material; however we were surprised to find acetone as a major volatile product, present in quantities similar to those for phenol.* Smaller quantities of simple ketones including butanone and a pentanone were also identified. These findings are discussed further below.

The elemental analyses from the work at 350°C are presented in Table 1. The %-oxygen values are by direct O-analysis. The final columns in the table show calculated compositions based on specific loss of the elements of CO_2 and H_2O, and values for the net loss of OH are also shown for comparison. Clearly CO_2 loss is not significant, and water loss fits rather well. Curiously loss of OH fits the measured values even better, although the accuracy of the measured values may not warrant our modeling the results to such a degree. The product coals from the 150° and 250°C work showed no O-loss.

Thus at 350°C we see about a 30% loss of oxygen, but significantly the loss is independent of the presence of added water. Kahn et al recorded about a 20% O-loss for Wyodak coal with steam at 304-320°C,[4] and we have noted that about half the oxygen in Illinois No. 6 coal is lost in water/N_2 at 400°C.[13] The present results show that at least for Wyodak coal the loss is strictly thermally promoted and does not require added water. *However it is notable that the loss of water in the hydrothermal case occurs at a partial pressure of water of 160 atm.* The process is thus highly irreversible, and obviously does not involve bound or sorbed molecular water. One candidate water source are coal clays, which dehydrate at elevated temperatures.[14] However that process is reversible, and at any rate is very highly suppressed below around 475°C under just a few torr of water vapor.[15]

We conclude that the water loss must involve the dehydration specifically of chemically bound elements of water in the organic phase of the coal. The dehydration may be tied to the fact that catechol is a prominent thermal product. And as we have shown in other work, catechol thermally dehydrates and forms oligomers at 300°-400°C in the presence of kaolinite, one of the clays in coal. We expect to develop a better understanding of this process in further work.

Volatilities

Several different py-FIMS measurements were made of separate samples of the as received coal on different days to establish the reproducibility of the method and the stability of the instrument, and the results of those runs (points) along with those for 150° and 250°C treatments (curves) are presented in Figure 1. The data for the as received coal fall essentially upon one another, demonstrating a satisfactory precision. The similar alignment of the data from the treated coal shows that little change in the coal takes place at 150°, while some activity is seen at the 250° level. The volatile fractions in these cases and in those below was consistently 25-30%.

The shape of the curves for the as received coal demonstrates two regions of activity. Below 300°-320°C the small quantities of preexisting volatile material in the coal are evaporated into the instrument. Then at higher temperatures pyrolytic fragmentation of the coal occurs, and products of that process are recorded. Thus for the as received coal and the 150° sample, no more than about 10% of the ultimately volatile material emerges in the first region. For the 250° treatment, since that temperature was below the point of substantial thermolysis, the increased volatiles for that run must be due specifically to the action of water in the treatment.

---

* The possibility of adventicious acetone was considered. However the presence of acetone solely in runs from the 350°C treatment confirmed its formation in the process.

This point is demonstrated more clearly for the 350° work in Figure 2. The figure presents the curves for 30 min runs at 350°C both with added water (2 runs) and without added water, with some data for the as received coal are shown again for comparison. In this case to assure no confusion from possible thermal effects from oven drying, the as received coal was used for the run with no water.

The effects tied specifically to the hydrothermal conditions are evident from the profiles. They are emphasized by comparing the %-volatile values at an abscissa value of 350°C, the temperature at which the coal was treated, and for the as received, no water, and hydrothermal samples the volatilities are respectively 22%, 37% and 52%. The jump from 22 to 37% reflects a thermal effect that can be anticipated since the treatment temperature was in the pyrolysis range, although we cannot rule out some action by the water driven out of the coal. (Work with dried samples is in progress.) The remaining increase to 52%, however, must be due specifically to the presence of water.

Recognizing that the treatment involves holding coal samples at temperature for 30 min, and that the py-FIMS heating rate is 2.5°C/min, another useful comparison can be made over the interval 350° to ~425°C (i.e. 350°C to ~[350° + 2.5 x 30]). The pertinent data are presented in Table 2, which shows that the weight average molecular weights $(M)_w$ for the tars from the hydrothermally treated coal are consistently greater than those for both the as received and thermally heated samples, a result in turn consistent with the view that added water specifically affects the subsequent pyrolytic properties.

An effect is apparent as well from inspection of the Pyrex inserts after the runs. For the hydrothermal treatment they showed considerable quantities of tar deposited on the walls. For the thermal treatment case, however, the walls were clean, except for droplets of water which was driven from the coal during the treatment. Some insight into the these effects can be developed with inspection of the various FIMS spectra, with attention to the effects of treatment on individual compound classes.

FIMS Spectra and Coal Tars

Treatment at 350°C. FIMS spectra are presented in Figure 3 for the as received coal and for the 350° treatment both with and without water. Each spectrum is the accumulated signal for each sample up to a py-FIMS temperature of 300°C, and the differences in volatilities shown in Figure 2 are evident here.

Specific effects of the addition of water can be gathered from the difference spectrum shown in Figure 4. The figure represents [hydrothermally treated] *minus* [thermally treated], and is derived from the respective spectra for the full volatiles fractions evolved to 500°C. The data from the two runs have been normalized, so that the differences reflect changes in the compositions. Thus the addition of water shifts the thermolytic behavior of the coal so that the volatiles are richer in dihydroxybenzenes and a broad range of coal tar material at m/z values 200-500 amu, and depleted in phenols.

Also very prominent in both spectra is m/z = 58, identified as acetone by vacuum line isolation and analysis. The difference spectrum shows that its levels are elevated relatively in the pyrolysate from the thermally treated coal, probably due to its solubility in water. Other simple ketones in smaller quantities were also identified as noted above. We are not aware of accounts of acetone or other simple ketones as products of coal thermolysis, although such compounds are identified in wood tars and are derived from cellulose.[16] This finding could reflect the presence cellulose residues in Wyodak coal, and we expect to look further into this matter in future studies.

The profiles for the generation of acetone, phenol and dihydroxybenzene as a function of temperature are shown in Figure 5. For the as received coal the activity is almost solely in the pyrolysis region, and dihydroxybenzene (most likely catechol) is the most prominent product, with its production peaking at around 400°C. Both the thermal and hydrothermal treatments shift the production of all three materials to lower temperatures, but the presence of added water does not appear to affect the phenol and acetone release. The addition of water clearly affects dihydroxybenzene evolution, however, moving it to lower temperatures.

The assignments in the figure are probably satisfactory to py-FIMS temperatures up to 300°C, and for m/z = 90 and 110 perhaps all the way to 500°C. However m/z = 58 above 300°C probably represents butane rather than acetone, although as the figure shows the point is moot since it is not significant in that region. On the other hand it is prominent at lower temperatures for the thermally and hydrothermally treated coal, its peaking coinciding closely with that for phenol. Given that all three compounds are volatile, it is surprising that the maximum in their lower temperature evolution falls at around 140°C. For the hydrothermally treated coal there is some immediate evolution which then declines, and we assign this behavior to some material fully released by the water, and thus simply "sitting" on coal and readily pumped into the FIMS instrument. However the delayed, common peaking temperature for much of the phenol, dihydroxybenzene, and acetone suggests that they are present together in a nonvolatile, complexed form generated in initial thermal or hydrothermal treatment. We expect to continue work in this system to develop a better understanding of the sources of these materials.

Treatment at 250°C. Just as for the 350° work, treatment at 250°C promoted the production of coal tar, albeit at a lower level. The fact that tar was produced with treatment at a temperature below the pyrolysis region is another reflection of the specific action of water in the treatment. However there were significant differences between the 350° and 250° results. First, as shown in Figure 6, the phenols and benzenediols for the treated coal emerge fully in the pyrolysis region, and no acetone is seen. In this regard the treated coal acts like the as received coal, and the result is not surprising since from the 350° work we learned that the phenols and acetone were pyrolytically produced.

Second, several prominent peaks appear in the FIMS of the tars of the treated coal, but are present in neither the as received nor the 350°-treated coal. These compounds emerge at py-FIMS temperatures around 100°C, with m/z values corresponding to the parent masses of some biomarkers. They include peaks at 234, 268 and 270 amu, which correspond respectively to retene, pristane, and ferruginol. A prominent peak also appears a m/z = 252, and we are aware of no corresponding biomarker.

We emphasize that while these parent masses correspond to the biomarkers, at present we have no additional information on the structures. However with this caveat, it appears that there is some hydrolytic release of biomarkers. The mechanism of that action is of interest, particularly in the case of hydrocarbons such as retene and pristane which have no "handles" for the action of water. The question of the role of mineral matter in these processes must be raised, including aspects of coal structure which might provide substantial and widely ranging interaction between the organic and mineral components in coal.

DISCUSSION

Our accumulated evidence thus far shows that there are both water-independent and water-promoted modes of release of tars and specific compounds. Phenols and acetone are evolved thermally at temperatures above 300°C, while hydrothermal conditions affect the dihydroxybenzene evolution. The question remains as to what features in the structure are responsible for this behavior. The production of acetone and other simple ketones may reflect the presence of some cellulose-related residue in the coal.

The water-promoted evolution of tars and biomarkers seems similar to the observations from the hydrous pyrolysis studies of oil shale. For oil shale such chemistry probably involves interfacial chemistry at the boundary joining the organic and mineral surfaces. In the case of coal, Allen and VanderSande have estimated that ultrafine mineral matter in the organic phase may represent up to 15% of the total quantity of mineral material in coal,[17] and the distribution of such a fine mineral material throughout the organic phase would lead to a significant interfacial volume. Our results may thus mirror the existence of such a volume, and specific interfacial chemistry generating and/or liberating volatile materials.

Finally, a possible parallel between oil shale and coal structure leads to an interesting surmise regarding the distribution of heteroatom components in coal. The heteroatom-containing fractions of oil shale are concentrated at the mineral surfaces,[18] presumably migrating over geologic time to acid/base sites in the clays. Were such a condition to exist in coal, we would then expect a nonrandom distribution of

heteroatom components, localized at the mineral inclusions within the organic phase. Such a picture of coal is considerably different from the structures commonly considered, and could be significant to the processing coal.

ACKNOWLEDGEMENT

We acknowledge support of the US DOE on Contract No. DE-AC22-89PC89880. We also are pleased to acknowledge helpful discussions with R. Malhotra and D. McMillen of SRI, and T. Milne of SERI.

REFERENCES

1. P. R. Beinkowski, R. Narayan, R. A. Greenkorn, and K-C Chao, Ind. Eng. Chem. Res., 26, 202-205 (1987).
2. S. D. Brandes and R. A. Graff, Am. Chem. Soc. Div. of Fuel Chemistry Preprints, 32 (3), 385-393 (1987).
3. R. A. Graff and S. D. Brandes, Energy and Fuels, 1, 84-88 (1987).
4. M. R. Kahn, W-Y. Chen and E. Suuberg, Energy and Fuels, 3, 223-230.
5. T. G. Rozgonyi, M. S. Mohan, R. A. Zingaro, and J. H. Zoeller, Jr., in *Proceedings of the 2nd International Conference on Processing and Utilization of High Sulfur Coals*, Y. Chugh, R. Caudle, C. Muchmore, and A. Sinha, Dds. (Elsevier, New York, 1988)
6. David S. Ross and Albert Hirschon, Am. Chem. Soc. Div. of Fuel Chemistry Preprints, 35, 000-000 (1990).
7. a) M. D. Lewan, J. C. Winters, and J. H. McDonald, Science, 203, 897-899 (1979)..
8. T. C. Hoering, Organic Geochemistry, 5, 267-278, (1984).
9. M. Monthioux,.P. Laniais, and J-C. Monin, Organic Geochemistry, 8, 275-292 (1985).
10. E. Tannenbaum and I. R. Kaplan, Nature, 317, 708-709 (1985)
11. P. G. Hatcher, H. E. Lerch, III, R. K. Korta, and T. V. Verhayen, Fuel, 67, 1069-1075 (1988).
12. Z. H. Baset, R. J. Pancirov, and T. R. Ashe in Adv. Org. Geochem.1979, A. G. Douglas and J. Maxwell, eds., Pergamon Press, Oxford, pp. 619-630.
13. D. S. Ross, T. K. Green, R. Mansani, and G. P. Hum, Energy and Fuels, 1, 292-294, (1987).
14. J. Unsworth, C. Fowler, N. Heard, V. Weldon and V. McBrierty, Fuel, 67, 1111-1119, (1988).
15. R. L. Stone, J. Am. Ceram. Soc., 35, 96-99, (1952); G. W. Brindley and J. Jemaitre in Chemistry of Clays and Clay Minerals, A. Newman, ed., Longman Scientific and Technical, London, 1987, pp. 327-329
16. R. J. Evans and T. A. Milne, Energy and Fuels, 1 (2), 123-137, (1987).
17. R. M. Allen and J. B. VanderSande, Fuel, 3, 24-29 (1984).
18. J. J. McKay and R. S. Blanche, Liquid Fuels Technology, 3 (4), 489-521, (1985).

Table 1

Analyses of As Received and 350°C-Treated Wyodak Coal

	Starting Coal	Treated Coal		Calculated For Loss Of[a]		
		With Water	No Water	CO_2	H_2O	"OH"
%C	66.47 67.60	71.56	72.17	70.45	71.67	71.34
%H	5.10 5.02	4.89	4.99	5.62	4.61	5.04
%N	0.85 0.86	0.95	0.94	0.93	0.91	0.91
%O	20.92 21.63	14.92	15.88	15.48	15.49	15.41
% ash	8.23 8.58	9.04	9.08	9.08	8.87	8.88

a. Calculated for loss of elements of CO_2, H_2O and OH from the starting coal, to match a final O-content of 15.4-15.5%.

Table 2

Weight Average Molecular Weights of Tars from As Received,Thermally Treated, and Hydrothermally Treated Wyodak Coal

py-FIMS Temperature Interval (°C)	Sample[a]	$\bar{M}_w$
332-359	As received	458
	Thermal	434
	Hydrothermal	518
362-389	As received	455
	Thermal	449
	Hydrothermal	516
392-419	As received	431
	Thermal	427
	Hydrothermal	507
422-449	As received	366
	Thermal	356
	Hydrothermal	403

a. Thermal and hydrothermal samples heated at 350°C/30 min.

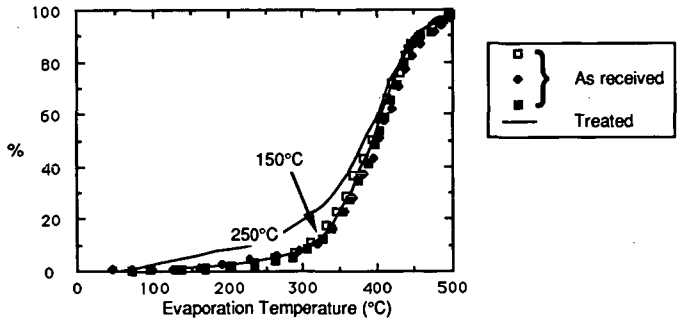

Figure 1. Evaporation curves for the as received coal and the 150° and 250°C coal products.

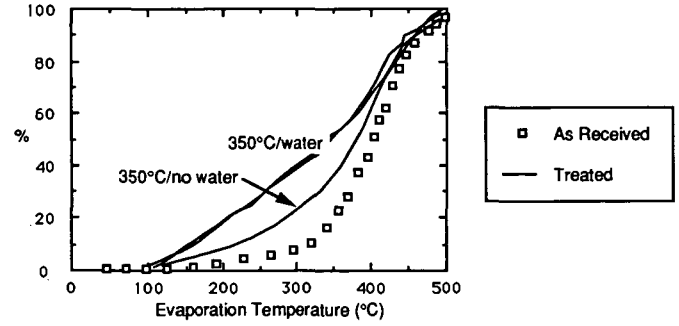

Figure 2. Evaporation curves for the as received coal, and products from 350°C runs both with (2 runs) and without water.

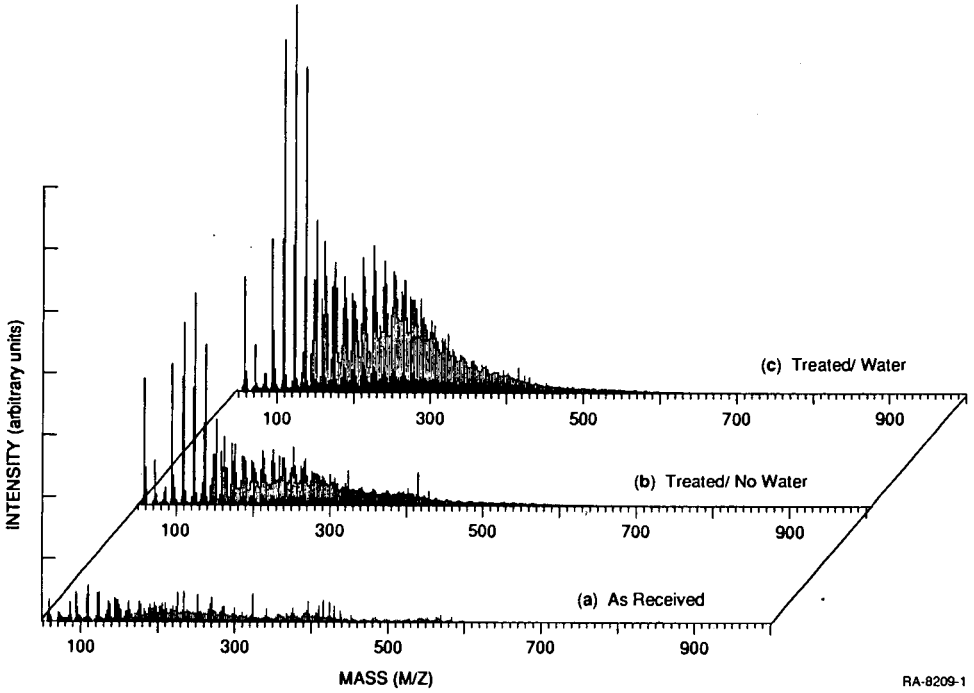

Figure 3. FIMS spectra for the as received coal, and for the coals treated at 350°C both thermally and hydrothermally.

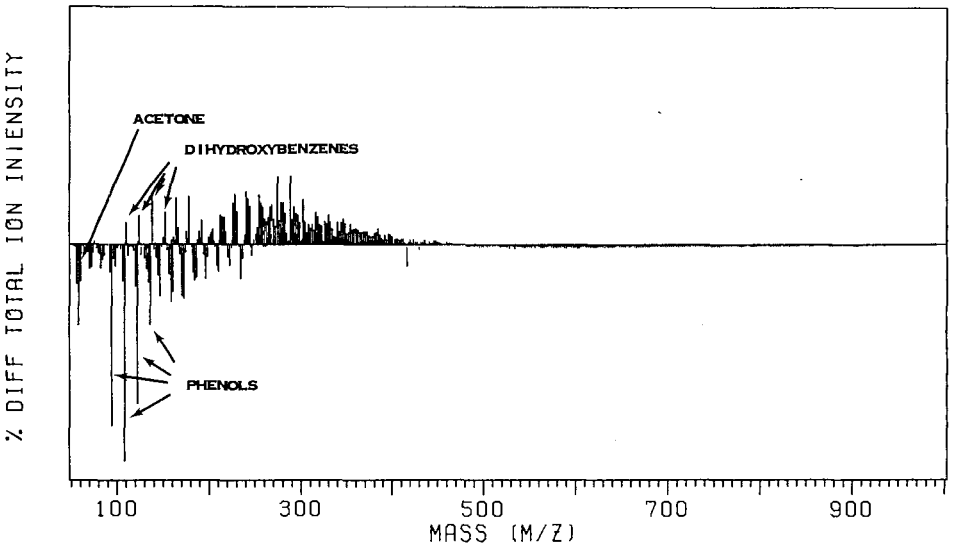

Figure 4. FIMS difference spectrum representing [hydrothermally treated] *minus* [thermally treated] for the volatiles evolved from ambient to 500°C.

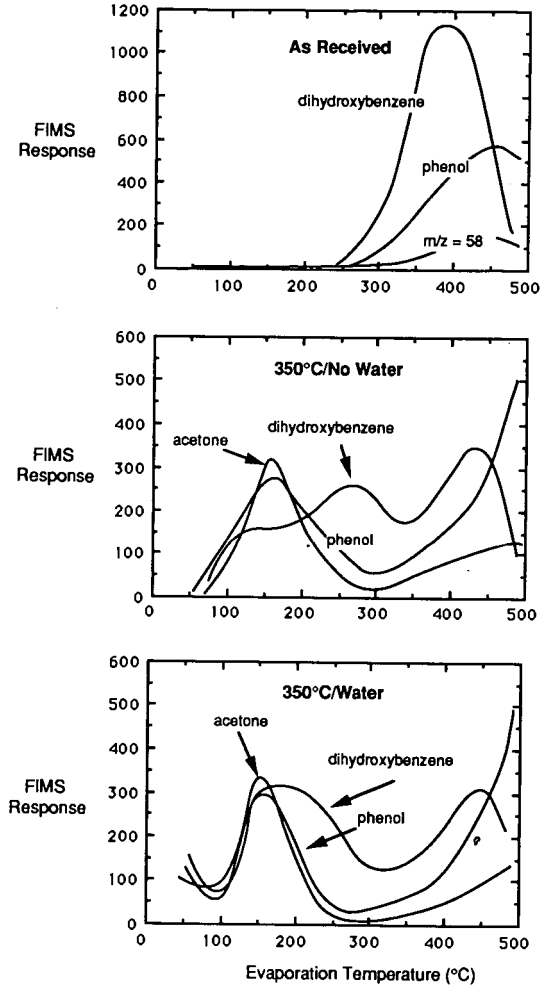

Figure 5. FIMS-derived profiles for acetone, phenol and dihydroxybenzene for runs at 350°C. The dihydroxybenzene is primarily catechol.

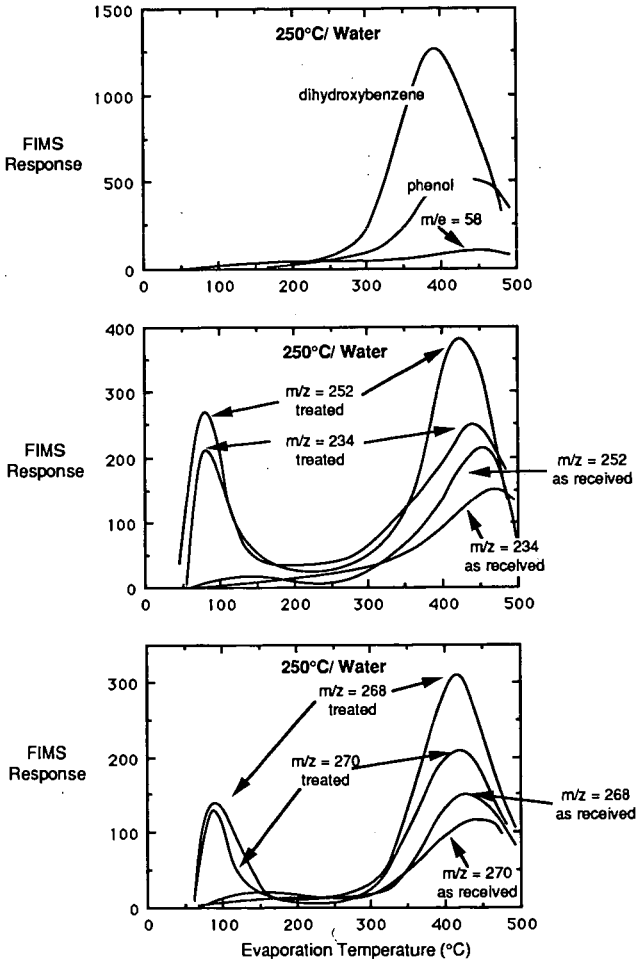

Figure 6. FIMS-derived profiles for several products from runs at 250°C. The m/z values at 234, 268, and 270 correspond to the parent masses for retene, pristane and ferruginol respectively.

INVESTIGATION OF ORGANIC SULFUR STRUCTURE AS A FUNCTION OF COAL RANK

S.Mitra, F.E.Huggins, N.Shah, and G.P.Huffman
Consortium for Fossil Fuel Liquefaction Science
University of Kentucky, Lexington, KY 40506-0107

Keywords: Sulfur, Coal Rank, XAFS Spectroscopy

INTRODUCTION

X-Ray Absorption Fine Structure (XAFS) spectroscopy is proving to be a very promising method by which information on the electronic bonding state and atomic environment of dilute elements in complex samples can be readily obtained. Of especial importance to coal science, is the technique's demonstrated ability to provide detailed information on organic sulfur in coal[1-5]. In this paper, we present the results of an XAFS investigation into the occurrence of various forms of sulfur present in a series of coals and maceral separates of different ranks.

EXPERIMENTAL PROCEDURE

Samples were selected for this study on the basis that they contain predominantly organic sulfur. A large number of the samples were maceral separates prepared by density gradient centrifugation (DGC), which effectively removed inorganic sulfur forms. A detailed description of the DGC methods can be found elsewhere[6-8]. Other samples were whole coals or coal extracts with very little inorganic sulfur contents. Samples were prepared for XAFS spectroscopy by grinding representative samples to less than 100 mesh. The samples were then cold-pressed into pellets of boric acid of approximately 2.5 cm diameter or placed in thin Mylar bags for the XAFS experiments.

Some of the sulfur K-edge XAFS measurements on the coals were performed at the Stanford Synchrotron Radiation Laboratory on wiggler beam-lines VII-3 and IV-1. Electron energies were 3.0 and 3.3 GeV and beam currents were typically in the range 40 to 80 mA. Other XAFS measurements were conducted at the National Synchrotron Light Source at Brookhaven National Laboratory on beam-line X19-A, with electron energies 2.53 Gev and beam currents 90-200 mA. At both synchrotron facilities, Si (111) double crystal monochromators were used to vary the X-ray energy from about 100 eV below to as much as 600 eV above the sulfur K-shell absorption energy (2472 eV). An all-helium pathway was used to minimize absorption of the X-rays. Thin Mylar windows (6μm) were also used for the same reason. Fluorescent experiments were performed for this study with a Stern-Heald type detector.

Complementary studies with Mössbauer and X-Ray Photoelectron spectroscopies (XPS) were also performed on some of the samples to ascertain the amounts of pyritic sulfur, iron sulfates, and oxygen-bonded sulfur compounds that might be present in the samples.

RESULTS AND DISCUSSION

The XAFS structure can be divided into two regions: the near edge structure, known as XANES, within about ±30 eV of the edge, and the extended region, the EXAFS, from about 30 eV to 300-400 eV above the edge. The XANES region of the spectrum provides information on the

bonding and oxidation state of the sulfur atoms. The EXAFS region, on the other hand, gives information about the local structural environment of the atoms.

In this study, we have concentrated on the XANES region of the spectra. The XANES structure typically consists of one or more peaks superimposed upon an absorption step. The peaks in the XANES region are derived either from transitions to vacant, bound levels, or from low energy scattering resonances. The first large peak in the XANES of all sulfur compounds, the white line, arises from the electronic transition from the 1s level to vacant np, or ns levels. A least-squares analysis of the XANES structure can be made by fitting the data to the sum of an arctangent edge step, which represents the transition of the photoelectron to the continuum, and a number of lorentzian peaks, which represent transitions to vacant bound states or scattering resonances. Each different sulfur compound exhibits one or more peaks and an edge step. Hence, the sulfur K edge of a coal sample that has a number of distinct organic sulfur forms, should exhibit a number of 1s to np/ns transitions and a corresponding number of transitions to the continuum. In practice, however, we have found that in the least-squares analysis at most only two arctangent steps are needed to obtain an adequate fit. The lower energy step represents the transition to the continuum for the sulfur bonded to carbon and the other step represents the corresponding transition for sulfur bonded to oxygen. The relative areas under the peaks can then be used in a semi-quantitative manner to show the variation of organic sulfur forms from sample to sample. However, it should be emphasized that there is at present no direct relationship between peak area and the abundance of a given organic form of sulfur, because of our lack of knowledge concerning transition moments, selection rules, etc. for the transitions in different sulfur compounds. Such relationships remain to be established in future work.

In the analysis procedure, the zero point of energy for the sulfur XANES spectra is defined as the major peak in the differential of the elemental sulfur spectrum. Relative to this point, pyritic sulfur has its white line at about 1.5 eV, and organic sulfides, such as dibenzyl sulfide, have white lines at about 2.2 eV. Thiophenic sulfur compounds, such as dibenzothiophene, have their major peaks at about 2.8 eV. Among sulfur-oxygen compounds, organic sulfoxides and sulfones have white lines at about 4.9 and 9.9 eV, respectively, whereas inorganic sulfates have white lines at around 11.4 eV. The edge step for these different compounds also exhibit similar displacements. The positive shift with increasing sulfur oxidation state is because of decreased screening of the nuclear charge for the 1s level electrons as valence electrons are transferred to the oxygen anions. In various coal spectra, fitted peaks at about the correct positions can be associated with all the sulfur forms listed above.

Coals and maceral separates of high rank appear to have little or no sulfur-oxygen bound components and the relatively small peak at 8-12 eV is believed to be principally a scattering resonance[9,10]. Such samples were fit with only one arctangent function, as shown in Figure 1. Other samples, principally of lower rank, did need a second step for a better fit and exhibited a much larger peak at 8-12 eV, as shown by the XANES spectrum of leonardite in Figure 2. Virtually all of the sulfur in this sample is thought to be organic as all common inorganic forms-of-sulfur, namely pyrite, iron sulfates, and gypsum, were not detected by iron Mössbauer spectroscopy or calcium K-edge XAFS spectroscopy.

A tabulation of the areas under the different peaks for the samples examined in this study is shown in Table 1. Weight percent carbon (dry, ash-free) from ultimate analyses is used as an approximate measure of the rank of the coals. A systematic variation with coal rank is found in the relative amounts of higher energy peaks compared to the lower energy peak components. The lower rank coals show very pronounced peaks at 8-12 eV, suggestive of the increasing amounts of sulfur-oxygen forms, and the percentages of the areas under these peaks are considerably higher, as shown in Table 1. Figure 3 shows how the peak intensities vary for three coals of different ranks.

CONCLUSIONS

The sulfur K-edge XANES data obtained to date on coals of low inorganic sulfur abundances show a variation in both type and abundance of organic sulfur forms that was not expected. Low-rank coals appear to contain appreciable amounts of sulfur-oxygen compounds and such compounds appear to increase relative to sulfides and thiophenes as rank decreases. It should be emphasized that the percentages quoted in Table 1 are merely for areas under peaks in the least-squares fit. It remains to be established what the relationship is between peak areas and abundances for the different sulfur species and further studies are planned towards this end.

ACKNOWLEDGMENTS

The work described in this paper is supported in part by the Electric Power Research Institute through contract No. RP-8803-20 and in part by the Department of Energy through contract No. DE-FC22-89PC89852.

REFERENCES

1. Spiro C.E., Wong J.,Lytle F., Greegor R.B., Maylotte D., Lampson S.; Science, (1984), **48**, 226.
2. Huffman G.P., Huggins F.E., Shah N., Bhattacharyya D., Pugmire R.J., Davis B., Lytle F.W., Greegor R.B.; ACS Div. Fuel Chem. Preprints, (1988), **33(1)**, 200.
3. Huffman G.P., Huggins F.E., Shah N., Bhattacharyya D., Pugmire R.J., Davis B., Lytle F.W., Greegor R.B.; Processing and Utilization of High Sulfur Coals II; Chugh Y.P., Caudle R.D., Eds., Elsevier, Amsterdam, (1987), 3.
4. George G.N., Gorbaty M.L.; J. Am. Chem. Soc., (1989), **111**, 3182.
5. Stock L.M., Wolny R., and Bal B.; Energy & Fuels, (1989), **3(6)**, 652.
6. Karas J., Pugmire R.J., Woolfenden W.R., Grant D.M., Blair S.; Int. J. Coal Geol., (1985), **5**, 315.
7. Keogh R., Poe S., Chawla B., Davis B.; Coal Science and Technology, **Vol.II**, 289.
8. Cooperative Research in Coal Liquefaction Infratechnology and Generic Technology Development, Final Report, DOE Contract No. DE-FC22-86PC90017, Consortium for Fossil Fuel Liquefaction Science, Lexington, KY, (1988).
9. Huffman G.P., Huggins F.E., Mitra S., Shah N., Pugmire R.J., Davis B., Lytle F.W., Greegor R.B.; Energy & Fuels, (1989), **3**, 200.
10. Huffman G.P., Huggins F.E., Mitra S., and Shah N.; International Conference on Coal Science (Tokyo), in press, (1989).

Table 1. XANES peak areas for various coals investigated.

Sample	%C, daf Whole Coal	% Area of Xanes peaks					
		1	2	3	4	5	6
PSOC 733, WV							
Exinite	87.4	0	60	20	6	14	0
Vitrinite	87.4	0	49	22	9	20	0
Inertinite	87.4	0	52	14	7	27	0
UKCAER 71155, KY							
Vitrinite	84.2	5	48	23	17	5	0
OHIO #5							
Vitrinite	83.5	4	52	20	5	20	0
OHIO #6							
Vitrinite	83.5	0	62	17	16	6	0
UKCAER 91864, KY							
NMP Extract	82.2	4	59	17	6	13	0
UKCAER 71094, KY							
Vitrinite	80.0	6	44	22	15	13	0
Inertinite	80.0	11	41	15	9	24	0
Exinite	80.0	5	44	24	17	10	0
Coal	80.0	7	46	26	11	11	0
PSOC 1110, Utah							
Exinite	72.5	10	30	13	25	14	8
Vitrinite	72.5	10	27	13	31	14	5
PSOC 1108, Utah							
Vitrinite	68.0	5	25	11	30	20	9
Leonardite							
Sample-A	60.1	4	23	21	39	11	2
Sample-B	60.0	5	20	18	24	33	0

Peaks occur in the following energy ranges:
Peak 1: 1.0- 2.2 eV, Peak 2: 2.0- 3.1 eV, Peak 3: 4.5- 4.9 eV,
Peak 4: 9.3-10.3 eV, Peak 5: 11.5-12.0 eV, Peak 6: 15.0-17.5 eV.

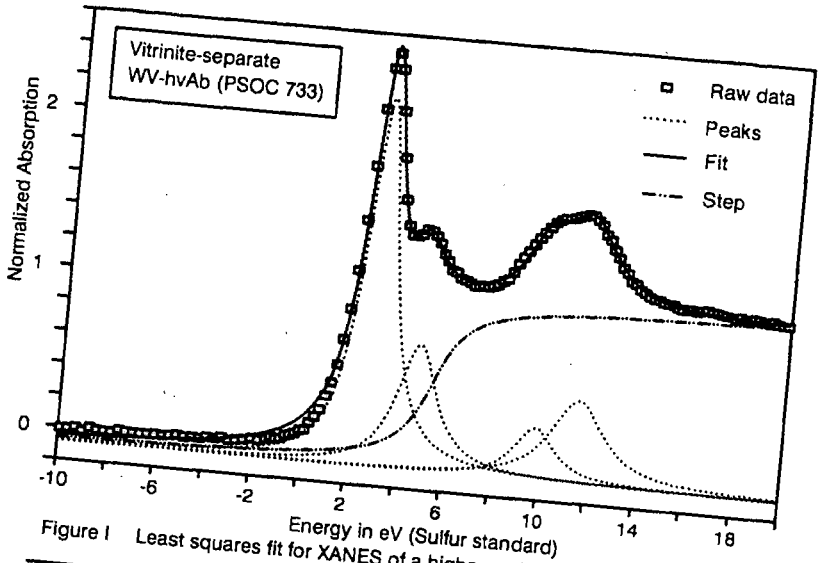

Figure 1 Least squares fit for XANES of a higher rank coal maceral with one step

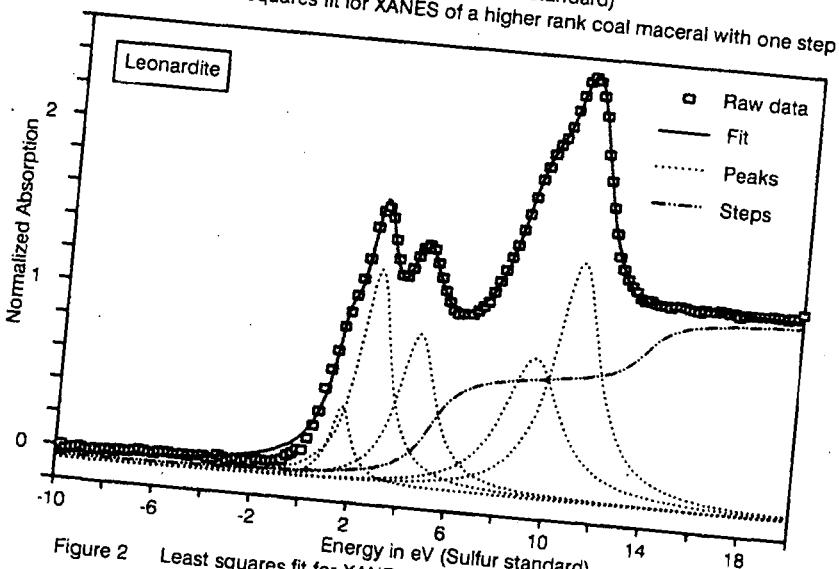

Figure 2 Least squares fit for XANES of a lower rank coal with two steps

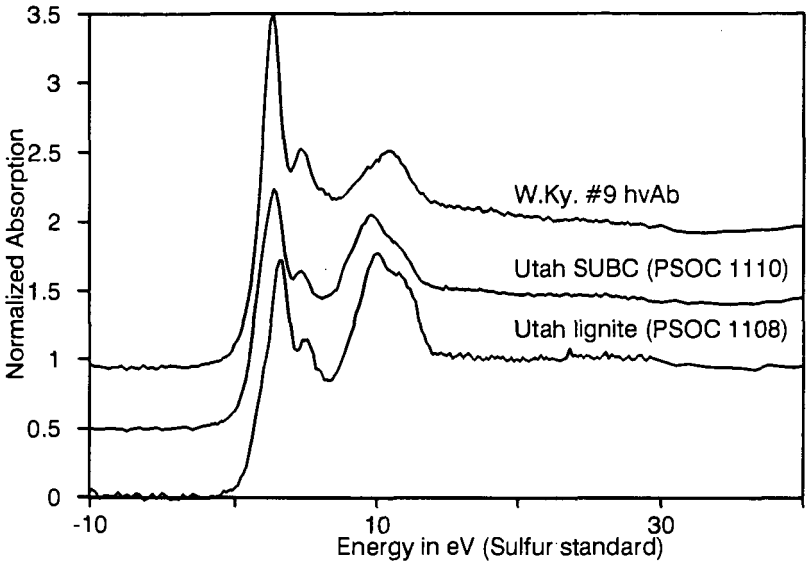

Figure 3 Sulfur XANES of coals of different ranks

Iron K-Edge EXAFS Investigation of Ash Deposits From Coal Combustion

Muthu S. Sundaram, Thomas A. Butcher,
C. R. Krishna and Bernard M. Manowitz
Department of Applied Science
Brookhaven National Laboratory
Upton, New York 11973

and

Melvin L. Zwillenberg
Public Service Electric & Gas Company
80 Park Plaza, T16
Newark, New Jersey 07101

INTRODUCTION

The formation and buildup of the slag deposits on wall tubes is one of the most serious problems in pulverized coal combustion for power generation. This phenomenon, traditionally called wall slagging, is known for its undesirable effects on heat and mass transfer. Many empirical formulationsa based on the silica percentage and acid/base ratio have been developed in the past to describe the slag characteristics. Unfortunately, due to variation of several factors such as flame pattern turbulence, residence time, temperature distribution, gas velocity, etc. within the boiler, these empirical formulations are of limited use in the prediction of the behavior of the slag. In addition, these formulations do not take into consideration of the interaction between the constituents of the coal mineral matter. Another problem in this area is the lack of information on the transition of fluid slag to a solid form and the mechanism of formation of sticky deposits.

Further work in understanding the chemical "structure" of the slags should be profitable in relating the major issue of the influence of coal mineral matter on the operational characteristics of the commercial boilers. Application of Synchrotron-Induced X-Ray Absorption Fine Structure (EXAFS) in such studies was explored and an understanding of the local structure of the iron atoms in the slags derived from a commercial boiler forms the scope of this study.

EXAFS has now become a standard tool for structural determinations. Through EXAFS, it is possible to study the local environment of specific atomic species regardless of the physical state of the material under investigation and one could derive radial structure functions for the short range order near an absorbing element. In simpler terms, EXAFS represents the oscillatory structure due to interference between the outgoing photoelectron wave propagating from the x-ray absorbing atom and the incoming wave backscattered by the neighboring atoms. The EXAFS structure is observed over several hundred electron volts past the absorption edge and many excellent review articles are available on the theory and practice of EXAFS (1-4).

EXPERIMENTAL PROCEDURE

The slag samples for EXAFS analysis were taken from the upper furnace wall of the Mercer Station of Public Service Electric & Gas company, Newark, New Jersey. This is a "wet bottom" unit which means that ash is removed from the furnace bottom as molten slag. This type of furnace design is commonly used with coal which have lower fusion temperatures.

The slag deposits were derived from a Virginia Pocohontas No. 5 bituminous coal. Three samples were analyzed by EXAFS technique: (1) an ASTM ash of the original coal, (2) an inner part of the slag deposit close to the tube wall, and (3) an outer part of the deposit thought to be formed at a higher temperature. The EXAFS materials were sampled from a large block of several feet long slag deposit which was about 6-in. to 8-in. thick.

The EXAFS measurements were made at room temperature on beamline X-19A, in the National Synchrotron Light Source (NSLS), at Brookhaven National Laboratory. The X-19A beamline is equipped with a NSLS boomerang-type double-drystal fixed-exit monochromator. An Si(III) crystal with a Brag angle range of 8° to 15.5°, corresponding to an energy range of 2.12 to 7.93 keV was employed in this study. The electron energy was 2.5 GeV and the beam current was within the range of 90 to 125 mA. The vertical beam height was 0.5 mm and the energy resolution was in the order of 0.7 eV. An Fe foil, obtained from Alpha Products, Danvers, Massachusetts, was used for energy calibration, and the first inflection point in the spectra was noticed at 7111.3 eV. This value was used as energy shift in plotting the spectral data contained in this paper.

A fluorescent ionization detector was employed. The direct beam detector, in front of the sample, was filled with He gas and the ionization detector was filled with a gentle stream of Ar gas. A 6 μm thick manganese filter was used to improve the fluorescent detection.

The raw data was analyzed using EXASCAN data analysis program, originally developed at the University of Washington, Seattle, Washington, and later modified by Mark Eglington of the Unviersity of West Virginia, Morgantown, West Virginia. The principles underlying complicated EXAFS data analysis were discussed in detail by Teo (5).

RESULTS AND DISCUSSION

Figure 1(a) shows an example of the expanded version of the raw spectrum of standard α-Fe_2O_3, -100 eV to +200 eV from the first point of inflection. This spectrum is indicative of the x-ray absorption near edge structure (XANES) which contains information about the chemical environment of the absorbing element. The structure in the XANES region (-20 eV to +50 eV from the absorption edge) is believed to be due to electronic density of the states and is not caused by interference effects from backscattering.

The pre-edge feature has been assigned to a 1s -> 3d transition and the shoulder in the absorption edge, just prior to the edge crest, is considered to be due to 1s -> 4s transition. Even though the observed spectral features are explainable on the basis of electronic transitions, it has been suggested that there is a strong possibility of them to be due to "shape resonances" which are much more sensitive to the ligand geometry and coordination number (6).

Figure 1(b), (c) and (d) shows the expanded version of the raw spectra of the ASTM ash, inner deposit (FETUBA) and outer deposit (FESLAG), respectively. All of these spectra contain a clearly resolved pre-edge peak due to the 1s -> 3d transition as in the case of the standard α-Fe_2O_3.

The intensity of the pre-edge peak is typical of iron in its +3 oxidation state (Fe^{3+}). The magnitude of the intensity of 1s -> 3d transition has been correlated to the degree of the site distortion from a perfect octahedron on the basis of Mossbauer studies (7).

In comparison with the α-Fe_2O_3 spectrum, the 1s -> 4s feature was broadened out in all the samples derived from coal. All spectra clearly showed a sharp edge crest in identical position within the limits of experimental error. Since the Fe^{3+} in α-Fe_2O_3 is highly symmertrical and 6-coordinated, this may be true of the other samples investigated. However, the effect of other nearest neighbor bonding with Fe^{3+} on the XANES feature is not known at this time. Additional standards, incorporating (alkali, alkaline earth metals and Fe) -O bonding have to be evaluated.

Figure 2 shows the Fourier transforms (FT) of K^3-weighted K-edge EXAFS of Fe in the above samples without taking into consideration of the phase shift. There are two major peaks in the FT's corresponding to two different shells: the first peak at ~1.5 Å is attributed to Fe-O atom pair correlation. Considering the fact that EXAFS derived bond-lengths are accurate to 0.02 Å, there are only minor variations in the pseudo radial distribution functions (PRDF), which is representative of the actual bond length in the absence of phase shift corrections, of the samples studied. The coordination (N) of Fe by oxygen decreased to 5.0, 4.5 and 4.0, respectively, for the ASTM ash, inner deposit and outer deposit, respectively, in comparison with N = 6 for α-Fe_2O_3.

The second peak around r = 2.7 Å corresponds to Fe-Fe atom pair correlation and none of the samples from the PSE&G boiler showed intensity similar to that of α-Fe_2O_3. Furthermore, there is considerable variation in the shape of this peak. Whereas this peak was a triplet in the case of α-Fe_2O_3, ASTM ash and the inner deposit, it was a singlet in the case of the outer deposit. It appears that the nature of the deposit formed in the boiler may be related to the second peak in the FT. The shape of the peak may be correlated to the type of the neighboring atom and the intensity of the peak may be used to determine the aggregation of the Fe atoms. The inner part of the deposit, which is close to the relatively cool tube, may be expected to be enriched with volatile alkalis which condense from the gas phase and the iron from the boiler tube. In any case, the

results show that the chemical nature of iron in the boiler deposits is different from that of Fe_2O_3 and there is a continuous variation in its nature across the deposit as additional layers are formed. This characteristic feature can be employed to establish the relationship between the processing conditions and the nature of ash deposits.

CONCLUSIONS

Slagging of ash and fouling of heat exchange tubes are two major problem areas in combustion of coal and other carbonaceous feedstock containing appreciable amounts of mineral matter in it. From the results of this study, employing samples generated in a large-scale utility boiler, it appears that XANES/EXAFS can be used as a structural problem of the materials that cause slagging and fouling, in order to obtain greater insight into the mechanism of their production. The EXAFS study of several other key elements such as Na, K, Ca, Al and S will be required to obtain a clear picture of the slag formation characteristics. The results can be applied to other emerging clean coal technologies such as fluidized bed combustion, coal-fueled gas turbines, etc.

ACKNOWLEDGEMENT

This research was supported by the U.S. Department of Energy under Contract No. AC02-76CH00016.

REFERENCES

1. Koningsberger, D. C. and Prins, R. X-ray Absorption: Principles, Applications and Techniques of EXAFS, SEXAFS and XANES. John Wiley & Sons, New York, New York 1988.

2. Fay, M. J., Proctor, A., Hoffmann, D. P. and Hercules, D. M. Anal. Chem. 60(21), 1225A (1988).

3. Lees, P. A., Citrin, P. H. Eisenberger, P. and Kincaid, B. M., Rev. Mod. Phys., 53(4), 769 (1981).

4. Hayes, T. M., and Boyce, J. B. Solid State Phys., 37, 173 (1982).

5. Teo, B. K. EXAFS: Basic Principles and Data Analysis. Springerverlag, New York, New York (1986).

6. Dehmer, J. L., and Dill, D. J. Chem. Phys., 65, 5327 (1976).

7. Bancroft, G. M., Maddock, A. G. and Burns, R. G. Geochem. Cosmochem. Acta, 31, 2219 (1967).

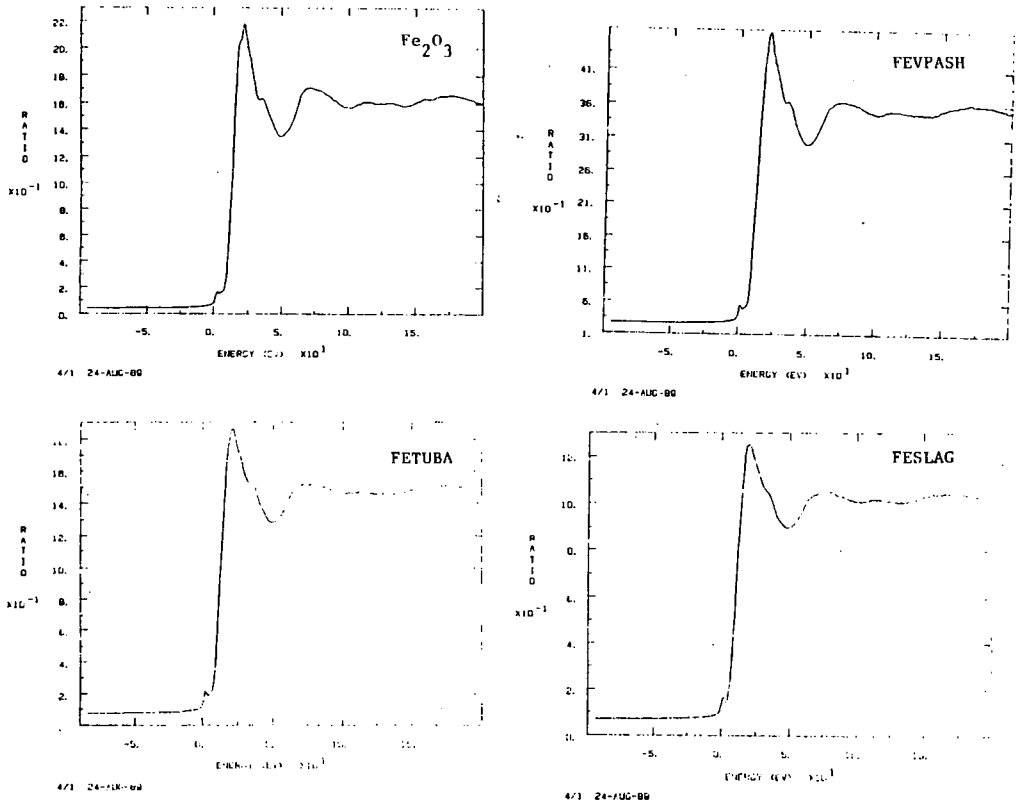

FIGURE 1. X-RAY ABSORPTION NEAR EDGE SPECTRA (IRON K EDGE)

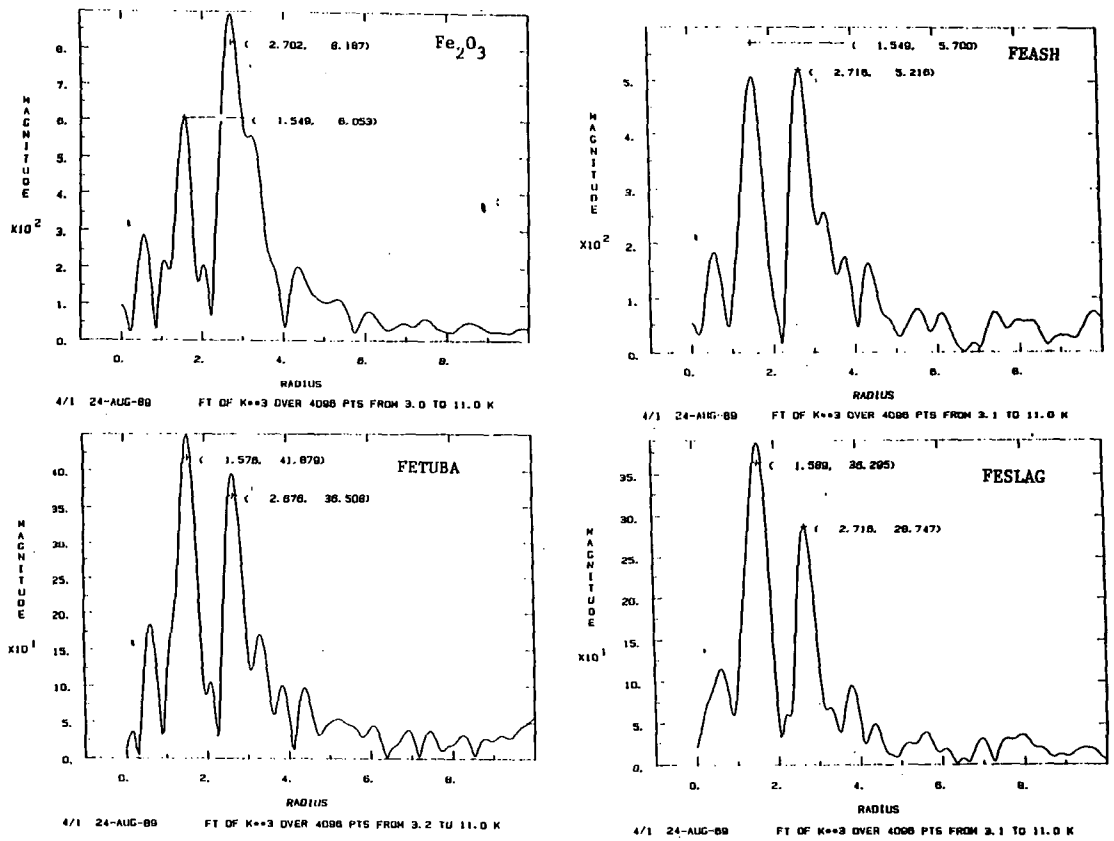

FIGURE 2. Fe K-EDGE PSEUDO RADIAL DISTRIBUTION FUNCTIONS